

The biochemical study of the *R*- and *S*-enantiomers of 2-(4-acetoxyphenyl)-2-chloro-*N*- methylethylammonium chloride (Compound A).

Liezel Maria Swart

Thesis presented in fulfilment of the requirements for the degree of
Master of Biochemistry in the Faculty of Natural Science at Stellenbosch University



Promoter: Prof Pieter Swart
Co-promoter: Prof Amanda C. Swart

March 2017

DECLARATION

By submitting this dissertation electronically, I declare that the entirety of the work contained therein is my own, original work, that I am the owner of the copyright thereof (unless to the extent explicitly stated otherwise) and that I have not previously in its entirety or in part submitted it for obtaining any qualification.

.....

L. M. Swart

March 2017

.....

Date

“Freedom of thought is best promoted by the gradual illumination of men’s minds, which follows from the advance of science.”

Charles Robert Darwin

In loving memory of my father and grandmother.

I am thinking of you always. You are a part of my life, heart and soul forever.

SUMMARY

The study describes:

- The synthesis of a racemic mixture of Compound A (2-(4-acetoxyphenyl)-2-chloro-*N*-methylethylammonium chloride), a synthetic analogue of the active compound isolated from the African shrub, *Salsola tuberculataformis* Botschantzev.
- The development of a strategy to separate the *R*- and *S*-enantiomers of Compound A.
- The isolation and purification of a highly purified substrate-free cytochrome P450 11 β -hydroxylase (CYP11B1) from ovine adrenals.
- The isolation of a partially purified mixture of the mitochondrial electron transport chain, adrenodoxin reductase and adrenodoxin from ovine adrenals.
- The investigation into the mechanism of action of the *R*- and *S*-enantiomers of Compound A on the spectroscopic properties of substrate-free CYP11B1.
- The investigation into the influence of the *R*- and *S*-enantiomers of Compound A on the mitochondrial electron transport chain by using cytochrome c as an electron acceptor.

OPSOMMING

Hierdie studie beskryf:

- Die sintese van 'n rasemiese mengsel van Verbinding A (2-(4-asetoksifeniel)-2-chloro-*N*-metielammoniumchloried), 'n sintetiese analoog van die aktiewe molekule wat in die Suider-Afrikaanse plant, *Salsola tuberculataformis* Botschantzev.
- Die ontwikkeling van 'n strategie om van die *R*- en *S*-enantiomere van Verbinding A te skei.
- Die isolering en suiwing van 'n hoogs gesuiwerde, substraat-vrye sitochroom P450 11 β -hidroksilase (CYP11B1) uit skaap-byniere.
- Die isolering van 'n gedeeltelike gesuiwerde mengsel van die mitokondriale elektrontransportketting, adrenodoksienreduktase en adrenodoksien uit skaapbyniere.
- 'n Ondersoek na die meganisme van werking van die *R*- en *S*-enantiomere van Verbinding A op die spektroskopiese eienskappe van 'n gesuiwerde substraat-vrye CYP11B1.
- 'n Ondersoek na die invloed van die *R*- en *S*-enantiomere van Verbinding A op die mitokondriale elektrontransportketting met behulp van sitochroom c as 'n elektronakseptor.

ACKNOWLEDGEMENTS

Immeasurable appreciation and my deepest gratitude for the help and support are extended to the following people, who in one way or another have contributed to making this study possible:

- **Prof Pieter** and **Prof Amanda Swart** for your unimaginable knowledge, your enthusiasm for science and your willingness to help in all aspects in life. Thank you for guiding me to become the best person and scientist I can be and allowing me to put family above everything. The last few years have been a journey that I will never forget and one I will always be proud of.
- **To my mother**, the strongest woman I know. Thank you for all your support, love guidance and for always allowing to follow my own path. You are truly an inspiration and I am so proud to call you my mother.
- **Ralie Louw**, the best lab manager a student could ever ask for. Thank you for always being understanding, even when I came bearing bad news after breaking glassware. You truly set the standard for how a lab should be managed.
- **Stefan Hayward, Timo Tait, Tandeka Magcwebeba, Jonathan Quanson** and **Liezl Bloem**, for your continued assistance, patience, encouragement and sense of humour during the two years. You have become more than my mentors; you have become my friends. Thank you for everything.
- **Lise Barnard, Desmaré van Rooyen, Charl Lotter** and **René Olsen** for your highly cherished friendship. You have made life outside the lab an adventure.
- The central analytic facility (CAF), with a special thanks to **Mr Malcolm Taylor** and **Dr Marietjie Stander** from mass spectrometry and **Dr Jaco Brand** and **Mrs Elsa Malherbe** from NMR. Thank you for your incredible knowledge in your fields and your assistance and interpretations of MS and NMR data.
- **Tomis Abattoir** for your hospitality and allowing me to collect adrenals.
- The financial assistance of the **National Research Fund (NRF)** towards this research is hereby acknowledged.
- The **University of Stellenbosch** for financial support.
- Finally, I would like to express my unconceivable gratitude to **Lachlan James McEvoy** who has constantly supported and encouraged me to complete this dissertation. You have become my pillar in my life and with your love and support you made this pipedream of completing my masters a reality. I am truly thankful for having such an amazing person in my life. I cannot wait to start the next chapter of my life with you.

TABLE OF CONTENTS

SUMMARY	I
OPSOMMING	II
ACKNOWLEDGEMENTS	III
TABLE OF CONTENTS	IV
LIST OF ABBREVIATIONS	VII
LIST OF FIGURES	XI
LIST OF TABLES	XVII
CHAPTER 1	1
General Introduction	1
CHAPTER 2	10
Adrenal steroidogenesis and cytochrome P450 enzymes	10
2.1 Introduction	10
2.2 The anatomy of the adrenal gland	10
2.3 Cholesterol, the precursor of adrenal steroid hormones	12
2.4 Adrenal steroid metabolism	14
2.5 The regulation of glucocorticoid biosynthesis via ACTH	16
2.6 Cytochrome P450 enzymes	17
2.6.1 Active site of cytochrome P450.....	18
2.6.2 Catalytic cycle of cytochrome P450 enzymes.....	21
2.6.3 The mechanism of cytochrome P450-dependent hydroxylation reactions	23
2.6.4 Spectral properties of cytochrome P450 enzymes	25
2.6.4.1 Cytochrome P450 activity assay - CO-induced difference spectra	26
2.6.4.2 Substrate-induced difference spectra.....	26
CHAPTER 3	31
Synthesis of a racemic mixture of CpDA and the chiral resolution of the R- and S-enantiomers of CpDA	31
3.1 Introduction	31

3.2	Experimental	36
3.2.1	Materials and reagents.....	36
3.2.2	Methods.....	37
3.2.2.1	Synthesis of CpDA.....	37
3.2.2.2	Separation of the R- and S-enantiomers of CpDA	38
3.2.2.3	Mass Spectrometry analysis.....	39
3.2.2.4	Nuclear magnetic resonance – analysis.....	40
3.2.2.5	Preparation of a P450-containing mitochondrial acetone powder from ovine adrenals	41
3.2.2.6	Protein determination assay	41
3.2.2.7	Cytochrome P450 activity assay – (CO-induced difference spectrum)	42
3.2.2.8	Difference spectra.....	42
3.3	Results and discussion	44
3.3.1	Synthesis of CpDA	44
3.3.1.1	Mass spectrometry analyses of CpDA	44
3.3.1.2	NMR analysis of synthesised CpDA.....	50
3.3.1.3	Screen for biological activity of CpDA	52
3.3.2	Separation of the R- and S-enantiomers of CpDA.....	56
3.3.2.1	Mass spectrometry of the R- and S-enantiomers of CpDA	56
3.3.2.2	NMR analysis of the R- and S-enantiomers of CpDA	62
3.3.2.3	Biological activity of the R- and S-enantiomers of CpDA	63
3.4	Conclusion	65
CHAPTER 4	67
	The interaction of CpDA and its enantiomers with purified ovine adrenal cytochrome P450 11β-hydroxylase and adrenal mitochondrial electron transport.....	67
4.1	Introduction	67
4.2	Experimental	68
4.2.1	Materials and reagents.....	68
4.2.2	Methods.....	69

4.2.2.1	The preparation of a P450-containing mitochondrial acetone powder from ovine adrenals	69
4.2.2.2	The preparation of ADXR/ADX from ovine adrenal mitochondrial powder	69
4.2.2.3	BCA protein determination assay	69
4.2.2.4	Cytochrome P450 activity assay.....	69
4.2.2.5	Isolation and purification of substrate bound ovine CYP11B1	70
4.2.2.6	SDS-PAGE analyses of purified CYP11B1 and ADX/ADXR.....	72
4.2.2.7	Western Blot analysis of CYP11B1 and ADX/ADXR.....	72
4.2.2.8	Preparation of substrate-free CYP11B1	73
4.2.2.9	Spectral assays	74
4.2.2.10	Influence of the CpDA and the R- and S-enantiomers on the partially purified ADX/ADXR electron transport system	77
4.3	Results and discussion	78
4.3.1	Isolation and purification of purified substrate-free CYP11B1	78
4.3.1.1	Cytochrome P450 activity assay of partially purified CYP11B1	78
4.3.1.2	Elution profile of purified substrate-bound CYP11B1 from ovine adrenal	80
4.3.1.3	SDS-PAGE and Western blot analysis of purified CYP11B1	83
4.3.1.4	Degree of purity of substrate-bound CYP11B1	85
4.3.1.5	Cytochrome P450 activity assay of substrate-free CYP11B1	86
4.3.1.6	Spectral assays with substrate-free CYP11B1.....	87
4.3.2	Isolation of the adrenal mitochondrial electron transport chain	92
4.3.2.1	SDS PAGE and Western blot analysis of isolated ADXR/ADX	92
4.3.2.2	The influence of CpDA and the enantiomers of CpDA on the reduction of cytochrome c by the ADX/ADXR electron transport system	94
4.4	Conclusion.....	100
CHAPTER 5	102
General discussion	102
REFERENCES	106

LIST OF ABBREVIATIONS

¹H-NMR	proton nuclear magnetic resonance
¹³C-NMR	carbon nuclear magnetic resonance
3βHSD2	3 β -hydroxysteroid dehydrogenase $\Delta^{4,5}$ -isomerase
11-DOC	11-deoxycorticosterone
17OH-PREG	17 α -hydroxy-pregnenolone
17OH-PROG	17 α -hydroxy-progesterone
Å	Angstrom
A4	androstenedione
ACAT	acyl-coenzyme A cholesterol acyltransferase
ACTH	adrenocorticotrophic hormone
ADX	adrenodoxin
ADXR	adrenodoxin reductase
ALDO	aldosterone
AR	androgen receptor
Az	aziridine
BCA	bicinchoninic acid
BSA	bovine serum albumin
cAMP	cyclic adenosine monophosphate
CO	carbon monoxide
CORT	corticosterone
Cl⁻	chlorine ion
CNBr	cyanogen bromide
CpDA	Compound A
CYP_{scc}	cytochrome P450 side chain cleavage
CYP11A1	cytochrome P450 11 α -hydroxylase

CYP11B1	cytochrome P450 11 β -hydroxylase
CYP11B2	cytochrome P450 aldosterone synthase
CYP17A1	cytochrome P450 17 α -hydroxylase/17, 20 lyase
CYP21A2	cytochrome P450 21-hydroxylase
Da	Dalton
D₂O	deuterium oxide
dH₂O	deionised water (Milli Q)
DOC	deoxycorticosterone
DTT	dithiothreitol
DHEA	dehydroepiandrosterone
DHEAS	dehydroepiandrosterone-sulfate
EDTA	ethylenediaminetetraacetic acid
ER	endoplasmic reticulum
EI-MS	electron ionization-mass spectrometry
ESI-MS	electrospray ionization-mass spectrometry
FAB-MS	fast atom bombardment-mass spectrometry
FAD	flavin adenine dinucleotide
Fe^{II}	ferrous iron
Fe^{III}	ferric iron
Δ	field splitting energy
FSH	follicle stimulating hormone
G6P	glucose-6-phosphate
G6PD	glucose-6-phosphate dehydrogenase
GC	gas chromatography
GC-MS	gas chromatography-mass spectrometry
GR	glucocorticoid receptor
HIC	hydrophobic interaction chromatography

HPA-axis	hypothalamic-pituitary-adrenal-axis
HPLC	high performance liquid chromatography
HDL	high density lipoprotein
HSL	hormone-sensitive lipase
IgG	immunoglobulin G
IMM	inner mitochondrial membrane
KCl	potassium chloride
kDa	kilo Dalton
LDL	low density lipoprotein
LH	luteinizing hormone
M	molar
Mr	relative molecular weight
ϵ	molar extinction coefficient
MS	mass spectrometry
NaCl	sodium chloride
NADH	nicotinamide adenine dinucleotide hydrogen
NADP⁺	nicotinamide adenine dinucleotide phosphate (oxidized)
NADPH	nicotinamide adenine dinucleotide phosphate (reduced)
NMR	nuclear magnetic resonance
NaOH	sodium hydroxide
OMM	outer mitochondrial membrane
P	spin-pairing energy
PEG	polyethylene glycol
PREG	pregnenolone
PROG	progesterone
LC-Q-ToF MS	liquid chromatography quadrupole time-of-flight mass spectrometry
SDS-PAGE	sodium dodecyl sulphate polyacrylamide gel electrophoresis

SR-B1	scavenger receptor class B type 1
StAR	steroidogenic acute regulatory protein
<i>Salsola tuberculata</i>	<i>Salsola tuberculatisformis</i> Botschantzev
TEMED	tetramethylethylenediamine
UV	ultra violet

LIST OF FIGURES

Figure 1.	Inhibitory effect on the estrus cycle after feeding rats with <i>Salsola tuberculata</i> . Lucerne meal was used as a control. Redrawn from (7), original image from (6).....	2
Figure 2.	Chemical structures of the compounds found in the <i>Salsola tuberculata</i> extract. Biologically active ketone derivatives namely, A, 4-hydroxy-acetophenone and B, 4-hydroxy-3-methoxy-acetophenone, respectively and the biologically inactive aldehyde derivative, C, 4-hydroxy-benzaldehyde. Redrawn from (4).....	3
Figure 3.	Chemical structure of metyrapone, a synthetic inhibitor of CYP11B1. Redrawn from (4).	4
Figure 4.	Chemical structure of (A) synephrine and (B) aziridine, the chemical precursors of the S2 fraction. Redrawn from (4).....	5
Figure 5.	Chemical structure of CpDA, the synthetic analogue of the S2 fraction. Redrawn from (4).	6
Figure 6.	Cross-sectional schematic of the adrenal gland, with the capsule encapsulating the cortex and the medulla. The adrenal cortex is divided into three distinct layers, namely the zona glomerulosa, zona fasciculata and zona reticularis. Each of these layers produce the mineralocorticoids, glucocorticoids and adrenal androgen precursors, respectively. Reproduced from (57).	11
Figure 7.	Chemical structure of cholesterol, representing the backbone of all the steroid hormones. Redrawn from (60).....	12
Figure 8.	Representation of the utilization of free cholesterol for adrenal steroid metabolism. LDL cholesterol esters bind to the LDL receptor, where they enter the cell via endocytosis. Free cholesterol is transported from the OMM to the IMM, via the protein, StAR. HDL cholesterol esters enter the cell via the SR-B1 receptor. Once in the cell, it can be stored as a lipid droplet, or it can be converted to free cholesterol by the enzyme, HSL. Only free cholesterol can enter the IMM. Free cholesterol can also be synthesized <i>de novo</i> from acetate in the ER and it can be stored as a lipid droplet by the enzyme, ACAT. Reproduced from (53).	13
Figure 9.	Adrenal steroidogenesis pathway. All steroid hormones are derived from cholesterol by a network of enzyme-catalysed reactions. Reproduced and adapted from (54).....	14
Figure 10.	Schematic representation of the HPA-axis. Reproduced from (64).	16
Figure 11.	Schematic representation of the active site of cytochrome P450 dependent enzymes. The 5 th axial position is co-ordinated to the iron by a thiol anion and a cysteine residue, whereas the 6 th axial position is co-ordinated with a water molecule. Redrawn from (7).	18

- Figure 12.** Distribution of electrons in the 3d orbital of the ferric- (Fe^{III}) and ferrous (Fe^{II}) iron, respectively. Image redrawn from (7)..... 19
- Figure 13.** Energy levels of the valence electrons in the 3d orbital influence by the field splitting energy (Δ). Image redrawn from (7). 19
- Figure 14.** Distribution of valence electrons in the 3d orbital in Fe^{III} and Fe^{II} when the field splitting energy (Δ) is smaller than the spin-pairing energy (P). Image represents the high-spin state of the iron. Redrawn from (7)..... 20
- Figure 15.** Distribution of valence electrons in the 3d orbital in Fe^{III} and Fe^{II} when the field splitting energy (Δ) is larger than the spin-pairing energy (P). Image represents the low-spin state of the iron. Redrawn from (7)..... 20
- Figure 16.** Representation of the position of the iron in low- and high-spin state. Upon substrate binding, the iron moves out of the plane of the protoporphyrin IX ring cavity. Redrawn from (7). 21
- Figure 17.** Schematic representation of the adrenal steroidogenic short electron transport system in the mitochondria. (E) represents the mitochondrial enzyme, CYP11B1. (S) denotes the natural substrate, DOC. ADXR is the NADPH-specific FAD containing flavoprotein, whereas ADX is the non-heme protein. Adapted from (7). 23
- Figure 18.** The catalytic cycle of P450-dependent hydroxylation reactions. The iron atom is a representation of the enzyme, whilst the RH (red block) and ROH (blue block) represent the substrate and the product, respectively. Modified image from (71). 24
- Figure 19.** CO-induced dithionite reduced difference spectrum of mitochondrial cytochrome P450 from ovine adrenal. Maximum peak at 450 nm denotes an active cytochrome P450 enzyme (red), whereas a maximum peak at 420 nm represents the inactive form (blue), known as cytochrome P420. Redrawn from experimental work..... 26
- Figure 20.** Representation of Spectral Assay A. CpDA inhibits the binding of DOC to CYP11B1. ... 28
- Figure 21.** Representation of Spectral Assay B. CpDA induced a Type II-induced difference spectrum with an absorbance maximum at 430 nm and absorbance minimum at 412 nm..... 29
- Figure 22.** Biologically active CpDA (2-(4-acetoxyphenyl)-2-chloro-N-methyl-ethylammonium chloride) in which the ring-opened aziridine precursor cyclises into biological inactive form of CpDA (2-(4-acetoxyphenyl)-1-methylaziridine), with a ring closed structure. Redrawn from (28). 32
- Figure 23.** Theoretical interaction of the R- and S-enantiomers of a chiral drug on the drug binding sites of a chiral enzyme. The R-enantiomer aligns directly to the binding sites of the enzyme, whereas the C and A substitutes of the S-enantiomer do not. In this theoretical scenario, the R-enantiomer will be biologically active, whereas the S-enantiomer will interfere with the pharmacological effects of a chiral drug. Adapted from (83). 34

Figure 24.	Chiral separation of 1-phenylethylamine.	35
Figure 25.	Schematic representation of the synthesis of CpDA.	37
Figure 26.	Schematic representation of the chiral resolution of the R- and S-enantiomers of CpDA.	38
Figure 27.	Q-ToF MS of (1 mg/mL) CpDA prepared in deionised water.	46
Figure 28.	ESI-MS spectrum of peak one at 2.57 minutes of the Q-ToF MS analysis of synthesized CpDA.	47
Figure 29.	ESI-MS spectrum of peak two at 3.02 minutes of the Q-ToF MS analysis of synthesized CpDA.	48
Figure 30.	ESI-MS spectrum of peak three at 4.60 minutes of the Q-ToF MS analysis of synthesized CpDA.	49
Figure 31.	¹ H-NMR analysis of synthesized CpDA.	50
Figure 32.	¹³ C-NMR analysis of synthesized CpDA.	51
Figure 33.	CO-induced difference spectrum of a crude mitochondrial-acetone preparation, 2mg/mL, in 0.1 M phosphate buffer, containing 10% ethylene glycol. [P450], 0.686 nmol P450/mg protein.	52
Figure 34.	Influence of CpDA on the DOC-induced difference spectrum of a mitochondrial suspension, 2mg/mL, in 0.1 M phosphate buffer, containing 10% ethylene glycol. [P450], 0.686 nmol P450/mg protein; [DOC], 3.21 μM; % inhibition of CpDA at 250 μM, 16.85%; 500 μM, 30.84%; 750 μM, 50,30%; and 1000μM, 64.53%.	53
Figure 35.	Type II-induced difference spectrum of CpDA (200 μM). [P450], 0.686 nmol P450/mg protein.	54
Figure 36.	Screen for biological activity of synephrine and tartaric acid. (A). Influence of synephrine (500 μM) and tartaric acid (500 μM) on the DOC-induced difference spectrum of a mitochondrial suspension, 2mg/mL, in 0.1 M phosphate buffer, containing 10% ethylene glycol. [P450], 0.686 nmol P450/mg protein; [DOC] = 3.21μM; no inhibition was observed. (B) Type II-induced difference spectrum of synephrine (200μM) and tartaric acid (200μM). [P450], 0.686 nmol P450/mg protein.	55
Figure 37.	Q-ToF MS of the R- and S-enantiomers (1 mg/mL) of CpDA prepared in deionised water.	58
Figure 38.	ESI-MS spectra of the Q-ToF MS spectrum of CpDA enantiomers. (A) R-enantiomer and (B) S-enantiomer at 1.18 minutes (peak 1); (C) R-enantiomer at 2.17 minutes and (D) S-enantiomer at 2.23 minutes (peak 2).	59

- Figure 39.** ESI-MS spectra of the Q-ToF MS spectrum of CpDA enantiomers. (A) R-enantiomer and (B) S-enantiomer at 2.54 minutes (peak 3); (C) R-enantiomer at 2.93 minutes and (D) S-enantiomer at 2.95 minutes (peak 4). 60
- Figure 40.** ESI-MS spectra of the Q-ToF MS spectrum of CpDA enantiomers. (A) R-enantiomer and (B) S-enantiomer at 3.44 minutes (peak 5); 61
- Figure 41.** Stacked ¹H-NMR spectra of the R- and S-enantiomers of CpDA. 62
- Figure 42.** (A) Influence of CpDA (750 μM) and the R-enantiomer (750 μM) and the S-enantiomer (750 μM) on the DOC-induced difference spectrum of a mitochondrial suspension, 2mg/mL, in 0.1 M phosphate buffer, containing 10% ethylene glycol. [P450], 0.686 nmol/mg protein; [DOC], .3.21 μM; % inhibition of CpDA and the R- and S-enantiomers of CpDA was 51.05%,18.96 % and 31.54%, respectively (B) Type II-induced difference spectrum of the R-enantiomer in red (200μM) and S-enantiomer in blue (200μM) of CpDA. [P450], 0.686 nmol P450/mg protein. 64
- Figure 43.** Schematic representation of the specially designed centrifuge tube. The sample application chamber (1) is connected to a 1 mL reactivial sample collector chamber (5), screwed into one another by the membrane support holder (4). The 0.4 μm filter membrane (7), cut to the right size using a punch, is supported by a porous poly-ethylene membrane support (3) and sealed by an O-ring (2). An air vent placed at a 65°angle on the sample application chamber prevents air trapping in the system. Redrawn from (18). 74
- Figure 44.** CO-induced difference spectrum of mitochondrial preparation containing CYP11B1. Mitochondrial preparation, 20mg/mL standard buffer; [P450], 2.350 nmol P450/mg protein. 79
- Figure 45.** Elution profile of substrate-bound CYP11B1. The dialysed CYP11B1 was applied to an equilibrated Phenyl-Sepharose CL-4B column (8cm x 1cm), washed with equilibration buffer, and eluted at 1 mL per minute, with an elution buffer. 81
- Figure 46.** CO-induced difference spectrum of collected fractions 2-4, (Fig 45 peak 1). The maximum at 420 nm represents the inactive form of CYP11B1. 82
- Figure 47.** CO-induced difference spectrum of collected fractions 13-18 (Fig 45 peak 2). The peak at 450 nm represents the active form of CYP11B1. The concentration of the pooled chromatographic fractions was 8.327 nmol/mg protein..... 82
- Figure 48.** (A) SDS-PAGE analysis of purified-substrate bound CYP11B1 with apparent molecular mass of 46 kDa. Column eluate samples were separated on a 12% gel. Lane 1: Precision Plus Protein™ Kaleidoscope™ marker (10-250 kDa); Lane 2, fraction 2, 10 x dilution 20 μg protein; Lane 3, fraction 3, 10 x dilution 25 μg protein; Lane 4, fraction 4, 10 x dilution 7.5 μg protein; Lane 5, fraction 16, 15 μg protein; Lane 6, fraction 17, 13 μg protein; Lane 7, fraction 18, 10 μg protein; Lane 8, pooled chromatographic fractions of 2nd elution peak, 18 μg protein; and Lane 9 partially purified extract, 30 x dilution 12.30 μg protein. (B)

- Western blot analysis of purified substrate-bound CYP11B1. Lanes 1 – 3, fractions 16, 17 and 18; and Lane 4 pooled chromatographic fractions of 2nd elution peak. CYP11B1 was detected with rabbit anti-sheep IgG against CYP11B1 (1:4000) and goat anti-rabbit IgG (1:20 000) was used as the secondary antibody. Immunoblot bands were visualised by chemiluminescence. 84
- Figure 49.** CO-induced difference spectrum of reduced purified substrate-free CYP11B1 in standard buffer. [CYP11B1] = 10.950 nmol P450/mg protein; black trace, CYP11B1 immediately after the filtration process; red trace; CYP11B1 after a 45 minutes; 86
- Figure 50.** (A) Influence of the racemic mixture of CpDA on the DOC-induced difference spectra with purified CYP11B1. CpDA, 750 μ M, inhibition, 52.30%; [CYP11B1] = 10.950 nmol/mg protein. [DOC] = 10 μ M. (B) CpDA-induced type II difference spectrum of purified CYP11B1. [CYP11B1] = 10.950 nmol/mg protein. [DOC], 10 μ M; and [CpDA], 200 μ M. 89
- Figure 51.** (A) Influence of the R-enantiomer of CpDA on the DOC-induced difference spectra with purified CYP11B1. R-enantiomer, 750 μ M, inhibition, 14.90%; [CYP11B1] = 10.950 nmol/mg protein. [DOC] = 10 μ M. (B) R-enantiomer of CpDA-induced type II difference spectrum of purified CYP11B1. [CYP11B1] = 10.950 nmol/mg protein. [DOC], 10 μ M; and [CpDA], 200 μ M. 90
- Figure 52.** (A) Influence of the S-enantiomer of CpDA on the DOC-induced difference spectra with purified CYP11B1. S-enantiomer, 750 μ M, inhibition, 35.18%; [CYP11B1] = 10.950 nmol/mg protein. [DOC] = 10 μ M. (B) S-enantiomer of CpDA-induced type II difference spectrum of purified CYP11B1. [CYP11B1] = 10.950 nmol/mg protein. [DOC], 10 μ M; and [CpDA], 200 μ M. 91
- Figure 53.** (A) SDS-PAGE of ADX and ADXR. Lane 1, Kaleidoscope protein marker; Lane 2, crude ADXR/ADX preparation; and Lane 3 concentrated ADXR/ADX preparation. In each lane, 20 μ g protein was loaded. (B) Western blot analysis of ADX. Lane 1, crude ADXR/ADX preparation and Lane 2, concentrated ADXR/ADX preparation. In each lane, 20 μ g protein was loaded. Rabbit anti-sheep ADX IgG 1:6000. (C) Western blot analysis of ADXR. Lane 1, crude ADXR/ADX preparation and Lane 2, concentrated ADXR/ADX preparation. In each lane, 20 μ g protein was loaded. Rabbit anti-sheep ADXR IgG, 1:6000; goat anti-rabbit IgG (1:20 000). 93
- Figure 54.** Reduction of cytochrome c by the ADX/ADXR electron transport system. The red curve represents the incubation mixture of the sample well (cytochrome c, ADX/ADXR, G6P and G6PD). The black line represents the incubation mixture of the reference well without the ADX/ADXR preparation. 96
- Figure 55.** (A) Reduction of cytochrome c by the ADX/ADXR electron transport system. The red curve represents the incubation mixture of the sample well (cytochrome c, ADX/ADXR, G6P and G6PD). The black line represents the incubation mixture of the reference well without the ADX/ADXR preparation. The blue curve represents the incubation mixture with CpDA, 750

μM , and the green curve the incubation mixture with CpDA, 375 μM . (B) Linear regression of the first 30 seconds of the curves..... 97

Figure 56. (A) Reduction of cytochrome c by the ADX/ADXR electron transport system. The red curve represents the incubation mixture of the sample well (cytochrome c, ADX/ADXR, G6P and G6PD). The black line represents the incubation mixture of the reference well without the ADX/ADXR preparation. The orange curve represents the incubation mixture with the R-enantiomer, 750 μM , and the light green curve the incubation mixture with the R-enantiomer, 375 μM . (B) Linear regression of the first 30 seconds of the curves. 98

Figure 57. (A) Reduction of cytochrome c by the ADX/ADXR electron transport system. The red curve represents the incubation mixture of the sample well (cytochrome c, ADX/ADXR, G6P and G6PD). The black line represents the incubation mixture of the reference well without the ADX/ADXR preparation. The purple curve represents the incubation mixture with the S-enantiomer, 750 μM , and the light blue curve the incubation mixture with the S-enantiomer, 375 μM . (B) Linear regression of the first 30 seconds of the curves. 99

LIST OF TABLES

Table 1.	Characteristics of the substrate- and inhibitor-induced difference spectrum of cytochrome P450 enzymes. Redrawn from (7).....	27
Table 2.	Chromatographic elution gradient of CpDA separated on an UPLC/Q-ToF/ ESI-MS system	40
Table 3.	Chromatographic elution profile for CYP11B1	71
Table 4.	Design protocol for Spectral Assay A.....	75
Table 5 .	Design protocol for Spectral Assay B.....	76
Table 6.	Purification table for CYP11B1 isolated from ovine adrenals.....	85

CHAPTER 1

General Introduction

Salsola tuberculatisformis Botschantzev (*Salsola tuberculata*) is a robust and hardy shrub native to the arid regions of the Namibian desert. During periods of low rainfall, this drought-resistant shrub is a highly valued source of nutrition for livestock (1). In 1906, Ploss described the utilization of an aqueous extract of plants belonging to the genus *Salsola* (Family: Chenopodiaceae) as an oral contraceptive for Algerian women (2). In addition, Sir Laurens Jan van der Post, an authority on Bushmen folklore and culture, also noted the utilization of the aqueous extracts of this genus as an oral contraceptive by the local Bushmen women (3, 4).

The biological effects of this African shrub were first brought to scientists' attention in 1961, when De Lange observed a syndrome of prolonged gestation in Karakul sheep, which occurred during periods of severe drought in the Keetmanshoop region of southern Namibia (5). This syndrome, known as "Grootlamsiekte", prolonged the normal gestation period of Karakul sheep from \pm 149 days to 213 days, which affected the vigour, size and pelts of the new born. At birth, the Karakul lambs have high quality, soft, strong and tightly-curved black wool, which is used to make a variety of soft, warm and elegant garments for international export. However, when the lambs grow older the tightly curved wool becomes straight, changes to a greyish colour and loses its silky appearance. Lambs are therefore slaughtered within 24 hours after birth to preserve the high-quality pelts (6). It is thus clear that "Grootlamsiekte" had detrimental financial implications for the world renowned Karakul industry, as the pelts of the new born were considered worthless for international trade.

The heavy losses that the Karakul farmers experienced initiated an investigation into identifying this syndrome and eliminating the cause. In 1969, Basson *et al*, discovered that ingestion of the hardy African shrub by the Karakul ewes was the agent responsible for this condition (6). The logical response to Basson's discovery was to isolate and characterize the active compound(s) in the shrub. The highest priority was placed on developing a reliable bio-assay in order to investigate the biological mechanism of action of the active compound(s) in *Salsola tuberculata*. This was an extremely challenging task, as the hormonal changes in both the ewe and foetus responsible for maintenance of pregnancy are influenced by several factors (7–9). These factors are divided into four main groups, namely: maternal, foetal, genetic and environmental. Examples corresponding to each group include: the age of the

lamb, hormonal changes caused by pituitary and adrenal function, the genotype of the foetus, the maternal gestational diet, and lifestyle factors. Therefore, when considering the length of gestation and the various factors that influence the maintenance of pregnancy in ewes, it became apparent that using the Karakul sheep as experimental animals would not be appropriate for screening tests. Thus, sexually mature laboratory rats were considered a more appropriate experimental model, given their significantly shorter gestation period of 21-23 days. These test animals posed similar problems to the sheep, as the prenatal development of the foetus is interdependent on the numerous factors previously mentioned. Nevertheless, when the natural plant extract was fed to pregnant rats, screening tests revealed a rise in foetal resorption during early pregnancy, and foetal death during later stages of pregnancy. However, when virgin female rats were fed with various concentrations of the dry plant extract, they noticed an inhibitory effect in their oestrus cycle (6, 7, 9). The results obtained during this investigation are shown in **Figure 1**.

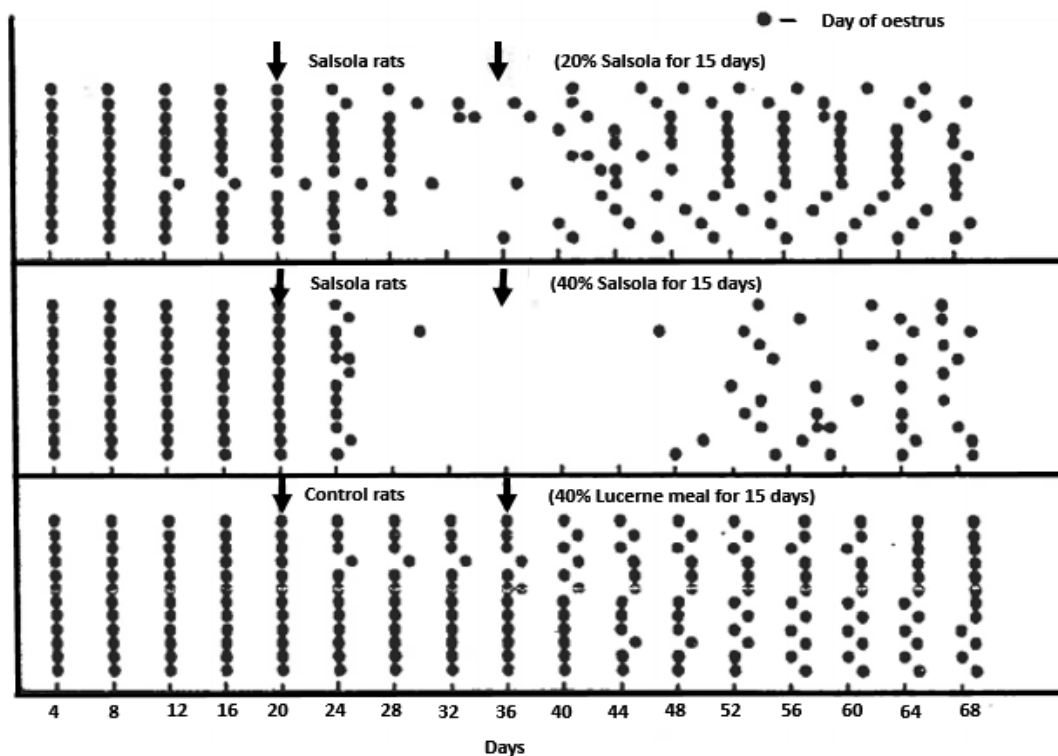


Figure 1. Inhibitory effect on the estrus cycle after feeding rats with *Salsola tuberculata*. Lucerne meal was used as a control. Redrawn from (7), original image from (6).

The results indicated that *Salsola tuberculata* possibly contained active compound(s) responsible for both the observed extended gestation period in Karakul ewes and the contraceptive effect in rats (6). These findings considered together with the notion that the Algerian and Bushmen women used the same plant for its contraceptive purposes motivated the development of a bio-assay which focused mainly on *Salsola tuberculata*'s contraceptive properties (2, 3, 6, 7). To perform this bio-assay in virgin rats, researchers administered the

plant extract and collected and analysed daily vaginal smears using appropriate staining techniques. In combination with this bio-assay, standard methanol extraction- and chromatographic procedures were used to extract the contraceptive agent from the plant. However, the methanol extract was highly labile and displayed rapid autocatalytic decomposition behaviour under standard laboratory conditions (6). Nevertheless, Van der Merwe *et al.* succeeded in isolating the contraceptive agents by treating the extract with the derivatizing reagent, trimethylammonium acetyl hydrazide chloride (Girard-T reagent), which is known to remove ketones and aldehydes (4, 9, 10). Subsequently, the reaction derivatives were subjected to standard solvent partitioning and, under acidic conditions, the derivatives decomposed into three organic compounds (**Figure 2**). These compounds were identified by electron ionization-mass spectrometry (EI-MS) and proton-nuclear magnetic resonance ($^1\text{H-NMR}$) as (**A**) 4-hydroxy-acetophenone (**Figure 2 A**), (**B**) 4-hydroxy-3-methoxy-acetophenone (**Figure 2 B**) and (**C**) 4-hydroxy-benzaldehyde (**Figure 2 C**). Biological studies revealed that the ketones (**A** and **B**) were to some extent biologically active in the rats, whereas the aldehyde (**C**) was entirely inactive. However, further investigations revealed that neither the ketones nor the aldehyde accounted for the contraceptive effects of the shrub. Unfortunately, the extracted compounds were sensitive to light, air, pH and heat and thus rapidly deteriorated under standard laboratory conditions (4, 9).

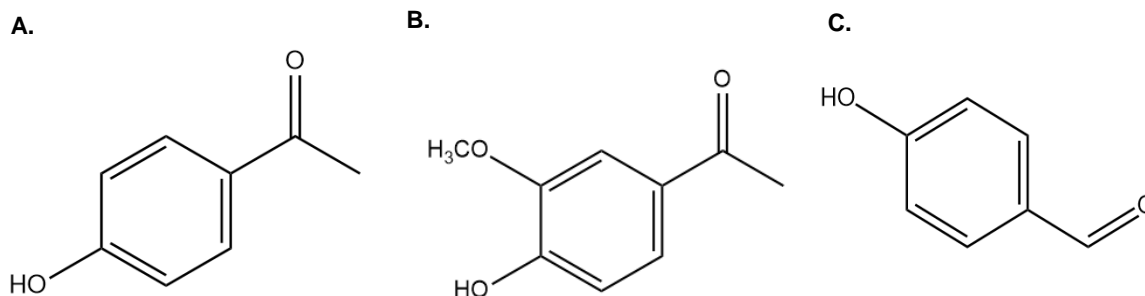


Figure 2. Chemical structures of the compounds found in the *Salsola tuberculata* extract. Biologically active ketone derivatives namely, **A**, 4-hydroxy-acetophenone and **B**, 4-hydroxy-3-methoxy-acetophenone, respectively and the biologically inactive aldehyde derivative, **C**, 4-hydroxy-benzaldehyde. Redrawn from (4).

Researchers were compelled to re-evaluate their extraction method and, due to the labile nature of the active compounds, replaced the time-consuming rat bio-assay with a more reliable, rapid, and sensitive method (9). The highly labile nature of the extracted bio-active compounds made the development of a new assay and extraction method a daunting task. Nevertheless, it appeared that two seemingly unrelated publications of Williamson and O'Donnell (1969) and Liggins and Fairclough (1973) offered new insights into resolving the problem (11, 12).

- The first publication revealed that the synthetic agent, metyrapone (**Figure 3**) (2-methyl-1,2-di-pyridin-3-yl-propan-1-one) inhibited the binding of the substrate, deoxycorticosterone (DOC) and deoxycortisol, to the terminal enzyme in the glucocorticoid biosynthesis pathway, cytochrome P450 11 β -hydroxylase (CYP11B1), resulting in the reduced production of corticosterone (CORT) and cortisol, respectively (11).
- The second publication discovered that a rise in the level of cortisol in foetal plasma triggers the onset of parturition in sheep (12).

The combined knowledge of the two publications led to the assumption that the active compound(s) of the shrub interfered with adrenal steroidogenesis and, more specifically, with the terminal reaction in the glucocorticoid biosynthesis pathway in both animals (7). It was, therefore, hypothesised that the active compound(s) in the shrub inhibited CYP11B1 and caused perturbations in cortisol production (7, 13, 14). This assumption was verified experimentally by feeding sexually mature female rats with metyrapone. Not only did metyrapone share structural similarities with the biologically active ketones (**Figure 3**), but metyrapone also mimicked the physiological consequences of the shrub (15).

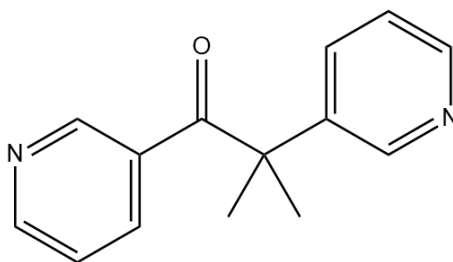


Figure 3. Chemical structure of metyrapone, a synthetic inhibitor of CYP11B1. Redrawn from (4).

The implications of these discoveries led to the development of a new bio-assay, which was based on the unique spectroscopic and catalytic properties of the adrenal steroidogenic enzyme, CYP11B1 (7, 14, 15). With the aid of difference spectroscopy, the unique spectral properties of CYP11B1 can be used to:

- Measure the interference of a test compound (inhibitor) on the binding of the natural substrate (DOC) with the enzyme (CYP11B1).
- Directly measure the interaction of a test compound (inhibitor) with the enzyme without the presence of natural substrate.

The mode by which a test compound (inhibitor) influences the spectroscopic properties of CYP11B1 can be used to understand its mechanism of action on a micro-scale (7, 16–18).

Since adrenal steroid metabolism and the spectroscopic properties of CYP11B1 play such an important role in this study, a detailed overview of adrenal steroid metabolism and cytochrome P450 enzymes will therefore be provided in Chapter 2.

The new bio-assays were successfully applied to a new screening method, which served as a more rapid and sensitive approach to identifying active compounds from *Salsola tuberculata* (7, 15, 18). Armed with a new screening method and high performance liquid chromatography (HPLC), Swart and Swart successfully isolated two biologically active HPLC fractions from the shrub, namely S1 and S2 (7, 18). Due to the labile nature of both fractions, precautionary steps needed to be taken to preserve their activity. The fractions were therefore shielded from light and oxidation, and stored in an acidic environment. Even after these steps were taken, only the S2 fraction remained active in biological studies (7, 18, 19). Despite these advances, the highly labile nature of the S2 fraction severely hindered the investigation into its chemical structure. Additionally, the lack of modern nuclear magnetic resonance (NMR) and mass spectrometry (MS) facilities, and the use of gas chromatography-mass spectrometry (GC-MS), prevented the direct elucidation of the structure at the time. However, by acetylating the S2 fractions and by using analytical techniques, such as gas chromatography (GC) and fast atom bombardment mass spectrometry (FAB-MS), researchers confirmed that the acetylated S2 was the precursor of both synephrine (**Figure 4 A**) and a highly reactive aziridine (Az) (**Figure 4 B**) (20–23).

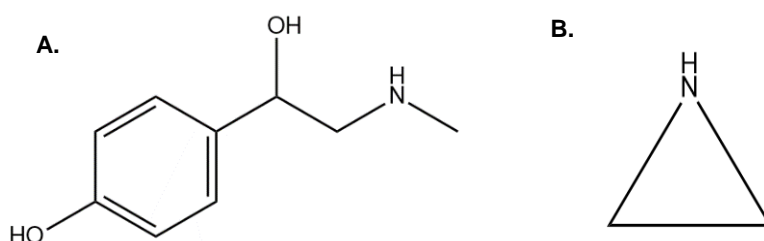


Figure 4. Chemical structure of (A) synephrine and (B) aziridine, the chemical precursors of the S2 fraction. Redrawn from (4).

Az, also known as ethylenimines, are highly reactive compounds, characterized by a three-membered ring structure, consisting of one amine group and two methylene bridges. The high lability and reactive characteristics of most aziridines are attributed to the high level of strain in the three membered ring structure. Therefore, to decrease the strain and increase the stability of the compound, Az readily reacts with a number of nucleophiles (which tend to be good leaving groups e.g. chlorine ion (Cl⁻), to form ring-opened products (4, 24, 25).

It was therefore hypothesized that the labile nature of the active compound(s) in the S2 fraction was attributed to the Az moiety (21–23). In an attempt to obtain a more stable derivative of the S2 fraction, an Az precursor was synthesized, known as Compound A (2-(4-acetoxyphenyl)-2-chloro-*N*-methylethylammonium chloride) (**Figure 5**) (24). Compound A (CpDA) served as an appropriate model for both *in vivo* and *in vitro* studies, as it mimicked the properties of its natural counterpart and the S2 fraction (26, 27). Additionally, it could be stabilised by steroid-binding globulins in plasma, thus enhancing its biological activity *in vivo* (28, 29).

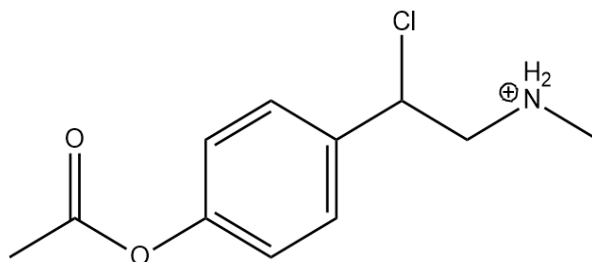


Figure 5. Chemical structure of CpDA, the synthetic analogue of the S2 fraction. Redrawn from (4).

To date, evidence has shown that CpDA acts as a non-steroidal multi-target androgen receptor (AR) and glucocorticoid receptor (GR) modulator (30). *In vivo* studies have revealed that CpDA has anti-cancer properties by repressing AR function (31–33). Similarly, numerous *in vitro* studies have shown that like synthetic glucocorticoids, CpDA has anti-inflammatory and immunosuppressive properties (34–43). CpDA promotes the translocation of the GR into the nucleus, however, it prevents GR dimerization and consequently inhibits the GR transactivation pathway. Instead CpDA binds as a homodimer to the glucocorticoid response element and promotes the GR transrepression pathway. It is well known that the adverse effects associated with the chronic use of glucocorticoids are mediated by GR transactivation. Since CpDA diverts from GR transactivation, it has the unique ability to retain the anti-inflammatory and immunosuppressive potential of glucocorticoids, but with reduced side effects (30, 44–46). However, the use of CpDA has limitations, as it has a narrow range (± 1 –15 mg/mL) in which it can elicit a therapeutic response. High concentrations of CpDA became intrinsically toxic to the cells, whereas low concentrations had a limited anti-inflammatory response. Moreover, in contrast to glucocorticoids, a 10-fold increase in the concentration of CpDA is needed to induce the same anti-inflammatory effect (30). Because the unique pharmacological properties of CpDA can be applied in future clinical treatment of diseases associated with the AR/GR or both receptors, it would be beneficial to develop a method wherein the therapeutic window of CpDA can be improved.

CpDA is, however, a chiral compound consisting of a 1:1 ratio of the *R*- and *S*-enantiomers (24, 30). It is important to note that all biological and comparative studies on CpDA, both *in vitro* and *in vivo*, have been performed using a racemic mixture of the compound (30). Although enantiomers have the same chemical composition, it is well-known that, in a biological environment, most single enantiomers have their own pharmacological profile and that the enantiomers should be classified as two distinct compounds, unless proven otherwise. Therefore, one enantiomer may be pharmacologically active, whereas the other enantiomer may be inactive, and even result in severe side effects. Consequently, it is important to separate the *R*- and *S*-enantiomers of CpDA, as the single enantiomeric form could potentially lead to a simpler and improved pharmacological profile, provide a greater understanding of the biological nature of each enantiomer, and similarly offer an alternative means of increasing its therapeutic range. A powerful tool that could aid in increasing the therapeutic window of CpDA is known as chiral resolution, which involves the separation of the *R*- and *S*-enantiomers of a racemic compound (47–52).

Aim of the study

The aim of this study was to separate the *R*- and *S*-enantiomers of CpDA and to determine the biological activity of each enantiomer. The biological activities of the single enantiomers were investigated by using the spectroscopic properties of mitochondrial CYP11B1 from ovine adrenals. In addition, the influence of CpDA was also tested on the mitochondrial electron transport system from ovine adrenals by using cytochrome *c* as an electron acceptor. As part of a comparative study, the effects of the *R*- and *S*-enantiomers of CpDA was compared to the racemic mixture of CpDA. The hypothesis of this study is that either the *R*- or *S*-enantiomers of CpDA may yield a more effective inhibitory profile.

The objectives addressed in this study can be summarized as follows:

1. Synthesize a racemic mixture of CpDA.
2. Develop a method to separate the *R*- and *S*-enantiomers of CpDA.
3. Screen for biological activity of the *R*- and *S*-enantiomers of CpDA and the racemic mixture of CpDA by using the spectroscopic properties of partially purified CYP11B1 from ovine adrenals.
4. Isolate and purify CYP11B1 from ovine adrenals.
5. Investigate the mechanism of action of the *R*- and *S*-enantiomers of CpDA by using the spectroscopic properties of purified CYP11B1.
6. Isolate the mitochondrial electron transport chain, adrenodoxin (ADX) and adrenodoxin reductase (ADXR) from ovine adrenals.

7. Investigate whether the *R*- and *S*-enantiomers of CpDA influence the electron transport system of CYP11B1.

The approach to this study is reported in four chapters as outlined below:

Chapter 2 – Adrenal steroidogenesis and cytochrome P450 enzymes

In Chapter 2 of this thesis, a literature review of adrenal steroidogenesis and cytochrome P450 enzymes is provided. This chapter focuses on the structure and function of the adrenal gland, the biosynthesis of adrenal steroid hormones, and the regulation of enzymes involved in the glucocorticoid biosynthesis pathway. Furthermore, a comprehensive overview of cytochrome P450 enzymes is provided including the discovery, the unique active site, the mechanism of action of the P450-dependent hydroxylation reactions, the electron transport system in the hydroxylation reaction and finally, the unique spectral and catalytic properties of the P450-dependent enzymes.

Chapter 3 – Synthesis of a racemic mixture of CpDA and the chiral resolution of the R- and S-enantiomers of CpDA

This chapter reports on the synthesis and chiral resolution of the *R*- and *S*-enantiomers of CpDA. Liquid chromatography quadrupole time-of-flight mass spectrometry (LC-Q-ToF MS) was used for the accurate mass determination of CpDA and the *R*- and *S*-enantiomers of CpDA. Additionally, NMR spectroscopy were employed for direct structure elucidation. The spectroscopic properties of partially purified CYP11B1 was used to screen for biological activity of CpDA and the *R*- and *S*-enantiomers.

Chapter 4 – The interaction of CpDA and its enantiomers with purified ovine adrenal cytochrome P450 11 β -hydroxylase and adrenal mitochondrial electron transport

In Chapter 4, the isolation and purification of CYP11B1, and the isolation of ADX and ADXR are described. CYP11B1, ADX and ADXR were isolated from a P450-enriched mitochondrial powder prepared from ovine adrenals. The purification of CYP11B1 was achieved by using hydrophobic interaction liquid (HIC) chromatography on a Phenyl-Sepharose column. The purity of CYP11B1 and isolated ADX/ADXR solution was assessed by sodium dodecyl sulfate polyacrylamide gel electrophoresis (SDS-PAGE) and Western blot analysis. The biochemical mechanism of action of the *R*- and *S*-enantiomers were determined by using the spectroscopic properties of purified CYP11B1. The influence of single enantiomers was also tested on the mitochondrial electron transport chain by using cytochrome c as an electron acceptor. The results obtained during the spectroscopic assays with the enzyme and electron transport system were compared to the racemic mixture of CpDA.

Chapter 5 - General discussion

Chapter 5 presents a thorough discussion of the results described in Chapter 3 and Chapter 4, and highlights the main conclusions which can be drawn from the study. This chapter concludes with the significance of this research study and a proposal of future work.

CHAPTER 2

Adrenal steroidogenesis and cytochrome P450 enzymes

2.1 Introduction

The adrenal cortex, located within the adrenal glands, produces the adrenal steroid hormones which regulate crucial physiological and developmental processes throughout the body (53). These steroid hormones are all derived from a common precursor, cholesterol, with the aid of an intricate network of mono-oxygenase reactions that are catalysed by different cytochrome P450 enzymes (53, 54). The adrenal steroid hormones can be divided into three distinct classes, namely: mineralocorticoids, glucocorticoids and adrenal androgens (53–55). Each class has its own essential role in the body. Abnormalities within the expression levels and/or activity of steroidogenic enzymes result in perturbations in the delicate steroid hormone balance, causing abnormal physiological responses (7, 18, 54, 56). The occurrence of prolonged gestation in sheep and the contraceptive action in rats, discussed in Chapter 1, can be understood in terms of the active compounds in the shrub directly affecting the activity of CYP11B1, resulting in an inhibition of glucocorticoid production.

The following subdivision will be devoted to understanding adrenal steroid metabolism and the intricate role of cytochrome P450 enzymes in the adrenal cortex.

2.2 The anatomy of the adrenal gland

The adrenals are two small bilateral encapsulated endocrine glands situated above each kidney. These glands consist of two distinct types of tissues, the adrenal cortex and the adrenal medulla, which are structurally, functionally and biochemically distinct from one another (**Figure 6**) (7, 18, 54).

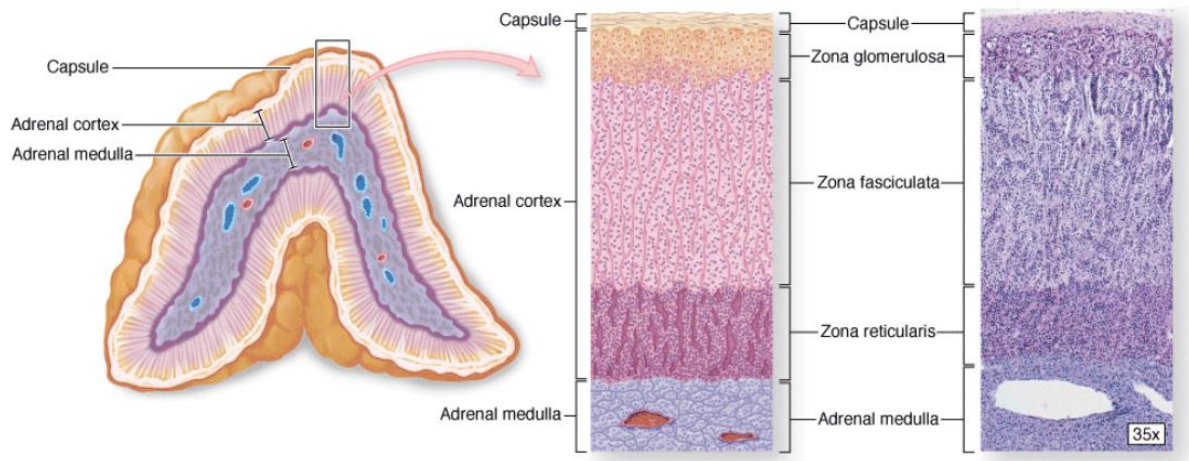


Figure 6. Cross-sectional schematic of the adrenal gland, with the capsule encapsulating the cortex and the medulla. The adrenal cortex is divided into three distinct layers, namely the zona glomerulosa, zona fasciculata and zona reticularis. Each of these layers produce the mineralocorticoids, glucocorticoids and adrenal androgen precursors, respectively. Reproduced from (57).

As shown in **Figure 6**, the adrenal is enclosed by a robust layer of connective tissue, known as the capsule (57). Beneath the capsule is the adrenal cortex, which consists of three morphologically distinct layers, namely: the outermost region - the zone glomerulosa; the middle region - the zona fasciculata; and the innermost region - the zona reticularis. The adrenal medulla is found in the centre of the adrenal and is encircled by the zona reticularis (57, 58). Each zone of the adrenal cortex produces a specific class of adrenal steroid hormone by following a range of enzymatic reactions unique to its production. The medulla produces the catecholamines, adrenaline and noradrenaline, which are responsible for the body's fight-and-flight response (54, 55, 58). The zona glomerulosa (outermost region) is responsible for the secretion of the mineralocorticoid aldosterone (ALDO), which controls the water and electrolyte balance in the body (54, 59). The zona fasciculata (middle region), which is continuous with the zona glomerulosa, is responsible for the biosynthesis and secretion of the glucocorticoids cortisol and CORT. The hormones released from this zona have numerous functions which aid in fat and protein metabolism, stress tolerance, and the suppression of inflammatory and immune responses. The innermost region of the adrenal cortex is known as the zona reticularis and is responsible for the biosynthesis of the adrenal androgen precursors, dehydroepiandrosterone (DHEA), dehydroepiandrosterone-sulfate (DHEAS) and androstenedione (A4) (54, 55, 59).

2.3 Cholesterol, the precursor of adrenal steroid hormones

All adrenal steroid hormones are fat soluble, organic compounds with a characteristic cyclopentanoperhydrophenanthrene ring structure derived from a common precursor, cholesterol (**Figure 7**) (7, 18, 53, 54).

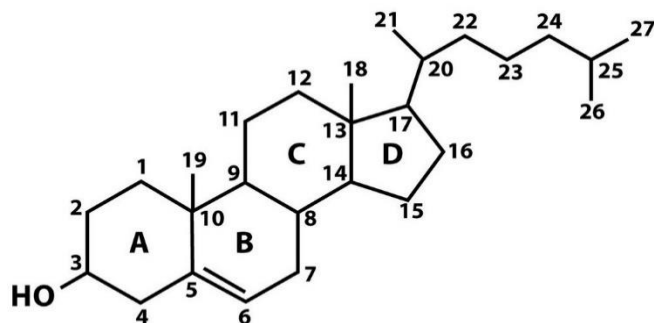


Figure 7. Chemical structure of cholesterol, representing the backbone of all the steroid hormones. Redrawn from (60).

Although adrenal steroid metabolism is regulated by tissue specific trophic hormones; a constant supply of cholesterol is essential for the optimum production of adrenal steroids (53, 54, 60). There are three ways in which cholesterol can be utilized in steroidogenic cells: Cholesterol can be biosynthesized *de novo* from acetate in the endoplasmic reticulum (ER) through a series of complex enzymatic reactions **Figure 8 (1)**. The cholesterol ester stored in the lipid droplet can be released as free cholesterol by a hydrolysis reaction **Figure 8 (2)** or cholesterol can be derived from two circulating lipoproteins in plasma namely, the low density lipoprotein (LDL) and the high density lipoproteins (HDL) **Figure 8 (3)** (53, 60). Although the first two mechanisms can potentially provide enough cholesterol to support adrenal steroidogenesis, evidence suggests that steroidogenic tissue and cells primarily utilize cholesterol from circulating lipoproteins for steroid hormone production (60). The utilization of LDL or HDL as the primary source of cholesterol is, however, species-dependent. Humans, cattle and pigs primarily use plasma LDL to obtain an adequate amount of cholesterol for steroid production, whereas rodents meet their cholesterol requirements for steroidogenesis by utilizing plasma HDL (53, 60).

The HDL cholesterol esters can enter the steroidogenic cell via the scavenger receptor class B type I (SR-B1) receptor-mediated pathway, which allows the direct transfer of HDL cholesterol esters into the cytoplasm. Once HDL cholesterol ester enters the cell, it is stored in a lipid droplet. However, when the demand for free cholesterol is high, the hormone-sensitive lipase (HSL) enzyme will convert the HDL cholesterol ester into free cholesterol (53, 54).

The uptake of LDL cholesterol ester from plasma into the cytoplasm of steroidogenic cells is mediated by the LDL-receptor through a process of receptor-mediated endocytosis (53, 54). The endosome, containing the LDL cholesterol ester, fuses with lysosomes (membrane-bound organelles that contains degradative enzymes) which hydrolyses the LDL cholesterol ester to release free cholesterol (53, 60). The steroidogenic acute regulatory protein (StAR) mediates the transfer of free cholesterol from the outer mitochondrial membrane (OMM) to the inner mitochondrial membrane (IMM). Only free cholesterol is transported into the adrenal IMM and initiate the biosynthesis of the steroid hormones production (53, 54). The initial step in adrenal steroidogenesis is catalysed by cytochrome P450 side chain cleavage (P450_{scc}) also known as the cytochrome P450 11 α -hydroxylase (CYP11A1), which converts cholesterol to pregnenolone (PREG) (7, 53, 54). PREG then serves as the precursor steroid metabolite to the three steroidogenic pathways, which will be discussed in Section 2.4. The conversion of cholesterol into PREG is also considered as the rate-limiting step of adrenal steroid metabolism and is highly dependent on the availability of free cholesterol (7, 18, 53, 54). Excess of free cholesterol will be esterified and stored in a lipid droplet by the enzyme, acyl-coenzyme A cholesterol acyltransferase (ACAT). If, however, the body requires a high amount of free cholesterol for adrenal steroid metabolism, HSL is activated and converts cholesterol esters in the lipid droplet to free cholesterol (53, 54, 60).

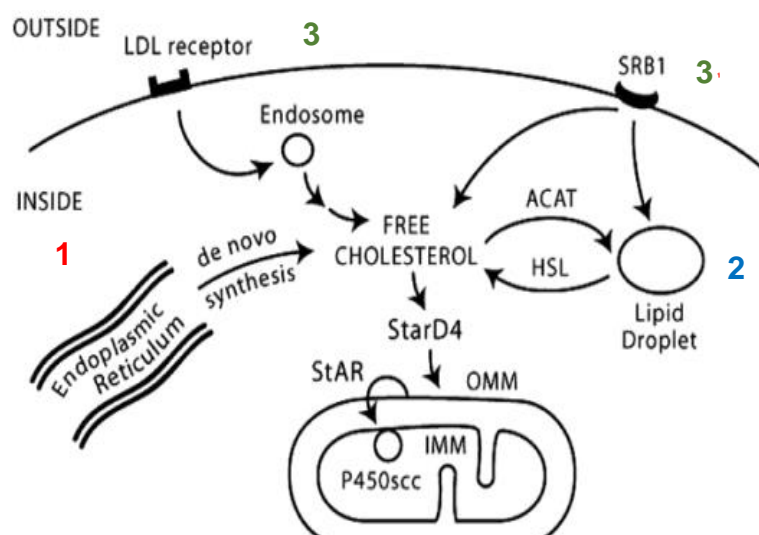


Figure 8. Representation of the utilization of free cholesterol for adrenal steroid metabolism. LDL cholesterol esters bind to the LDL receptor, where they enter the cell via endocytosis. Free cholesterol is transported from the OMM to the IMM, via the protein, StAR. HDL cholesterol esters enter the cell via the SR-B1 receptor. Once in the cell, it can be stored as a lipid droplet, or it can be converted to free cholesterol by the enzyme, HSL. Only free cholesterol can enter the IMM. Free cholesterol can also be synthesized *de novo* from acetate in the ER and it can be stored as a lipid droplet by the enzyme, ACAT. Reproduced from (53).

2.4 Adrenal steroid metabolism

In each zona of the adrenal cortex, there are two main types of enzymes that facilitate the biosynthesis of adrenal steroid hormones. These enzymes are known as cytochrome P450 enzymes and hydroxysteroid dehydrogenases (53, 54, 61–63). A schematic representation of the steroid hormone biosynthesis in the adrenal cortex is shown in **Figure 9**.

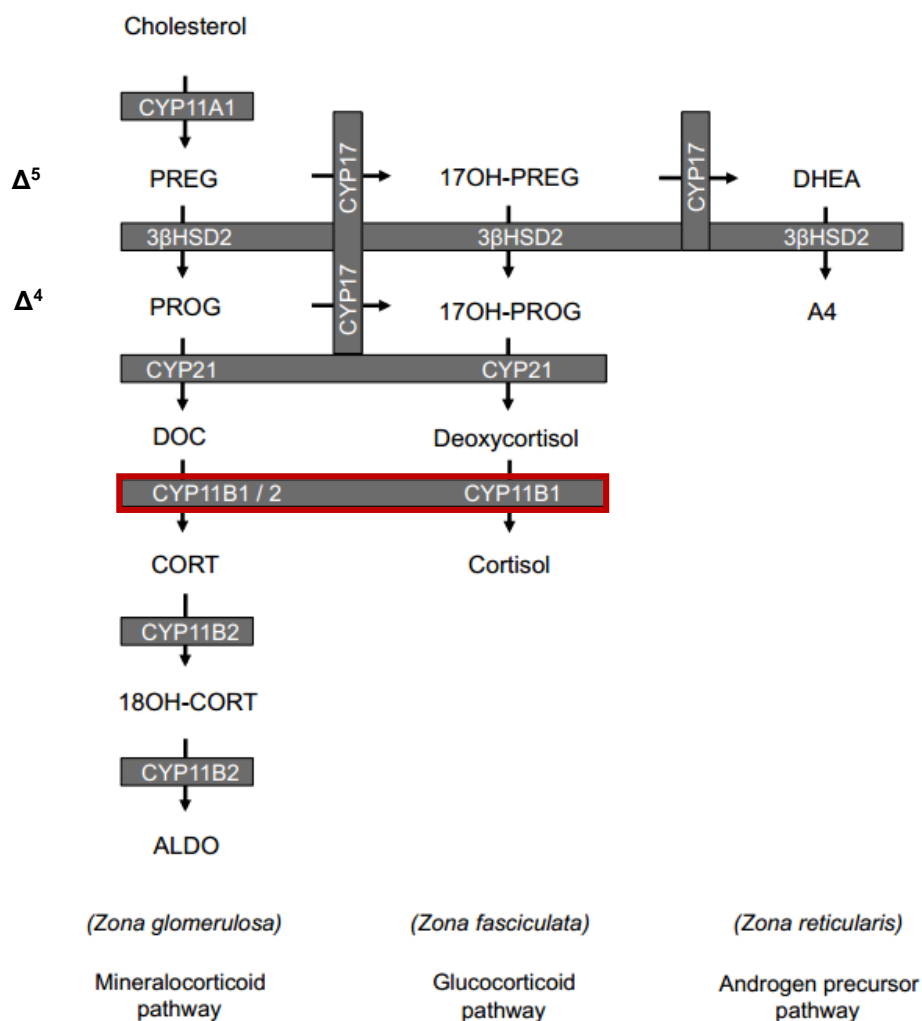


Figure 9. Adrenal steroidogenesis pathway. All steroid hormones are derived from cholesterol by a network of enzyme-catalysed reactions. Reproduced and adapted from (54).

Once cholesterol enters the IMM via the StAR protein, CYP11A1 converts cholesterol into PREG in three successive mono-oxygenase reaction; firstly, cholesterol is hydroxylated at C22, followed by a hydroxylation at C20 and finally, cleavage of the C20-22 bond by CYP11A1 to produce the adrenal steroid precursor, PREG (53, 60). The conversion of cholesterol into PREG is classified as the rate-determining step of adrenal steroid metabolism as it regulates the rate at which the overall reactions in the adrenal cortex proceed (7, 54).

PREG travels from the mitochondria to the smooth ER, where the pathway by which PREG is metabolised is modulated by trophic (peptide) hormones (53). The release of the trophic hormones, follicle stimulating hormone (FSH) and luteinizing hormone (LH), play a significant role in androgen production. Furthermore, angiotensin II and potassium ions, control the biosynthesis of ALDO in the zona glomerulosa, whereas the adrenocorticotrophic hormone (ACTH) regulates glucocorticoid biosynthesis (CORT and cortisol) in the zona fasciculata (53, 60).

The pathways by which PREG is converted to the respective adrenal steroid hormones in the different adrenal zone are the following:

Zona reticularis

In the zona reticularis of the adrenal cortex, PREG is converted to 17 α -hydroxy-pregnenolone (17OH-PREG) by cytochrome P450 17 α -hydroxylase (CYP17A1), which hydroxylates PREG at C17. 17OH-PREG is further metabolized by the 17,20 lyase activity of CYP17A1 to yield the adrenal androgen precursor, DHEA. 3 β -hydroxysteroid dehydrogenase or 3 β -hydroxysteroid dehydrogenase $\Delta^{4,5}$ -isomerase (3 β HSD2) converts the Δ^5 -steroid substrate, DHEA at C3, to the Δ^4 -steroid product, A4 (7, 18, 53, 54).

Zona glomerulosa

In the zona glomerulosa 3 β HSD2 converts PREG into progesterone (PROG) via an oxidation and isomerization reaction. Cytochrome P450 21-hydroxylase (CYP21A2) converts PROG into 11-deoxycorticosterone (DOC) via a hydroxylation reaction at C21. DOC moves back into the mitochondria where cytochrome P450 aldosterone synthase (CYP11B2) catalyses firstly the hydroxylation at C11 and the subsequent hydroxylation and oxidation reaction at C18 resulting in the final conversion of DOC into ALDO (7, 18, 53, 54).

Zona fasciculata

The glucocorticoids are produced in the zona fasciculata from two different Δ^4 -steroid substrates, PROG and 17 α -hydroxy-progesterone (17OH-PROG). PREG and 17OH-PREG are converted by 3 β HSD2 to PROG and 17OH-PROG. PROG is converted to DOC by CYP21A2 as previously mentioned, while 17OH-PROG is converted to 11-deoxycortisol by the same enzyme. PROG can also be converted to 17OH-PROG by CYP17A1. Both DOC and 11-deoxycortisol move to the mitochondria, where CYP11B1 catalyses the hydroxylation at C11 of both DOC and 11-deoxycortisol thus yielding CORT and cortisol, respectively (7, 18, 53, 54).

2.5 The regulation of glucocorticoid biosynthesis via ACTH

ACTH plays a significant role in the biosynthesis of glucocorticoids in the zona fasciculata of the adrenal glands. Stress, circadian factors, low glucose levels and inflammation are all examples of factors that can activate the trophic hormone (7, 54, 64). The mechanism of the ACTH-action is under the control of the hypothalamus, the anterior pituitary and the adrenal cortex, better known as the HPA-axis **Figure 10** (7, 54).

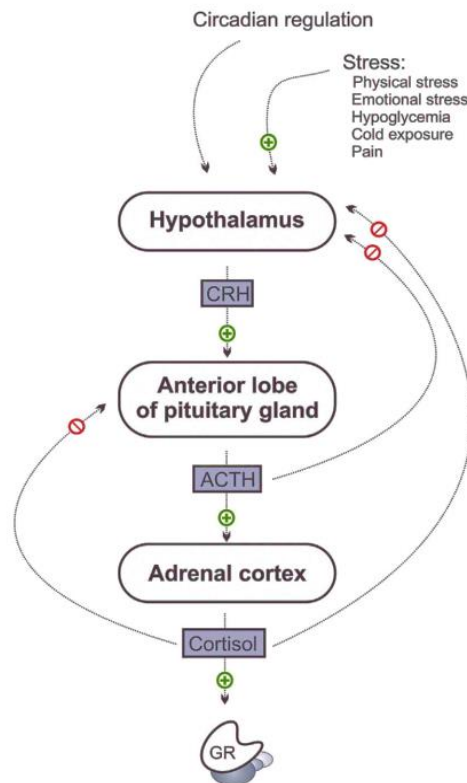


Figure 10. Schematic representation of the HPA-axis. Reproduced from (64).

Glucocorticoid levels regulate the secretion of ACTH through a negative feedback system (7, 18, 64). High glucocorticoid levels in plasma will inhibit the HPA-axis, whereas low glucocorticoid levels will activate the system (54). The activation of the HPA-axis, initiates the secretion of corticotropin-releasing hormone (CRH) and arginine vasopressin (AVP) from the hypothalamus, which in turn stimulates the release of ACTH from the anterior pituitary gland (7, 54, 59).

The release of ACTH affects the cells of the zona fasciculata in two ways: ACTH increases the permeability for certain ions to enter the membrane of the zona fasciculata and ACTH stimulates the production of cyclic adenosine monophosphate (cAMP) through the activation of adenylate cyclase. The production of cAMP results in the activation of a protein kinase A

signalling cascade which exerts both chronic and acute steroidogenic effects on the control of glucocorticoid production (7, 53, 60).

The acute steroidogenic response occurs within minutes and is characterized by the activation of the HSL and the rate-limiting enzyme, CYP11A1. The esterase activity of HSL increases the supply of free cholesterol in the steroidogenic cell, while CYP11A1 utilizes the free cholesterol for glucocorticoid production (7, 18, 65). Evidence has further revealed that the chronic activation of the ACTH steroidogenic responses alter the cytochrome P450 enzymes expressed in the adrenal cortex at a mRNA level, resulting not only in an altered production of adrenal steroid hormone, but also an altered steroid flux in the adrenal gland (18, 54, 65).

Perturbations of the HPA-axis, glucocorticoid receptor levels, or the expression and/ or activity of the enzymes involved in glucocorticoid production, can result in abnormal glucocorticoid levels, which can cause severe clinical conditions (54). In the case of “Grootlamsiekte” and the contraceptive action of the natural compounds of *Salsola tuberculata* in rats, inhibited the conversion of DOC and deoxycortisol to CORT and cortisol, respectively (7, 18, 27). In the next section, the importance of cytochrome P450 enzymes will be discussed.

2.6 Cytochrome P450 enzymes

The cytochrome P450-dependent enzymes involved in adrenal steroid metabolism belong to a large family of hemoproteins, which catalyse various hydroxylation reactions in both prokaryotic and eukaryotic organisms (7, 18, 54).

The discovery of cytochrome P450 enzymes was first reported independently by Klingenberg and Garfinkel in 1958, who revealed an intense absorption at 450 nm when carbon monoxide (CO) was bubbled through a sodium dithionite reduced suspension of rat liver microsomes (66, 67). The unique spectral properties of cytochrome P450 enzymes were, however, identified by Omura and Sato (68) who concluded that the newly discovered heme pigment was a b-type cytochrome(s). Evidence obtained during their research showed a maximum absorbance at 450 nm when the heme pigment was in a reduced form and complexed with CO. Because the pigment absorbed maximally at 450 nm, the name cytochrome P450 was given to the new b-cytochromes. Omura and Sato further revealed that treating cytochrome P450 containing microsomes with detergent gave rise to an inactive solubilized form, known as cytochrome P420 (P420). The membrane bound cytochrome P450 enzyme could therefore be distinguished from its solubilized (and active) form, since the P420 enzyme absorbed maximally at 420 nm under the same conditions (68).

Further investigations into the physiological function of cytochrome P450 enzymes revealed that the heme-pigment was the oxygen-activating component in various oxygenation

reactions. In 1964, Harding discovered cytochrome P450 enzymes in the mitochondria of the adrenal gland, where they served as the oxygen-activating component of the three mitochondrial cytochrome P450 enzymes systems, CYP11A1, CYP11B1 and CYP11B2 (69).

2.6.1 Active site of cytochrome P450

The distinct spectral and catalytic properties of all cytochrome P450 enzymes can be attributed to the unique conformation of the heme active site (**Figure 11**) (7, 18, 68).

The active site of a cytochrome P450 enzyme is comprised of an oxidized iron (Fe^{3+}) atom in the centre of a highly hydrophobic protoporphyrin IX ring (7, 18, 70, 71). The protoporphyrin IX ring structure is bound to the enzyme by hydrophobic forces and coulombic attractions, while the iron is bound to the protoporphyrin IX ring by four coordinate ion-covalent bonds (7, 18). The iron atom, however, can still bind two ligands, one in the fifth and the other in the sixth axial position. The sixth axial position is co-ordinated to the iron by an easily exchangeable ligand, such as water, and under reduced conditions, CO can occupy the sixth position. The fifth axial position, however, is different from other cytochrome enzymes, as the polypeptide chain of the enzyme contains a conserved cysteine residue in which the sulphur is a thiolate anion forming a cysteinyl ligation to the heme iron (7, 18, 70, 71).

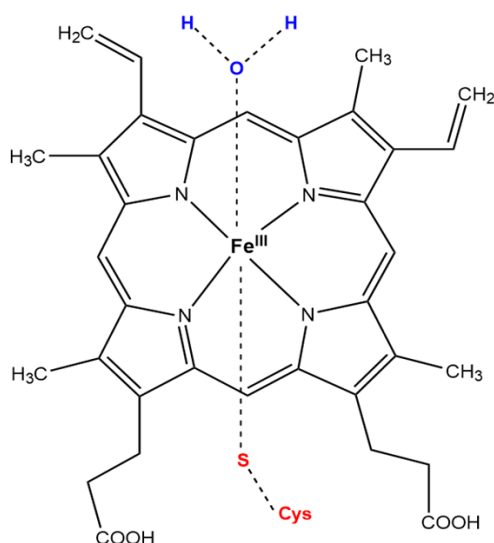


Figure 11. Schematic representation of the active site of cytochrome P450 dependent enzymes. The 5th axial position is co-ordinated to the iron by the thiol anion of a cysteine residue, whereas the 6th axial position is co-ordinated with a water molecule. Redrawn from (7).

The oxidation state of the heme iron and the thiolate axial ligand directly influences the unique spectral properties of P450-dependent enzymes. Iron exists in two oxidation states, namely, the ferrous iron (Fe^{II}) and the ferric iron (Fe^{III}). In a substrate -free environment, the ferric iron

has five valence electrons in the 3d orbital, whereas the ferrous iron has six (**Figure 12**) (7, 18, 72).

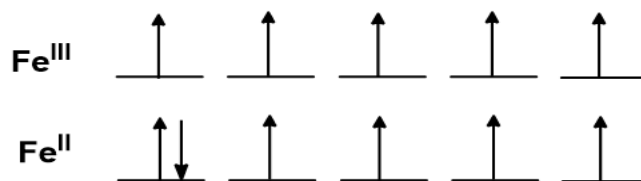


Figure 12. Distribution of electrons in the 3d orbital of the ferric- (Fe^{III}) and ferrous (Fe^{II}) iron, respectively. Image redrawn from (7).

The occupancy of valence electrons in the 3d orbital is influenced by the binding of a substrate or inhibitor to the iron. The spin state of iron is therefore influenced directly by the behaviour of the valence electrons in the 3d-orbital. When iron is bound to a substrate, the spatial arrangement of the 3d orbitals attains different levels of energy in relation to the substrate. This is known as field splitting energy (Δ). Once a substrate binds to iron, the orbitals are split (by the field splitting's energy) into two groups, two higher lying and three lower lying orbitals (**Figure 13**) (7, 18, 72).

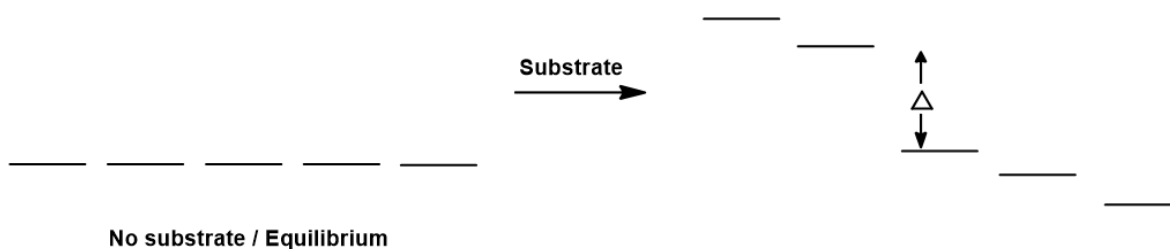


Figure 13. Energy levels of the valence electrons in the 3d orbital influence by the field splitting energy (Δ). Image redrawn from (7).

When the (Δ) is relatively small in comparison to the energy required for the electrons to pair (spin-pairing of electrons (P)), less energy is required for the five electrons of Fe^{III} and the six electrons of Fe^{II} to fill each orbital first before pairing. The iron will therefore be in a high-spin state with maximally unpaired electrons. The high-spin state Fe^{III} iron has five unpaired electrons, whereas Fe^{II} iron has four unpaired electrons (**Figure 14**) (7, 18, 72).

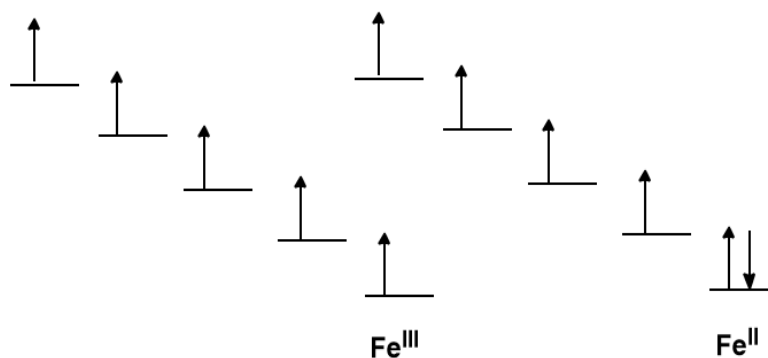


Figure 14. Distribution of valence electrons in the 3d orbital in Fe^{III} and Fe^{II} when the field splitting energy (Δ) is smaller than the spin-pairing energy (P). Image represents the high-spin state of the iron. Redrawn from (7).

Alternatively, when ($\Delta > P$), the valence electrons will occupy all the lower energy orbitals first, before moving to a higher orbital, giving rise to a low spin state iron with minimum unpaired electrons. The low-spin state Fe^{III} iron has one unpaired electron, whereas Fe^{II} has no unpaired electrons (**Figure 15**) (7, 18, 72).

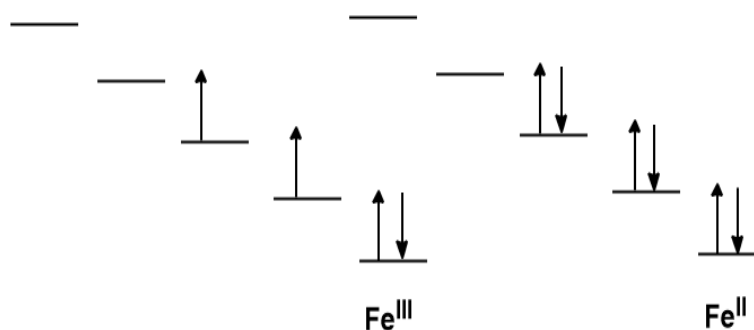


Figure 15. Distribution of valence electrons in the 3d orbital in Fe^{III} and Fe^{II} when the field splitting energy (Δ) is larger than the spin-pairing energy (P). Image represents the low-spin state of the iron. Redrawn from (7).

The valence electrons in the 3d orbital also influence the position of the heme-iron in the cavity of the protoporphyrin IX ring. The space of the protoporphyrin IX ring cavity is in a fairly rigid hexa-coordinated octahedral shape, with a diameter of 2.02 Å. As the valence electrons of the low-spin state iron do not occupy the higher lying orbitals, the low-spin form of the iron is more compact than the high-spin form, with a diameter of 1.91 Å. The space in the protoporphyrin IX ring is large enough to accommodate the low-spin state iron. Conversely, the high-spin state iron, which has a diameter of 2.6 Å cannot fit into the space of the protoporphyrin IX ring cavity. The substrate causes the displacement of the high-state iron out of the plane of the protoporphyrin IX ring cavity and changes the hexa-coordinated octahedral shape of the active site to a penta-coordinated square-pyramidal shape. The low-spin state iron is 0.3 Å out of the

plane of the protoporphyrin ring cavity, whereas the high-spin state iron is approximately 0.7 Å out of the plane (**Figure 16**) (7, 18, 72) .

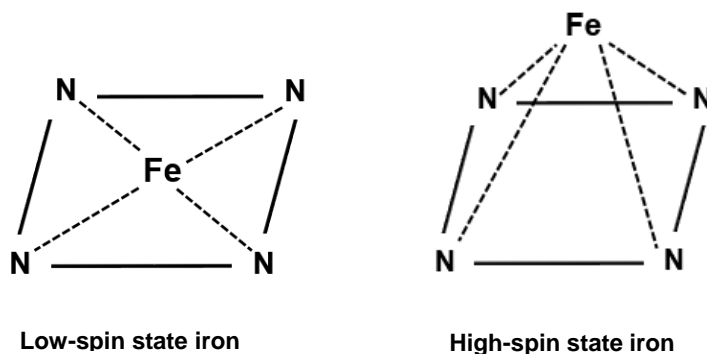
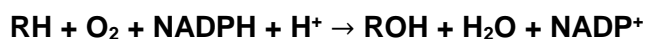


Figure 16. Representation of the position of the iron in low- and high-spin state. Upon substrate binding, the iron moves out of the plane of the protoporphyrin IX ring cavity. Redrawn from (7).

The spin state of iron is, therefore, influenced by two factors, namely: the oxidation state of the iron, and the specific substrate in the active site. The low- and high-spin state iron is characterised with specific spectral properties. Therefore, changes brought about by a specific substrate or inhibitor can be determined spectrophotometrically. The unique properties of P450-dependent enzymes give rise to difference spectra, which can be used to determine the spin state of the iron and the mechanism of action of these enzymes (7, 18, 72). The bio-assay used to determine the influence of *Salsola tuberculata* and CpDA on the terminal reaction of the glucocorticoid biosynthesis pathway, were based on these unique spectral properties of CYP11B1. Details of these assays will be described in Section 2.6.4.

2.6.2 Catalytic cycle of cytochrome P450 enzymes

Cytochrome P450 enzymes serve as the biocatalyst in mono-oxygenase reactions by incorporating a single oxygen atom into a non-polar substrate (RH), while reducing the second oxygen atom into water (7, 71, 73). Due to the unique structure of the hemo-protein (oxygen activation site), P450-dependent enzymes are the only heme-containing enzymes that can catalyse these mono-oxygenase reactions (7, 18, 73). The general redox reaction, catalysed by cytochrome P450 mono-oxygenases, is summarised in the following equation:



For the hydroxylation reaction to occur in adrenal steroid metabolism, the P450-dependent enzyme requires a source of electrons and an electron transport system. As mentioned in section 2.4, P450-dependent enzymes are found both in the ER and mitochondria of the adrenal cortex and can therefore be classified as microsomal or mitochondrial cytochrome P450 enzymes (53). Microsomal cytochrome P450 enzymes are expressed in the brain, lungs,

liver and adrenals, whereas mitochondrial cytochrome P450 enzymes are found in the liver, kidney and adrenal (7, 70).

Not only are the microsomal and mitochondrial cytochrome P450 enzymes substrate specific, but they also require a different mechanism of electron transport to support the cytochrome P450 catalysed reactions (7, 18, 53). However, for the purpose of this study only the electron transport system of the adrenal mitochondrial cytochrome P450 enzymes (CYP11A1, CYP11B1 and CYP11B2) will be discussed.

The mitochondrial cytochrome P450 enzymes utilize the reducing equivalents of NADPH via an electron transport chain which is embedded in the IMM (7, 18, 74). The mitochondrial electron transport chain is comprised of ADXR, ADX and the specific mitochondrial cytochrome P450 enzyme (75). ADXR is a NADPH-specific flavin adenine dinucleotide (FAD) containing flavoprotein, whereas ADX is a non-heme iron-sulphur protein (76). The flavoprotein contains one mole of FAD per mole of protein and has a molecular weight of approximately 52 000 Da (76, 77). During the hydroxylation cycle, the flavoprotein is capable of accepting a maximum of two electrons from NADPH, while the resulting NADP⁺ remains bound to the reduced flavoprotein. The reaction complex is represented as follows:



The non-heme protein contains two iron atoms and two moles sulphur per mole protein, and has an approximate molecular weight of 12 000 Da (7, 18, 78). Together, ADXR and ADX form a biomolecular complex and function as a short electron transport chain.

Upon substrate binding (**Figure 17**), two electrons are transferred from NADPH to the flavin protein in two separate cycles. The reduced ADXR transfers the electrons to the oxidised ADX (76, 78). The reduction of the iron-sulfur centre weakens the interaction between the biomolecular complex, thus promoting the dissociation of the reduced mobile shuttle. The reduced ADX re-associates with the substrate bound enzyme (CYP11A1, CYP11B1 or CYP11B2) and donates a single electron for the catalytic reaction. In the second phase of electron transfer, an electron from NADP⁺ is transferred to ADXR. The dissociation and association of ADX with the flavoprotein and cytochrome P450 enzyme respectively allows for the second cycle of electron transfer (7, 18, 76, 78).

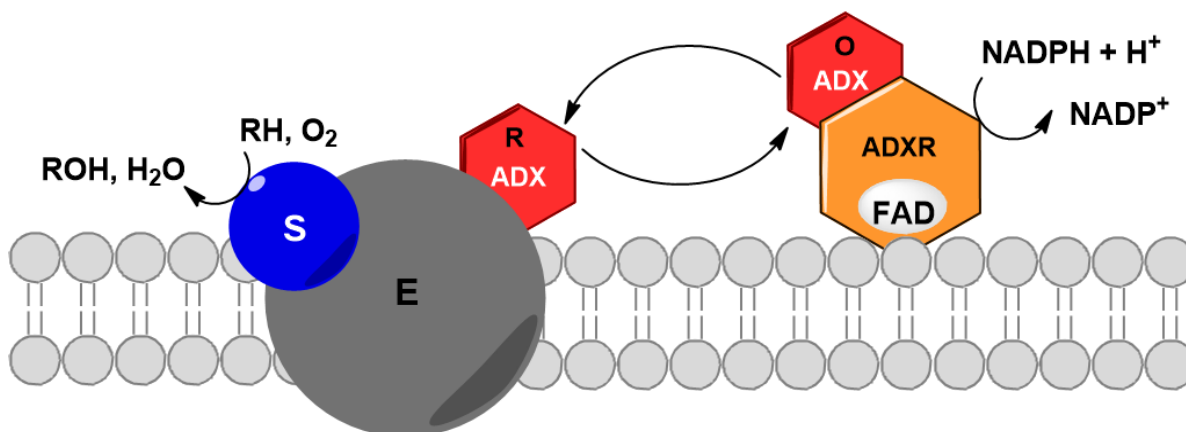


Figure 17. Schematic representation of the adrenal steroidogenic short electron transport system in the mitochondria. (E) represents the mitochondrial enzyme, CYP11B1. (S) denotes the natural substrate, DOC. ADXR is the NADPH-specific FAD containing flavoprotein, whereas ADX is the non-heme protein. Adapted from (7).

The mitochondrial electron transport system is also capable of reducing other mitochondrial proteins, such as cytochrome c (7, 79). Cytochrome c is a heme-containing protein with a molecular weight of 12 000 Da (79, 80). As cytochrome c and the mitochondrial electron transport system are located on opposite sides of the IMM, there is no physiological relevance in the reduction of this heme-containing enzyme (7, 79, 80). Cytochrome c can therefore be used as a mechanistic probe to determine the manner in which the adrenal mitochondrial hydroxylation system is influenced by CpDA, the cytochrome P450 inhibitor used in this study (80). If no inhibitory effect is observed in the reduction of cytochrome c, one would conclude that CpDA affects only the spin state of the purified CYP11B1 and not the mitochondrial electron transport chain. In Chapter 4, studies that explored the influence of CpDA, and the *R*- and *S*-enantiomer of CpDA on the mitochondrial electron transport chain by using cytochrome c as an electron acceptor are described.

2.6.3 The mechanism of P450-dependent hydroxylation reactions

The proposed representation for the mechanism of action of the catalytic cycle of P450-dependent enzymes, is shown in **Figure 18**.

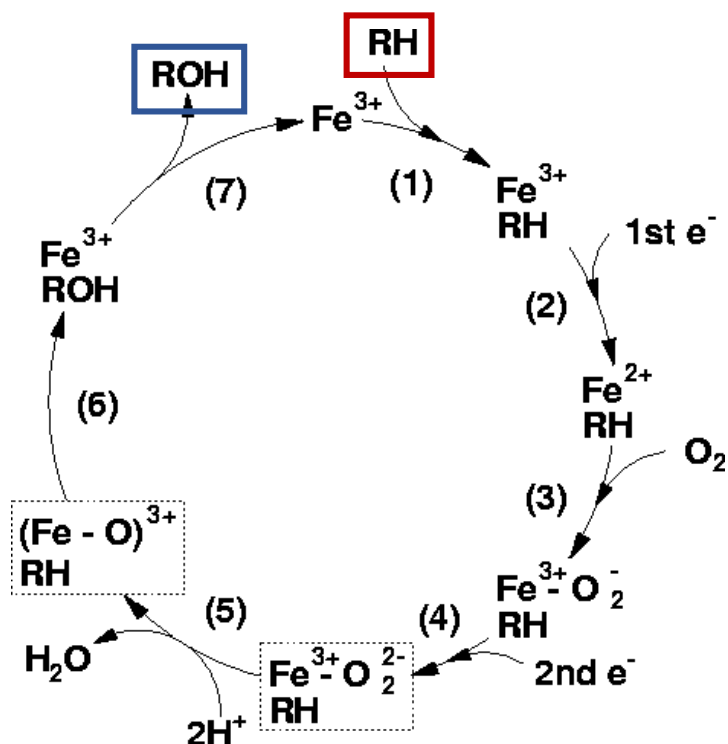


Figure 18. The catalytic cycle of P450-dependent hydroxylation reactions. The iron atom is a representation of the enzyme, whilst the RH (red block) and ROH (blue block) represent the substrate and the product, respectively. Modified image from (71).

The first step in the catalytic cycle entails the binding of a hydrophobic substrate, (RH), to the oxidised form of the cytochrome P450 enzyme **Figure 18 (1)**. This initiates the transfer of a single electron from NADPH via the short electron transport system to the enzyme-substrate complex, which leads to the reduction of the ferric iron (low-spin state) to the ferrous (high-spin state) iron **Figure 18 (2)**. At this point (**Figure 18 (3)**), a single oxygen molecule binds to the reduced enzyme-substrate complex, forming a superoxide complex with the ferrous iron ($\text{Fe}^{2+} - \text{O}_2$), which slowly converts to a more stable ferric enzyme-substrate complex ($\text{Fe}^{3+} - \text{O}_2^-$). The second electron from NADP^+ is required at this point to balance the stoichiometry of this redox equation, by converting the $\text{Fe}^{3+} - \text{O}_2^-$ complex to produce the rate-limiting complex, $\text{Fe}^{3+} - \text{O}_2^{2-}$ (**Figure 18 (4)**).

The oxygen at this stage will react with two protons from the surrounding environment, causing the oxygen-oxygen bond to break. The one oxygen atom is released as water (**Figure 18 (5)**), and the other oxygen atom ("activated oxygen") is inserted into a carbon-hydrogen bond of the substrate, yielding a hydroxylated product (ROH) (**Figure 18 (6)**). The completion of the catalytic cycle, entails the dissociation of the hydroxylated product and the regeneration of the cytochrome P450 dependent enzyme (**Figure 18 (7)**) (7, 18, 71).

2.6.4 Spectral properties of cytochrome P450 enzymes

In general, the heme-containing proteins, with the exception of cytochrome P450 enzymes, show substantial consistencies in their absorbance spectra (7, 18). The “usual” heme-containing proteins can be divided into two main groups, namely: the hemo-proteins (cytochromes) that function as electron carriers during processes such as oxidative reactions; and the heme-containing proteins (haemoglobin and peroxidase) that function as oxygen carriers and oxidizing agents, respectively. The oxidized form of the first group will exhibit a ferric low-spin type absorbance spectrum when oxidized and a ferrous low-spin type when it is reduced. Alternatively, the oxygen carriers and oxidizing hemo-proteins elicit a ferric high-spin and ferrous high-spin type spectrum when they are in their oxidized and reduced forms, respectively (7, 18, 70).

In contrast, the cytochrome P450 enzymes possess unique spectral properties which can be summarized as follows (7, 18, 70):

- As mentioned in Section 2.6, cytochrome P450 enzymes exhibit a maximum peak at 450 nm after the reduction with dithionite and treatment with CO, whereas a maximum peak at 420 nm is observed in the “usual” hemo-proteins.
- Unlike other hemo-proteins, which only exhibit spin state change upon cyanide, azide and fluoride binding, various substrates such as drugs, toxins and steroids, can induce spin state changes in cytochrome P450 enzymes.
- Variations in pH and ionic strength can also cause changes in the spin state of cytochrome P450 enzymes.
- Both the ferric high-spin and low-spin forms of the cytochrome P450 enzymes are converted to a ferrous high-spin form, upon reduction with dithionite or NADPH.
- The binding of ethyl isocyanide to the reduced form of cytochrome P450 enzyme will change the peak at 450 nm into two peaks, with an absorbance at 430 nm and 453 nm, respectively.

The unique spectral characteristics of cytochrome P450 enzymes suggest that the environment surrounding the active site is highly dynamic and therefore allows for spin state changes to occur upon substrate binding. The spectral changes can be attributed to the interaction of the prosthetic group with specific amino acids (histidine, methionine and cysteine) of the apoprotein in the dynamic hydrophobic environment of the active site. The thiolate anion, provided by a cysteine residue is responsible for the unique spectral characteristics of cytochrome P450 enzymes (70).

Difference spectroscopy is used to investigate the unique spectral characteristics of P450-dependent enzymes. There are two main types of difference spectra employed to study

cytochrome P450 enzymes – the cytochrome P450 activity assay, also known as the CO-induced difference spectra, and the substrate-induced difference spectra.

2.6.4.1 Cytochrome P450 activity assay - CO-induced difference spectra

A CO-induced difference spectrum of adrenocortical mitochondria provides information on the concentration and activity of the cytochrome P450 enzymes (68, 70). The concentration of cytochrome P450 is determined by bubbling CO through the adrenocortical mitochondria preparation, prior to the reduction by either sodium dithionite or NADH (70). When the enzyme is active, a peak with a maximum at 450 nm is observed, with a deep trough at 405 nm and a shallow trough at approximately 480-520 nm (**Figure 19**). Alternatively, when the cytochrome P450 enzyme is converted to its inactive form, a peak with a maximum peak at 420 nm will be observed.

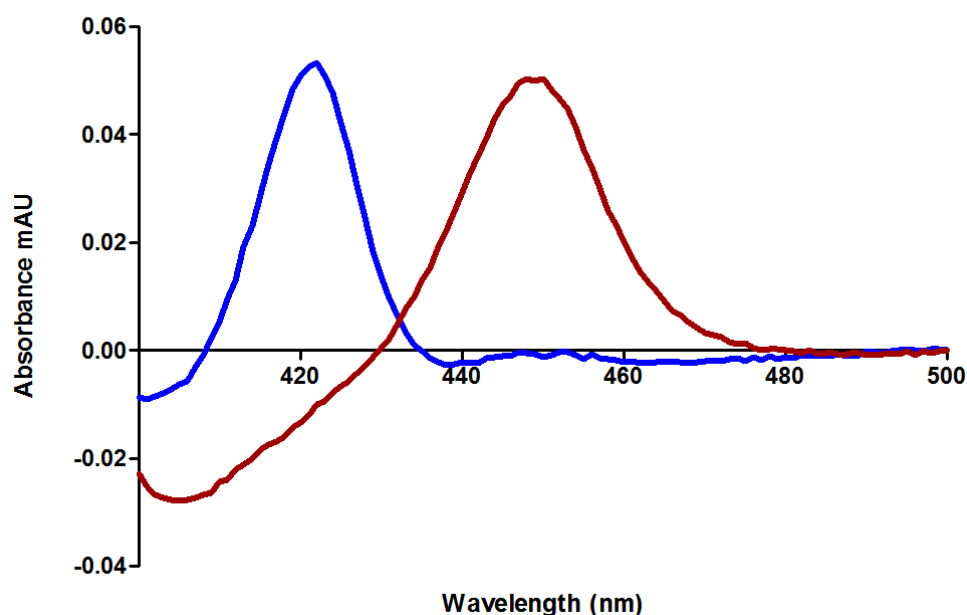


Figure 19. CO-induced dithionite reduced difference spectrum of mitochondrial cytochrome P450 from ovine adrenal. Maximum peak at 450 nm denotes an active cytochrome P450 enzyme (red), whereas a maximum peak at 420 nm represents the inactive form (blue), known as cytochrome P420. Redrawn from experimental work.

2.6.4.2 Substrate-induced difference spectra

The spectral properties of cytochrome P450 enzymes can provide valuable information about the mechanism of action of a particular test compound (7, 15, 18, 70). The unique spectral properties of CYP11B1 facilitated the development of two spectral assays, which served as a reliable, sensitive and rapid approach to screen for biological activity for the active compounds in *Salsola tuberculata* (7, 15).

The first two assays were based on the spectral properties of CYP11B1 and are denoted as Spectral Assay A (DOC-induced difference spectrum) and Spectral Assay B (Inhibitor-induced difference spectrum). These bio-assays were based on the ability of a test compound to bind to the active site of CYP11B1 and induce a difference spectrum. In order to induce a difference spectrum, active cytochrome P450 enzyme is required (maximum peak at 450 nm). If, however, the enzyme is in its inactive form (maximum absorbance at 420 nm), no substrate-induced difference spectrum will be observed. The type of substrate-induced difference spectrum is therefore dependent on the structure of substrate used, the source of cytochrome P450 and the spin state of the enzyme (7, 17, 18, 27, 70). The characteristic absorbance maximum, minimum and change in spin state of a substrate-induced difference spectrum are summarized in **Table 1**.

Table 1. Characteristics of the substrate- and inhibitor-induced difference spectrum of cytochrome P450 enzymes. Redrawn from (7).

	Maximum absorbance	Minimum absorbance	Spin state change
Type I	385-390 nm	420 nm	Low to high
Type II	430 nm	390 nm	High to low
Type II (Modified)	409-445 nm	365-410 nm	High to low

2.6.4.2.1 Spectral assay A: DOC-induced difference spectrum

Spectral assay A is used to determine the effect of an inhibitor on the binding of a substrate (DOC) to CYP11B1. When a substrate such as DOC binds to CYP11B1 it forms an enzyme-substrate complex, and changes the ferric iron (low spin state) to a ferrous iron (high spin state). It is important to note that the intensity of the substrate-induced difference spectrum is directly proportional to the concentration of substrate. The high spin state of the iron will elicit a Type I spectrum, which is characterized by an absorbance maximum at 385-390 nm and an absorbance minimum at 420 nm (**Figure 20**) (7, 17, 18).

An inhibitor will decrease the amplitude at the absorbance maxima value and increase the amplitude at the absorbance minima value (17).

2.6.4.2.2 Spectral assay B: Inhibitor-induced difference spectrum

In general, a natural substrate will bind to its cytochrome P450 enzyme and elicit a Type I spectrum. However, some compounds such as inhibitors, can also elicit a difference spectrum in P450. The inhibitor binds to the enzyme and forms an enzyme-inhibitor complex, which

stabilizes the low-spin state of the iron and induces a typical Type II difference spectrum. The Type II difference spectrum is characterized by an absorbance maximum and minimum of 430 nm and 390 nm, respectively (**Figure 21**) (7, 17, 18).

Investigations into the biological properties of the active compounds from *Salsola tuberculata* and CpDA revealed that both test compounds inhibit the DOC-induced difference spectrum and also induced a Type II difference spectrum, meaning that it stabilized the low-spin state of the enzyme (27, 28). The spectral properties of these assays was used to investigate and compare the effect of CpDA and the *R*- and *S*-enantiomers on both spin states of CYP11B1.

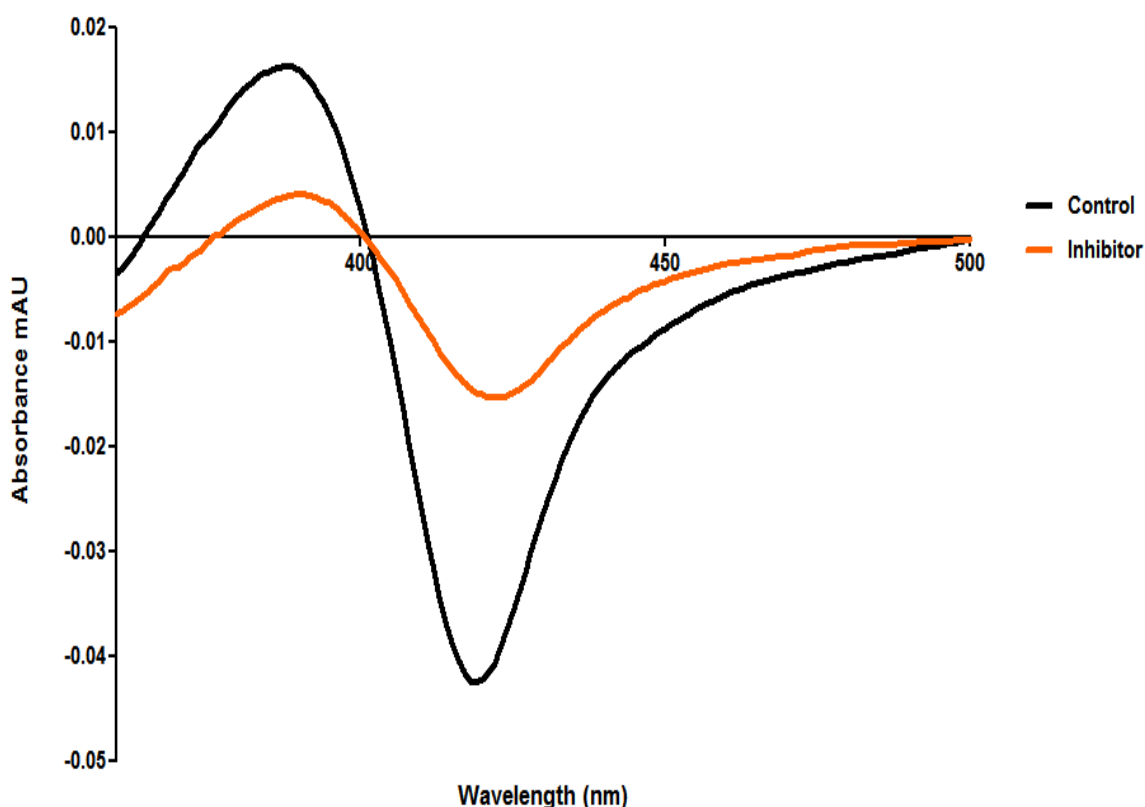


Figure 20. Representation of Spectral Assay A. CpDA inhibits the binding of DOC to CYP11B1.

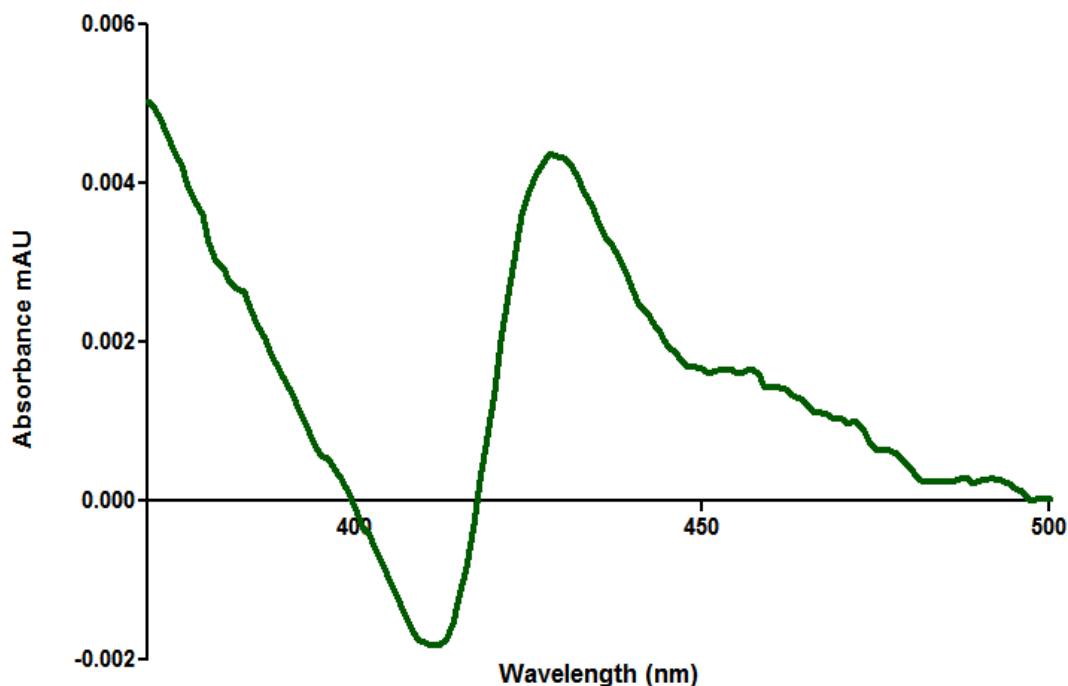


Figure 21. Representation of Spectral Assay B. CpDA induced a Type II-induced difference spectrum with an absorbance maximum at 430 nm and absorbance minimum at 412 nm.

Although difference spectroscopy serves as a reliable and rapid technique to investigate the substrate and inhibitor interaction with CYP11B1, there are a number of restrictions and precautions to be considered before recording and interpreting spectra (7, 17, 70). These restrictions and precautions are summarized as follows:

- a. Only optically matched cuvettes can be used during the recording of a difference spectrum. Any discrepancy in the cuvettes could result in an inaccurate recording of the baseline, therefore affecting the recording of the difference spectrum itself.
- b. As the recording of the difference spectra is influenced by pH, ionic strength, detergents, the volume and concentration of the solvent added should be considered. The enzyme may be influenced by the organic solvent should the substrate or compound not be soluble in an aqueous solution. In addition, the contents in the sample and reference cuvettes should always be equal before baseline recording. After baseline recording, substrate should be added to the sample cuvette and an equal volume of organic solvent should be added to the reference cuvette. The intensity of the substrate-induced difference spectrum may also be affected by the volume of solvent. Therefore, a small volume of the solvent and substrate should be added to minimize interference.

- c. In a partially pure mitochondrial preparation, contaminating proteins such as cytochrome c oxidase, haemoglobin, and P420, may interact with the added substrate and interfere with the difference spectra recorded.
- d. As the mitochondrial cytochrome P450 enzymes are membrane bound and in suspension, sedimentation of protein may occur during recording. Sedimentation of the mitochondrial preparation may be prevented by sonicating the preparation or decreasing the mitochondrial cytochrome P450 concentration prior to recording difference spectra.
- e. Only specialized instruments can be used to record the difference spectra of turbid samples. The instrument should ensure maximum sensitivity throughout the absorbance and wavelength ranges for each preparation.

The unique spectral properties of CYP11B1 served as the basis of bio-assays used in this study. In Chapter 3, experiments are described that utilised a partially purified mixture of CYP11B1 from ovine adrenals to screen for biological activities of CYP11B1 inhibitors (CpDA and the enantiomers of CpDA). Chapter 4 describes experiments used to distinguish between the biological activities of the *R*- and *S*-enantiomers of CpDA using a highly purified substrate-free CYP11B1 preparation.

CHAPTER 3

Synthesis of a racemic mixture of CpDA and the chiral resolution of the *R*- and *S*-enantiomers of CpDA

3.1 Introduction

CpDA (2-(4-acetoxyphenyl)-2-chloro-*N*-methyl-ethylammonium chloride) is a synthetic analogue of the highly unstable and reactive aziridine precursor found in the African shrub, *Salsola tuberculata* (4, 26, 27). Like its natural counterpart, CpDA interferes with the binding of the substrates, DOC and/or deoxycortisol, to CYP11B1, the terminal cytochrome P450 enzyme in the glucocorticoid biosynthesis pathway. By using the spectral properties of CYP11B1, studies have shown that CpDA inhibits the DOC-induced difference spectra and induces a Type II difference spectrum on its own (27). Initial chemical investigations indicated that the activity of the synthetic compound could be attributed to the formation of an aziridine when the nitrogen of the ethylammonium moiety carries out a nucleophilic attack on C2 to yield the 2-(4-acetoxyphenyl)-1-methylaziridine, as shown in **Figure 22**. It was, however, later established that the cyclisation of the aziridine precursor of 2-(4-acetoxyphenyl)-1-methylaziridine resulted in the inactivation of CpDA (**Figure 22**) (21, 24). As aziridines are reactive and chemically unstable compounds (24, 25), pH, light and oxygen influence the cyclization of CpDA.

The biologically active and inactive forms of CpDA can be distinguished from one another by electrospray mass spectrometry (ES-MS), as the open-ring structure has a molecular ion at 228/230, whereas CpDA in which the aziridine ring structure is intact has a molecular ion at 192. Biological studies have, however, revealed that the steroid-binding globulins in plasma can stabilize the ring-opened form of CpDA ($M+H]^+ = 228$), thereby enhancing its biological activity *in vivo* (4, 24, 28, 81).

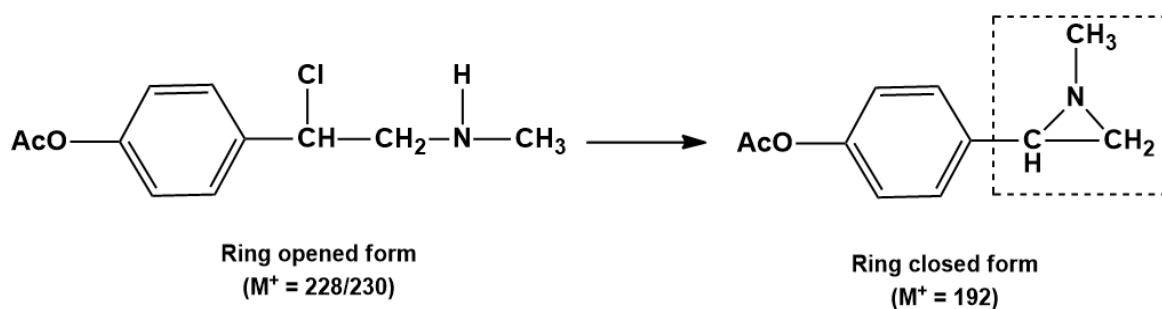


Figure 22. Biologically active CpDA (2-(4-acetoxyphenyl)-2-chloro-*N*-methyl-ethylammonium chloride) in which the ring-opened aziridine precursor cyclises into biological inactive form of CpDA (2-(4-acetoxyphenyl)-1-methylaziridine), with a ring closed structure. Redrawn from (28).

At present, CpDA has been identified as a selective glucocorticoid receptor modulator with both anti-inflammatory and anti-cancer properties in numerous *in vitro* and *in vivo* studies. Nonetheless, the racemic mixture of CpDA has a restricted therapeutic range of $\pm 1-15$ mg/mL (30). Therefore, in an attempt to possibly enhance its therapeutic range, the *R*- and *S*-enantiomers of CpDA were separated.

Chirality or chiral originates from the Greek word *cheir*, which translates to “handedness” and is used to describe the non-superimposability of an object with its mirror image (49, 82, 83). In chemistry, chirality is used to describe two structurally, physically and chemically identical molecules and/or compounds that cannot be super-imposed on one another (48, 49, 84). The two identical molecules/compounds are referred to as stereoisomers and more specifically enantiomers (48, 49, 82). Enantiomers are formed when the chiral centre (asymmetric centre) is attached to four different substituents and for a molecule/compound to be chiral, it should have at least one chiral centre (49, 83, 84). In most instances the different substituents will be attached to a carbon atom, while in some cases nitrogen, phosphorus and sulphur can also act as the asymmetric centre (49). Another important feature of enantiomers is that they exhibit optical activity, meaning that each enantiomer of a chiral compound can rotate polarized light by the same magnitude, but in an opposite direction (48, 49). Alternatively, an equal mixture (also known as racemic mixture or racemate) of both enantiomers of a specific chiral compound will be optically inactive (49, 82). The direction in which the enantiomers can polarise light can either be classified as dextrorotary (*d* or +) or levorotary (*l* or -), which is classified as rotating polarized light towards the right (clockwise) or left (anti-clockwise), respectively (49, 82). There are two ways by which the optical activity of an enantiomer can be determined, namely, through the use of a polarimeter or by circular dichroism. However, for both approaches a highly purified enantiomeric sample is required (49).

Enantiomers can further be distinguished from one another by their 3-D configurations in space (48, 82, 84). An important nomenclature system, known as the *R/S*-configuration system, has been employed to distinguish between the absolute 3-D configurations of the enantiomers by assigning the letter *R* or *S* to the chiral centres (48, 49, 83). The letters *R* and *S* originate from the Latin words *rectus*, meaning 'right' or 'clockwise,' and *sinister*, meaning 'left' or 'anti-clockwise'. The Cahn-Ingold-Prelog (CIP) sequence rules are used to determine whether the chiral centre is in an *R* or *S* configuration (49, 52, 83). These rules are based on re-orientating the four different substituents attached to the chiral centre in order of priority i.e. from highest to lowest molecular weight (highest = 1 to lowest = 4) (48, 49, 82). If the priority of the substituents attached to the chiral centre ascend in a clockwise direction, the chiral centre is in the *R* configuration; alternatively, if the priority of the substituents ascends in a counter-clockwise direction, the configuration is designated as *S* (52, 83).

In an achiral environment (non-living system), enantiomers have identical physical, chemical and biological properties (83, 85). However, as chirality is found in the most fundamental building blocks of life, such as amino acids, lipids, carbohydrates, as well as enzymes and receptors, the individual enantiomers of a chiral compound can behave differently in a living system (48, 83). Therefore, the *R*- and *S*-enantiomers of a chiral drug should be classified as two distinct compounds with different biological characteristics, unless proven otherwise (83). Figure 23 illustrates a theoretical interaction between the *R*- and *S*-enantiomers of a chiral drug and the binding site of a chiral enzyme. In this scenario, the *R*-enantiomer is biologically more active than the *S*-enantiomer, as the substituents of the *R*-enantiomer (A, B and C) directly interact with the binding sites of the chiral enzyme labelled a, b and c, respectively. However, as the *S*-enantiomer is in the "wrong" 3-D configuration, the C and A substituents do not interact with the a and c binding site of the enzyme. Therefore, in a racemic mixture, the *S*-enantiomer will be inactive, or in some cases cause severe side-effects. It was therefore deemed important and interesting to separate the *R*- and *S*-enantiomers of CpDA, as the single enantiomeric form could lead to a simpler and improved pharmacological profile (48, 83).

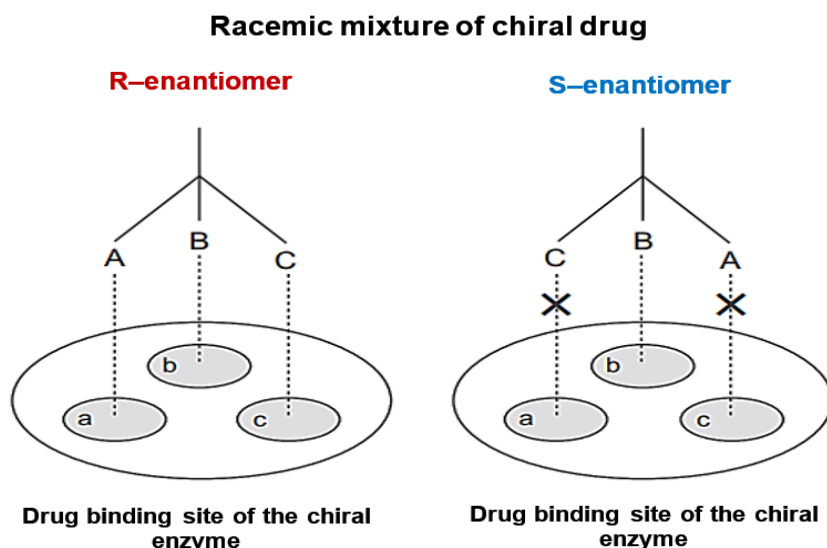


Figure 23. Theoretical interaction of the *R*- and *S*-enantiomers of a chiral drug on the drug binding sites of a chiral enzyme. The *R*-enantiomer aligns directly to the binding sites of the enzyme, whereas the C and A substitutes of the *S*-enantiomer do not. In this theoretical scenario, the *R*-enantiomer will be biologically active, whereas the *S*-enantiomer will be inactive. Adapted from (83).

Various techniques exist which can aid in the separation of the *R*- and *S*-enantiomers of a chiral compound. These techniques include, diastereomeric salt crystallization, bio-resolution, enzymatic kinetic-resolution, capillary electrophoresis, supercritical fluid extraction and chromatography. The separation of any given two enantiomers is not a simple task, as each chiral compound is different. Therefore, choosing a specific technique is dependent of the nature of the compound, the availability of resources and the time and cost of production (48, 49). Due to the limited resources and the cost of production, diastereomeric salt crystallization was chosen to separate the *R*- and *S*-enantiomers of CpDA, as this technique is more time efficient and cost effective, when compared to other methods of chiral separation.

In 1965, Ault used diastereomeric salt crystallization to separate the *R*- and *S*-enantiomers of racemic mixture of 1-phenylethylamine (Figure 24) (86). This separation was achieved by reacting 1-phenylethylamine with an optically pure form of L-(+)-tartaric acid, which produced two diastereomeric salt complexes i.e. (*R*)-amine, (*R*, *R*)-tartaric acid and (*S*)-amine, (*R*, *R*)-tartaric acid. In contrast to enantiomers, diastereoisomers have different physiochemical properties, and as such, the two salt complexes have different solubility in methanol. Figure 24 illustrates this conversion, whereby the (*R*)-amine, (*R*, *R*)-tartaric acid was more soluble in methanol and therefore stayed in solution, and the (*S*)-amine, (*R*, *R*)-tartaric acid was less soluble and precipitated as crystals. Once the diastereomeric complexes were isolated from one another, the individual complexes were treated with an excess of sodium hydroxide (NaOH), which freed the individual amine salts from tartaric acid (86). As

1-phenylethylamine is structurally similar to CpDA, a modified approach was employed to separate the *R*- and *S*-enantiomers of CpDA.

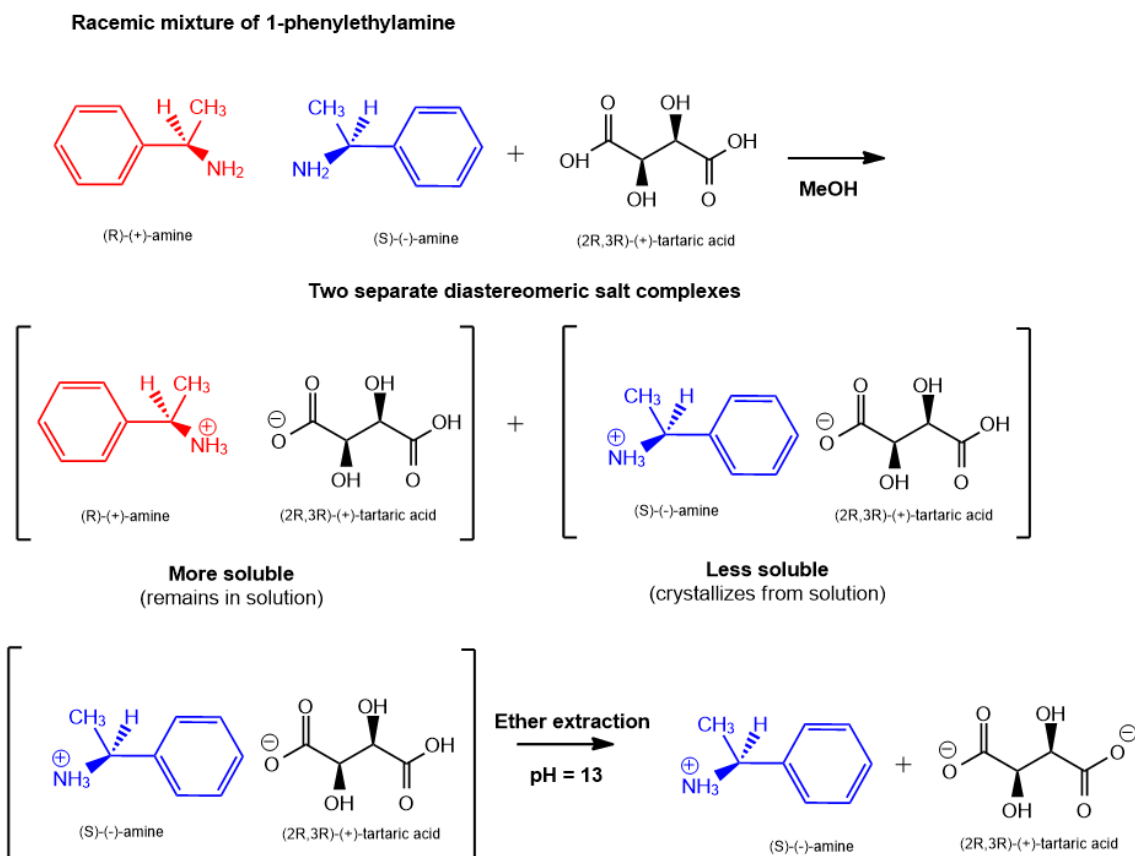


Figure 24. Chiral separation of 1-phenylethylamine.

Due to the amount of CpDA required to separate the enantiomers and the cost involved in buying commercially available CpDA, it was financially more viable to synthesise a racemic mixture of CpDA. It must, however, be emphasized that CpDA readily cyclises into its inactive form under standard laboratory conditions (28). Therefore, to preserve the biological activity of CpDA precautionary steps were employed, which involved working in a dark and inert environment. The purity of CpDA was tested by using Q-ToF/ESI-MS and NMR spectroscopy. In addition, the spectral properties of CYP11B1 were used to screen for biological activity of CpDA.

In this study CpDA was therefore synthesized after which the racemic mixture of CpDA was reacted with optically pure L-(+)-tartaric acid to produce diastereomeric salts, dissolved in methanol and separated by selective crystallization. The salts were converted to the respective enantiomers by treatment with hydrochloric acid (HCl) and the structures validated using Q-ToF/ESI-MS and $^1\text{H-NMR}$ spectroscopy. Their respective biological activities were determined using the spectral properties of CYP11B1.

3.2 Experimental

3.2.1 Materials and reagents

All solvents used (unless otherwise specified) were of laboratory grade (>95% pure) and purchased from trustworthy scientific companies. Acetone and ethanol absolute (analytic grade) were purchased from Merck Millipore (South Africa). Acetyl chloride, diethyl ether (analytic grade), hydrogen chloride, methanol (analytic grade) and glacial acetic acid (analytic grade) were obtained from Sigma- Aldrich Chemical Co. (St. Louis, MO, USA). Anti-bumping granules were purchased from BDH Chemicals Ltd Poole (England). Deionised water (dH₂O) was obtained from an in-house Milli-Q™ water purification system. Wilmad® NMR tubes (5 mm diameter) and deuterium oxide (99.9 atom %D), (±)-synephrine (≥ 98%), L-(+)-tartaric acid (≥99.5%) and DOC (≥ 97%, HPLC) were purchased from Sigma – Aldrich (St. Louis, MO, USA).

Fresh ovine adrenals were collected from Tomis Abattoir & Fresh Meats Wholesalers (Hermon, South Africa). A Beckman Coulter Avanti® J-E centrifuge was used for all centrifugation procedures. The mitochondrial cell membranes were disrupted by sonicating with a Branson B12 sonifier. Spectral assays were recorded on a Cary 100 UV-visible dual beam spectrophotometer from Agilent Technology (South Africa). Samples were concentrated on a Techne sample concentrator DB-3 or CentriVap benchtop vacuum concentrator from Labconco. The protein concentration of mitochondrial preparations was determined by using the Pierce bicinchoninic acid (BSA) protein quantification kit from Thermo Fisher Scientific (Rockford Ill, USA). Q-ToF/ESI-MS and NMR analyses were all performed at the Central Analytic Facility (CAF) at Stellenbosch University. The facility provided all materials and reagents needed for the analyses.

3.2.2 Methods

3.2.2.1 Synthesis of CpDA

CpDA was synthesized by a method previously published (24, 28). The schematic representation of the synthesis of CpDA is shown in **Figure 25**.

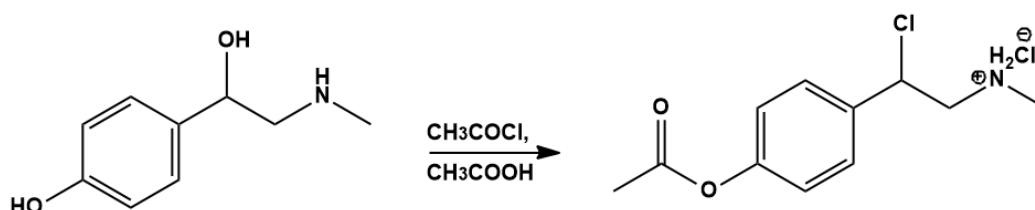


Figure 25. Schematic representation of the synthesis of CpDA.

(±)-Synephrine (10 g; 59.81 mmol) was dissolved in glacial acetic acid (27 mL, 28.35 g, 0.472 mol), whilst cooling down the entire mixture to 10°C on a water bath. Acetyl chloride (27 mL, 29.7 g, 0.378 mol) was slowly added to the mixture in a dropwise manner, while stirring continuously under an inert atmosphere. The temperature was kept below 30°C. A clear solution was formed within the first hour of this reaction and within 12 hours a white precipitate was produced. The precipitate was collected by filtration under nitrogen and washed three times with anhydrous cold ether (20 mL), followed by three consecutive washes with anhydrous cold acetone (20 mL). The white powder was kept in a vacuum desiccator (over silica gel) for 12 hours before storage at -80°C. The powder was highly hygroscopic and readily decomposed following the absorption of moisture or when it was left at room temperature. The structure and purity of CpDA were verified by ¹H-NMR, ¹³C-NMR and Q-ToF/ ESI-MS.

- **Product:** White powder; Yield: 13.229g, 57.76 mmol, 83.72%.
- **ESI-MS:** (*m/z*) [M+H]⁺ calculated for C₁₁H₁₅ClNO₂ (CpDA, open-ring structure of aziridine): 228.0791 g/mol, found 228.0764 g/mol.
- **¹H-NMR** (600 MHz, D₂O) δ 2.38 (s, 3H), 2.84 (s, 3H), 3.65 (dd, *J* = 13.5, 9.9 Hz, 1H), 3.77 (dd, *J* = 13.5, 9.9 Hz, 1H), 5.45 (dd, *J* = 9.9, 4.4 Hz, 1H), 7.26 (d, *J* = 4.8 Hz, 2H), 7.63 (d, *J* = 4.8 Hz, 2H),
- **¹³C-NMR** (600 MHz, D₂O) δ=21.07, 33.80, 49.66, 53.22, 55.14, 57.30, 72.15, 123.41, 128.36, 129.59, 134.17, 135.40, 151.48, 173.92.

3.2.2.2 Separation of the *R*- and *S*-enantiomers of CpDA

The *R*- and *S*-enantiomers of CpDA were separated by modifying the previously published diastereomeric salt crystallization method as applied to 1-phenylethylamine (86). The schematic representation of the chiral resolution of the *R*- and *S*-enantiomers are depicted in Figure 26.

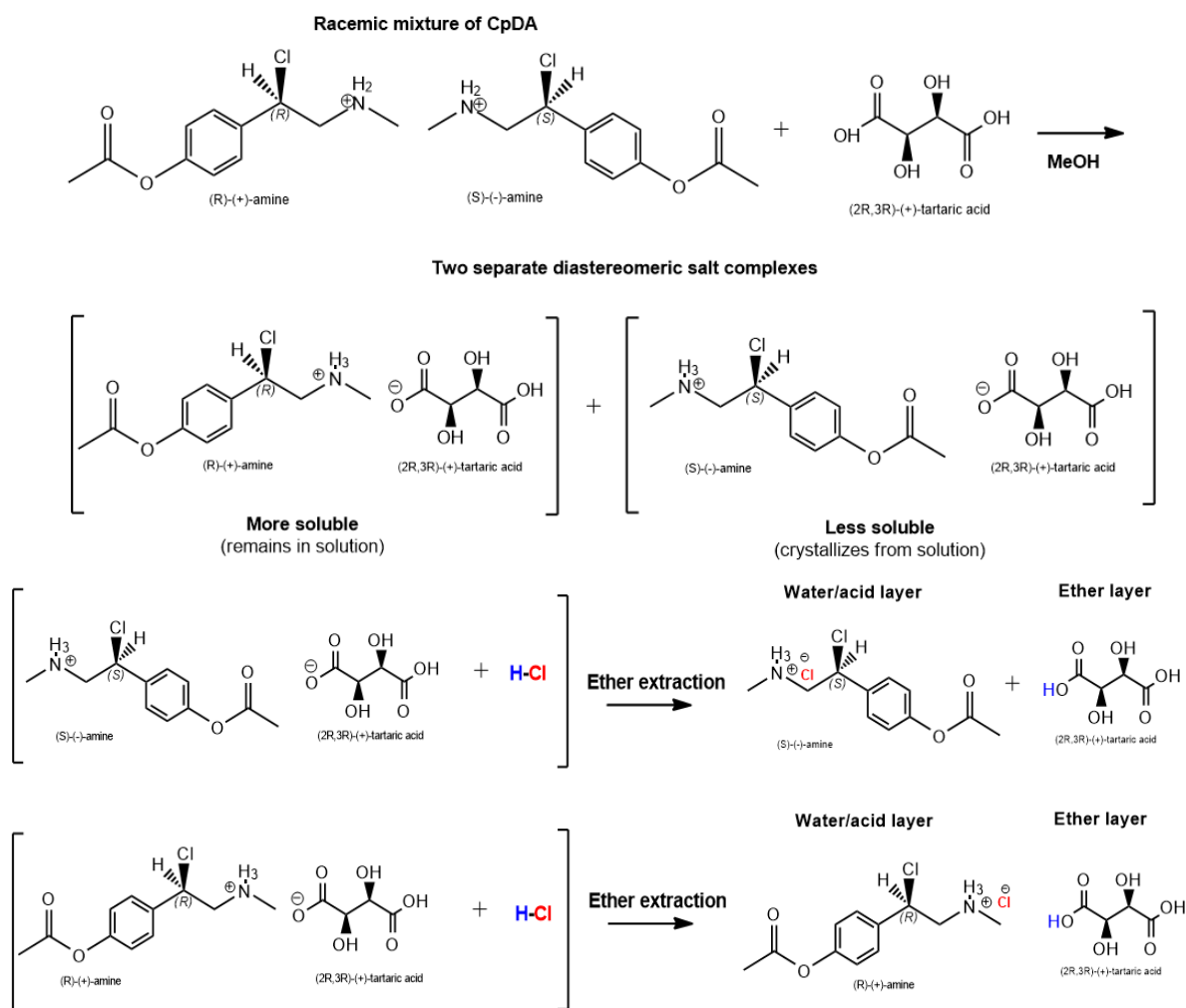


Figure 26. Schematic representation of the chiral resolution of the *R*- and *S*-enantiomers of CpDA.

Methanol (9.88 mL) was added to 0.691 g L-(+)-tartaric acid in a 50 mL round bottom flask. The mixture was heated to $\pm 40^\circ\text{C}$ (below boiling point) in a water bath and stirred with a magnetic stirrer for 10 minutes or until a homogenous solution was obtained. A racemic mixture of CpDA (1 g) was cautiously added to the hot methanol solution. The flask was stoppered and the reaction mixture stirred for approximately 60 minutes until the reaction mixture was clear. The homogenous reaction mixture was allowed to cool to room temperature. The (-)-amine-(+)-hydrogen tartrate is less soluble in methanol and thus crystallized out, whilst the (+)-amine-(+)-hydrogen tartrate remained in solution. Following,

centrifugation at 5000 x g for 10 minutes, the precipitate (crystals) were collected by vacuum filtration using a small Buchner funnel. The crystals were subsequently mixed with a 6 M aqueous hydrogen chloride (HCl) solution (10 mL). The pH change protonated the tartaric acid, making it less soluble in water. The tartaric acid was extracted with three 20 mL portions of ether. Any remaining ether was removed, by passing nitrogen over the surface of (-)-amine solution. The (-)-amine solution was further concentrated using a speed vac concentrator. The total yield of the (-)-amine was 41.5 mg (4.15%). The (+)-amine-(+)-hydrogen tartrate in solution was treated in the same way to remove the tartaric acid. The final yield of the (+)-amine product was 480 mg (48%).

- **R-enantiomer** – clear gel-like compound, highly hygroscopic; Yield 480 mg, 48%.
- **S-enantiomer** – clear gel-like compound; highly hygroscopic; Yield 41.5 mg, 4.15%
- **ESI-MS of the R- and S-enantiomers:** (m/z) $[M+H]^+$ calculated for $C_{11}H_{15}ClNO_2$ (CpDA, open-ring structure of aziridine): 228.0791 g/mol, found 228.0789 g/mol.
- **1H -NMR** – R-enantiomer (600 MHz, D_2O) δ 2.12 (s, 3H), 2.77 (s, 3H), 3.24 (dd, $J = 13.0, 3.3$ Hz, 1H), 3.32 (dd, $J = 13.0, 3.3$ Hz, 1H), 6.98 (d, $J = 8.6$, 2H), 7.32 (d, $J = 8.6$ Hz, 2H).
- **1H -NMR** – S-enantiomer (600 MHz, D_2O) δ 2.12 (s, 3H), 2.77 (s, 3H), 3.24 (dd, $J = 13.0, 3.3$ Hz, 1H), 3.31 (dd, $J = 13.0, 3.3$ Hz, 1H), 6.98 (d, $J = 8.6$, 2H), 7.32 (d, $J = 8.6$ Hz, 2H).

3.2.2.3 Mass Spectrometry analysis

The purity and accurate mass of the synthesized CpDA and the R- and S-enantiomers of CpDA were determined by using an ACQUITY Ultra Performance Liquid Chromatography (UPLC)/Q-ToF ESI-MS system equipped with an electrospray ionisation (ESI) source, which was operated in positive ion mode. CpDA and the R- and S-enantiomers of CpDA (1 mg/mL) dissolved in deionised water (Milli-QTM water purification system) and were separated on an Acquity UPLC[®] BEH C18 column (100 x 2.1mm) (Waters Corp, Milford, USA). The sample (5 μ L) was injected onto the column and eluted at a flow rate of 0.3 mL/min over a period of 10 minutes. Deionised water, containing 0.1% formic acid, was used as the Solvent A, whereas acetonitrile, containing 0.1% formic acid, was used as Solvent B. The gradient conditions for the chromatographic separation are listed in **Table 2**.

Table 2. Chromatographic elution gradient of CpDA separated on an UPLC/Q-ToF/ ESI-MS system

	Time (minutes)	Flow (mL/min)	%Solvent A Deionised water, 0.1% formic acid	% Solvent B Acetonitrile, 0.1% formic acid	Curve
1	Initial	0.300	98.0	2.0	6
2	0.50	0.300	98.0	2.0	6
3	7.00	0.300	20.0	80.0	6
4	8.00	0.300	1.0	99.0	6
5	8.10	0.300	98.0	2.0	6
6	10.00	0.300	98.0	2.0	6

The instrument setup for the separation was as follows: Capillary voltage, 2.50 kV; cone voltage, 15 V; extraction cone, 4 V; source temperature, 120 °C; desolvation temperature, 275°C; source gas flow, 50 L/h; and desolvation gas flow, 650 L/h. MassLynx 4.1 software was used to analyse the data obtained. The ESI-MS was performed by Mr M. Taylor or Dr M. Stander at the Central Analytic Facilities situated in Stellenbosch University.

3.2.2.4 Nuclear magnetic resonance – analysis

NMR spectroscopy was performed under the supervision of Dr J. Brandt from the Central Analytic Facility (CAF) at Stellenbosch University. ¹H-NMR and ¹³C-NMR analyses were performed on a Varian Unity INOVA 600 MHz spectrometer equipped with a 5-mm probe, operating at 25°C. Deuterium oxide (D₂O) was used as the solvent. ¹H-NMR and ¹³C-NMR spectra of CpDA (20 mg) were recorded by using 16 scans, whereas the ¹H-NMR spectra of the *R*-enantiomer (10 mg) and the *S*-enantiomer (4 mg) were recorded by using 32 and 128 scans, respectively. The raw NMR data were processed using MestReNova software, version 6.0.2.

3.2.2.5 Preparation of a cytochrome P450-containing mitochondrial acetone powder from ovine adrenals

Cytochrome P450-enriched adrenal mitochondrial acetone powder from ovine adrenals was prepared as previously published (87). Fresh ovine adrenals were collected from a local abattoir and immediately stored on ice. All procedures were conducted at 4°C. The capsules and connective tissue of the frozen adrenals were removed and washed with a 0.15 M KCl solution (pH 7.4). The decapsulated adrenals (100 g) were homogenised with a Waring-Blendor in 450 mL of Buffer A (10 mM Tris-HCl buffer, containing 1 mM EDTA and 0.25 M sucrose, pH 7.4). The adrenal homogenate was further homogenised with a Potter-Elvehjem glass homogeniser and the resulting homogenate centrifuged at 1000 x g for 20 minutes. The pellet, containing the extracellular debris and fat was discarded whilst the supernatant was retained. The supernatant was centrifuged at 12 000 x g for 15 minute, to yield the cytochrome P450-enriched mitochondrial pellet. The pellet was washed three times by resuspending and homogenising it once in 450 mL of Buffer B (10 mM Tris-HCl buffer, containing 1 mM EDTA, 0.15 M KCl, pH 7.4), and twice in 200 mL of Buffer C (10 mM Tris-HCl buffer, containing 1mM EDTA, 0.25 M sucrose and 1% (m/v) BSA; pH 7.4). After every wash step, a centrifugation step was carried out for 15 minute at 12 000 x g. The mitochondrial pellet was frozen with liquid nitrogen and lyophilized overnight. The dried pellet (6.8 g) was resuspended in 100 mL dry acetone and homogenised with the Potter-Elvehjem glass homogeniser. The homogenate was subsequently centrifuged for 15 minutes at 12 000 x g. The supernatant was decanted and the mitochondrial acetone pellet (6.2 g) lyophilized overnight. The lyophilized powder was stored at -20°C until further use as a source of cytochrome P450 for the investigation of enzyme-substrate and enzyme-inhibitor interactions.

3.2.2.6 Protein determination assay

The protein concentration of the crude mitochondrial powder and purified CYP11B1 were determined according to the instruction manual of the Pierce bicinchoninic acid (BCA) Protein Assay Kit. A standard protein series was prepared by making a triplicate serial dilution (ranging from 0 µg/mL to 2000 µg/mL) of a 2 mg/mL bovine albumin serum (BSA) standard that was provided in the kit. Ten µL of the BSA protein standard and the mitochondrial protein samples were pipetted in triplicate into a 96-well micro-titre plate. A BCA working reagent was prepared by mixing Reagent A and Reagent B in a 50:1 ratio. Thereafter, 200 µL of the BCA working reagent was pipetted, with a multi-channel pipette, into the respective wells containing either the BSA protein standards or the mitochondrial sample. The micro-titre plate was subsequently incubated for 30 minutes at 37°C, followed by measuring the absorbance at 560 nm on a Spark™ 10M multimode microplate reader. A standard curve was generated

from the absorbance values obtained from the protein standards and was used to determine the protein concentration of the samples.

3.2.2.7 Cytochrome P450 activity assay – (CO-induced difference spectrum)

The cytochrome P450 content of the crude cytochrome P450-containing mitochondrial acetone powder was determined spectrophotometrically as previously described (16). The mitochondrial powder (2 mg/mL) was resuspended in phosphate buffer (0.1 M, pH 7.4), containing 10% ethylene glycol (10% m/v). The mitochondrial preparation was homogenised with a Potter Elvehjem homogeniser. The resulting homogenate was sonicated for 5 min at 60 Watts. To prevent overheating of the mitochondrial sonicate, one minute intervals were included between each consecutive minute of sonication. CO was bubbled through the mitochondrial sonicate to saturate the binding sites of the heme iron. Equal volumes (1.5 mL) of the saturated mitochondrial sonicate were subsequently divided into two optically matched 1.5 mL quartz cuvettes. A corrected baseline was first recorded between 400-500 nm. Crystallized sodium dithionite (1 – 2 mg) was used to reduce the heme-iron from the ferric to the ferrous state, which was added to the sample cuvette and the contents inverted. A difference spectrum was recorded between 400 - 500 nm. The cytochrome P450 content was calculated using an wavelength at 450 nm, an extinction coefficient of $91 \text{ cm}^{-1}\text{mM}^{-1}$ and a path length of 1 cm (16).

3.2.2.8 Difference spectra

Difference spectra were recorded at 25°C in 1.5 mL optically matched quartz cuvettes. All spectral assays were recorded in phosphate buffer (0.1 M, pH 7.4), containing 10% ethylene glycol (10% m/v). The cytochrome P450 concentration for all difference spectra was 0.686 nmol P450/mg protein. The influence of an inhibitor was determined as previously published (87). For all spectral assays DOC was dissolved in ethanol, CpDA and *R*- and *S*-enantiomers in dH₂O.

3.2.2.8.1 Spectral assay A: DOC-induced difference spectrum

A substrate-induced difference spectrum of the crude mitochondrial powder was obtained as follows: Mitochondrial powder (2 mg/mL), suspended in phosphate buffer, was homogenised and the resulting homogenate sonicated for 5 minutes, with one minute intervals. The mitochondrial sonicate (3480 μL) was mixed with phosphate buffer (20 μL) to obtain a final mitochondrial volume of 3500 μL . An equal volume (1496 μL) of the mitochondrial enzyme/buffer preparation was pipetted into two optically matched cuvettes and a corrected baseline was recorded between 360-500 nm. DOC (3.2 μM , 4 μL), was added to the sample

cuvette and an equal volume of absolute ethanol to the reference cuvette. The content of both cuvettes were inverted gently and a difference spectrum recorded between 360-500 nm.

The influence of the inhibitor on the substrate-induced difference spectrum was determined by replacing the phosphate buffer with the inhibitor, prior to the division into the optically matched quart cuvettes.

The influence of the inhibitor on the substrate-induced difference spectrum was indicated by a decrease in amplitude, i.e. decreased maximum absorbance at 390 nm and an increase in minimum absorbance at 420 nm. The percentage inhibition was calculated by using the following equation:

- Enzyme/Buffer: $(Abs_{390nm} - Abs_{420nm}) = x$
- Enzyme/Inhibitor: $(Abs_{390nm} - Abs_{420nm}) = y$

$$Percentage\ inhibition = 100 - \left(\left(\frac{y}{x} \right) * 100 \right) \quad Eq. 1$$

3.2.2.8.2 Spectral assay B: Inhibitor-induced difference spectrum

The inhibitor-induced difference spectrum of the crude mitochondrial powder was prepared in the same manner as described for the substrate induced difference spectrum, prior to the addition of buffer/inhibitor to the mitochondrial sonicate. Equal volumes (1496 μ L) of the mitochondrial sonicate were added to both the reference and sample cuvettes and a corrected baseline was recorded between 360-500 nm. After the baseline correction, 4 μ L of inhibitor (200 μ M) was added to the sample cuvette and an equal volume of dH₂O was added to the reference cuvette. The contents of both cuvettes were inverted gently and a difference spectrum recorded between 360-500 nm.

3.3 Results and discussion

The present study includes the synthesis of a racemic mixture of CpDA and the separation of the *R*- and *S*-enantiomers of CpDA. Before the enantiomers of CpDA were separated, MS and NMR analysis were performed to determine the purity, the accurate mass and structure of the synthesized product. In addition, the spectroscopic properties of partially purified CYP11B1 from ovine adrenals were used to establish whether CpDA was biologically active. As the enantiomers of CpDA had, up until the present study, not been separated, the *R*- and *S*-enantiomers were also subjected to MS and NMR analysis for accurate mass and structure elucidation. To establish whether the enantiomers were biologically active, spectral assays were performed and the results compared to the racemic mixture of CpDA.

3.3.1 Synthesis of CpDA

Acetylation of synephrine with acetyl chloride in glacial acid gave rise to a racemic mixture of CpDA. However, it must be emphasized that CpDA readily cyclises to its inactive form (**Figure 27**) when exposed to light and oxygen, and converts back to synephrine when it is left at room temperature for an extended period of time. Therefore, precautionary steps were taken when working with CpDA, such as working in the dark and storing it at -80°C . The purity and structure were verified by MS and NMR analysis and the biological activity tested by using the spectral properties of CYP11B1 from ovine adrenals.

3.3.1.1 Mass spectrometry analyses of CpDA

The purity and accurate molecular weight of the newly synthesised CpDA was analysed using Q-ToF/ESI-MS. As shown in **Figure 27**, three distinct peaks were detected at approximately 2.57, 3.02 and 4.60 minutes. Each peak was further analysed and the results are shown in **Figure 28**, **Figure 29** and **Figure 30**, respectively.

The ESI-MS spectrum of peak one (at 2.57 minutes) (**Figure 28**) shows a $[\text{M}+\text{H}]^{+}$ peak at (m/z) at 192 and 210, respectively. The first molecular ion and its fragmentation pattern corresponds to formation of 2-(4-acetoxyphenyl)-1-methylaziridine ($[\text{M}+\text{H}]^{+} = 192$), whereas the second molecular ion corresponds to 2-(4-acetoxyphenyl)-2-hydroxy-*N*-methylethanamine ($[\text{M}+\text{H}]^{+} = 210$) the structure depicted in the spectrum.

Figure 29 displays the ESI-MS spectrum from peak two (at 3.02 minutes). This spectrum displays a $[\text{M}+\text{H}]^{+}$ peak at (m/z) at 192, 228 and 252, respectively. The fragmentation pattern of the molecular ion ($[\text{M}+\text{H}]^{+} = 192$) is consistent with the cyclisation of CpDA ($[\text{M}+\text{H}]^{+} = 228$) to the corresponding aziridine precursor (2-(4-acetoxyphenyl)-1-methylaziridine). The $[\text{M}+\text{H}]^{+}$ peak at 252 could not be identified, it is possibly an impurity.

ESI-MS analysis of peak three (**Figure 30**) shows various peaks with molecular ions at (m/z) at 192, 234, 294, 316 and 332, respectively. The molecular ions ($[M+H]^+=192$) and ($[M+H]^+=294$) were identified as 2-(4-acetoxyphenyl)-1-methylaziridine and acetylated synephrine, respectively. The structure of the acetylated synephrine is depicted in the spectrum. The remainder of the peaks could, however, not be identified.

Q-ToF/ESI-MS analysis revealed that the synthesized product was indeed CpDA. However, CpDA was not completely pure as the fragmentation patterns revealed the presence of 2-(4-acetoxyphenyl)-2-hydroxy-*N*-methylethanamine, acetylated synephrine and other unidentified impurities within the sample. Even though CpDA (228.0764 g/mol) is a more stable analog than the active compounds from the shrub, under the instrumental setup of the UPLC/Q-ToF MS, the Cl⁻ (good leaving group) leaves as the highly reactive aziridine ring forms (biologically inactive form of CpDA) with a molecule weight at 192.1008 g/mol.

It would have been possible to isolate peak 2 using HPLC. However, as CpDA is already labile under standard laboratory conditions, subjecting it to an additional HPLC step posed further risks for it to cyclise to its inactive form. It was, therefore, decided to use the synthesised mixture of CpDA as is for the separation of the enantiomers.

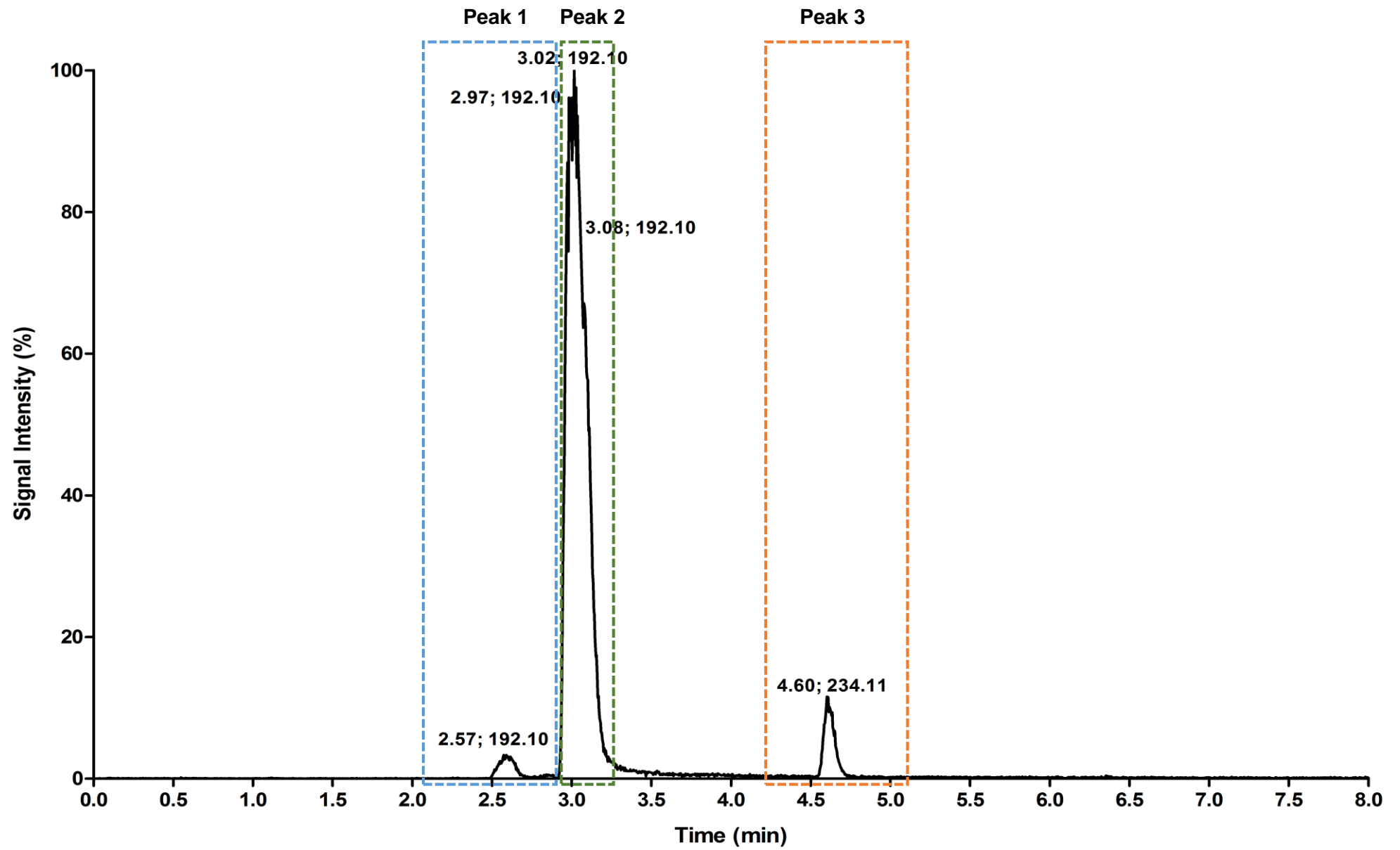


Figure 27. Q-ToF MS of (1 mg/mL) CpDA prepared in deionised water.

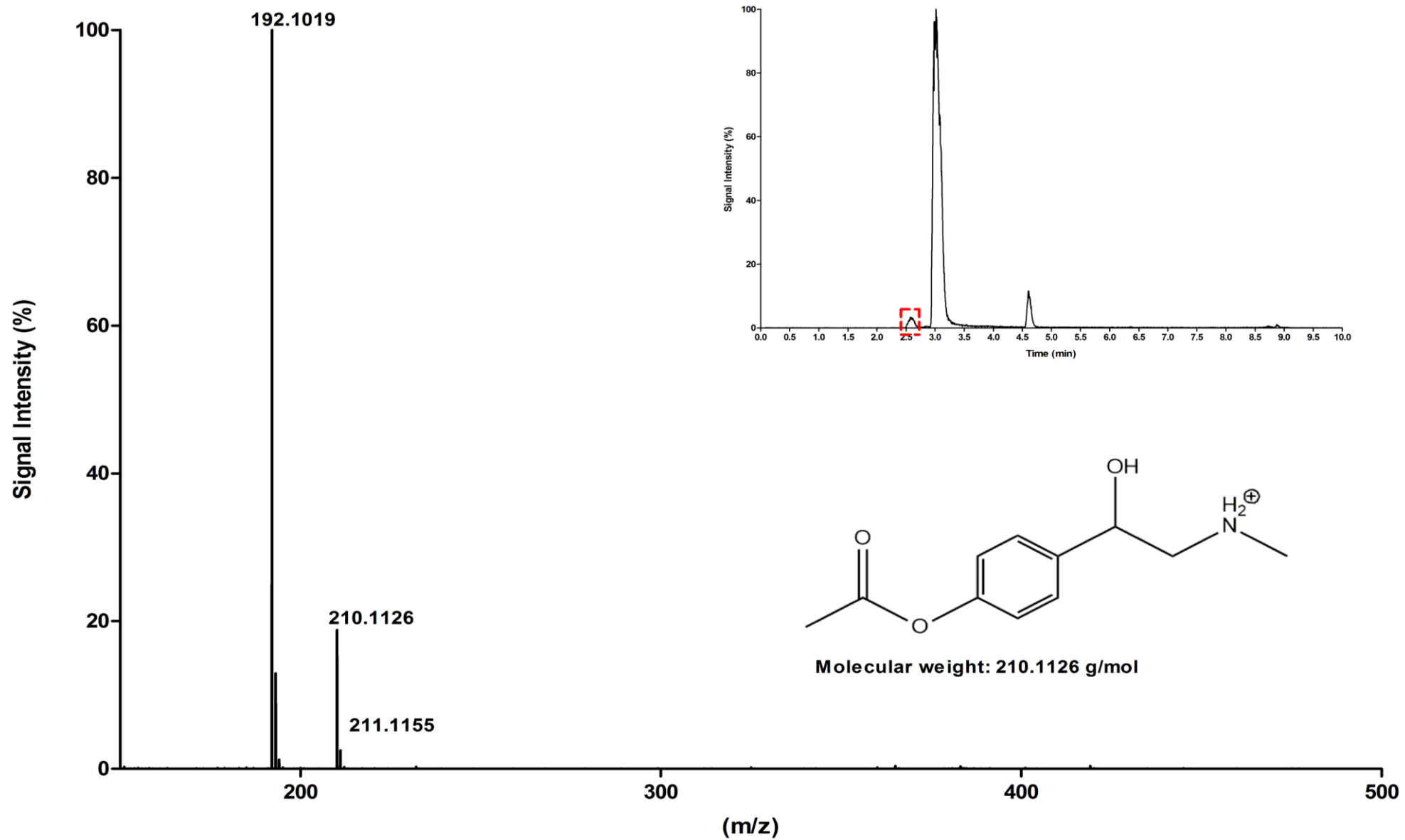


Figure 28. ESI-MS spectrum of peak one at 2.57 minutes of the Q-ToF MS analysis of synthesized CpDA.

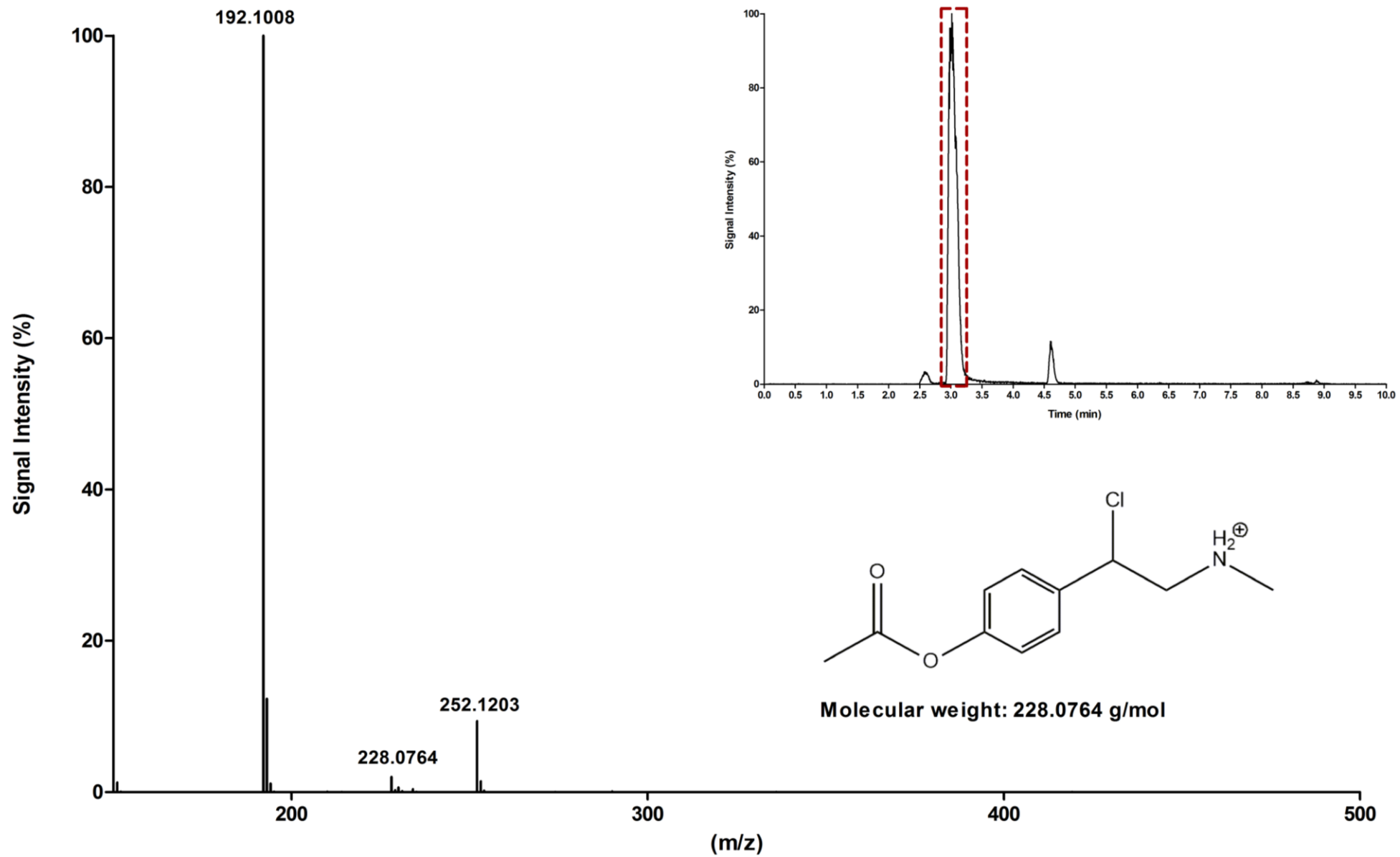


Figure 29. ESI-MS spectrum of peak two at 3.02 minutes of the Q-ToF MS analysis of synthesized CpDA.

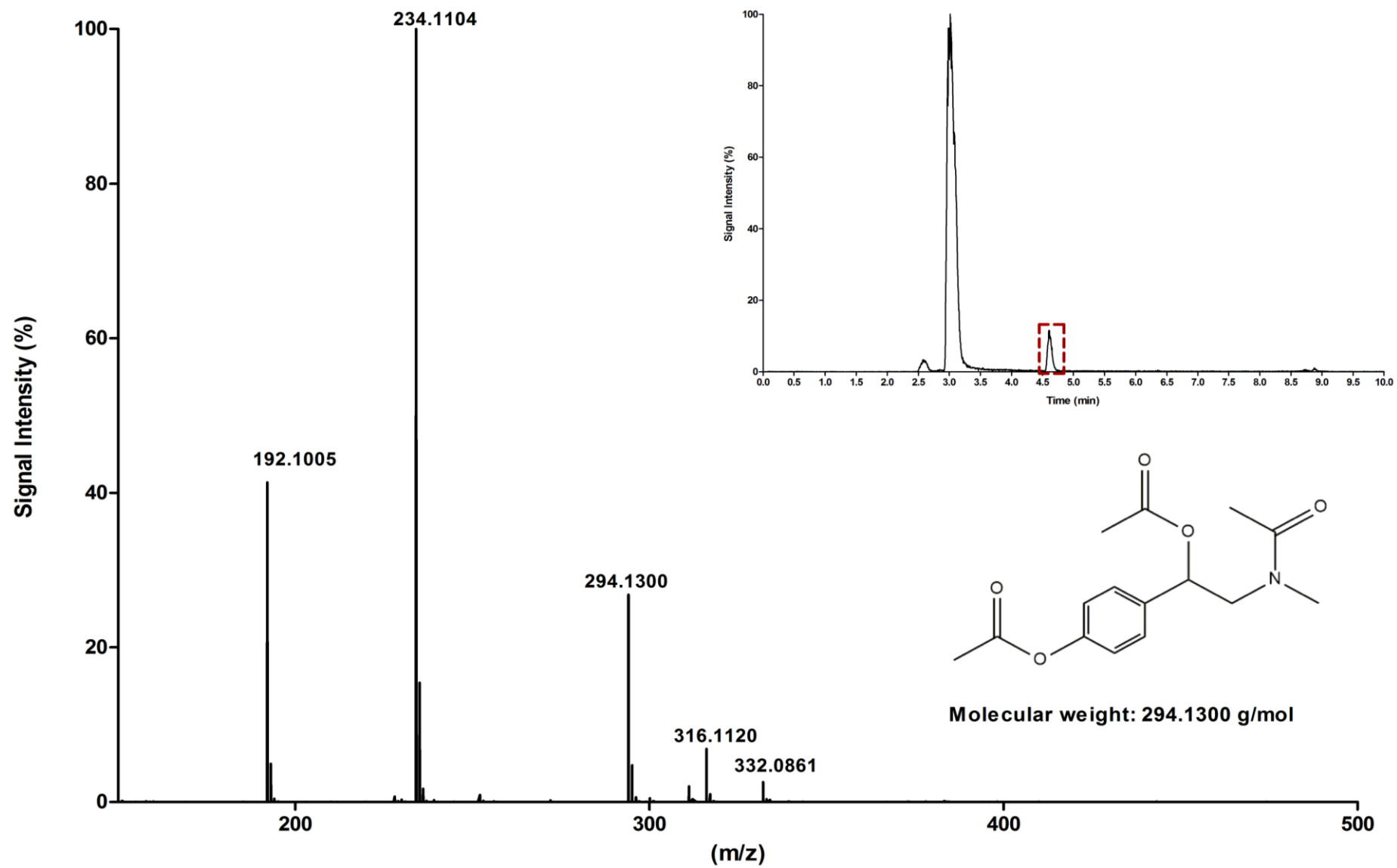


Figure 30. ESI-MS spectrum of peak three at 4.60 minutes of the Q-ToF MS analysis of synthesized CpDA.

3.3.3.2 NMR analysis of synthesised CpDA

The ^1H -NMR and ^{13}C -NMR analyses of the synthesized racemic mixture of CpDA are shown in **Figure 31** and **Figure 32**, respectively. As shown in the ^1H -NMR spectrum, the three protons of the $-\text{CH}_3$ group (labelled **a** and **b** in the spectrum) are represented as a single peak at 2.38 ppm and 2.84, respectively. The two protons of the $-\text{CH}_2$ group (labelled as **c**) are represented as a doublet of doublets (dd) at 3.65 and 3.77, respectively. The proton at position **f** should be a triplet, yet the results revealed a dd at 5.44 ppm. Furthermore, the two protons in the benzene ring (depicted as **d**) represents a doublet at 7.26 ppm. Similarly, the two protons (labelled as **e**) are also denoted as a doublet at 7.63 ppm. The amino group ($-\text{NH}_2$), however, should have a single peak at approximately 7 ppm. There is a small peak connected to the doublets (labelled as d) at 7.25 ppm, which could potentially represent the amino group. In addition, there should be nine carbon peaks on the carbon NMR spectrum, however, there were a total of fourteen carbon peaks. Taken together, NMR analyses confirm that the sample was CpDA, however it also confirms the presence of impurities in the sample.

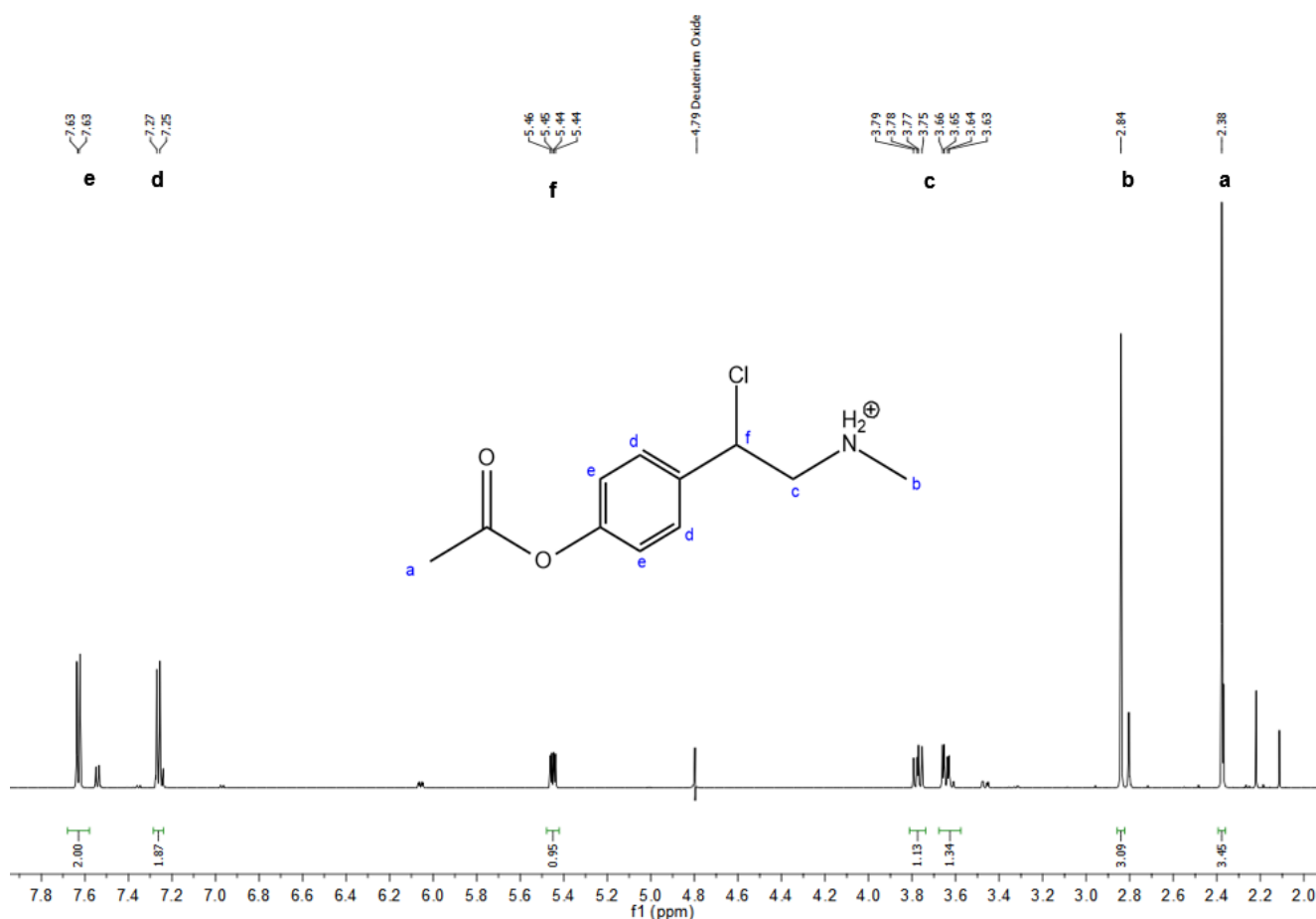


Figure 31. ^1H -NMR analysis of synthesized CpDA.

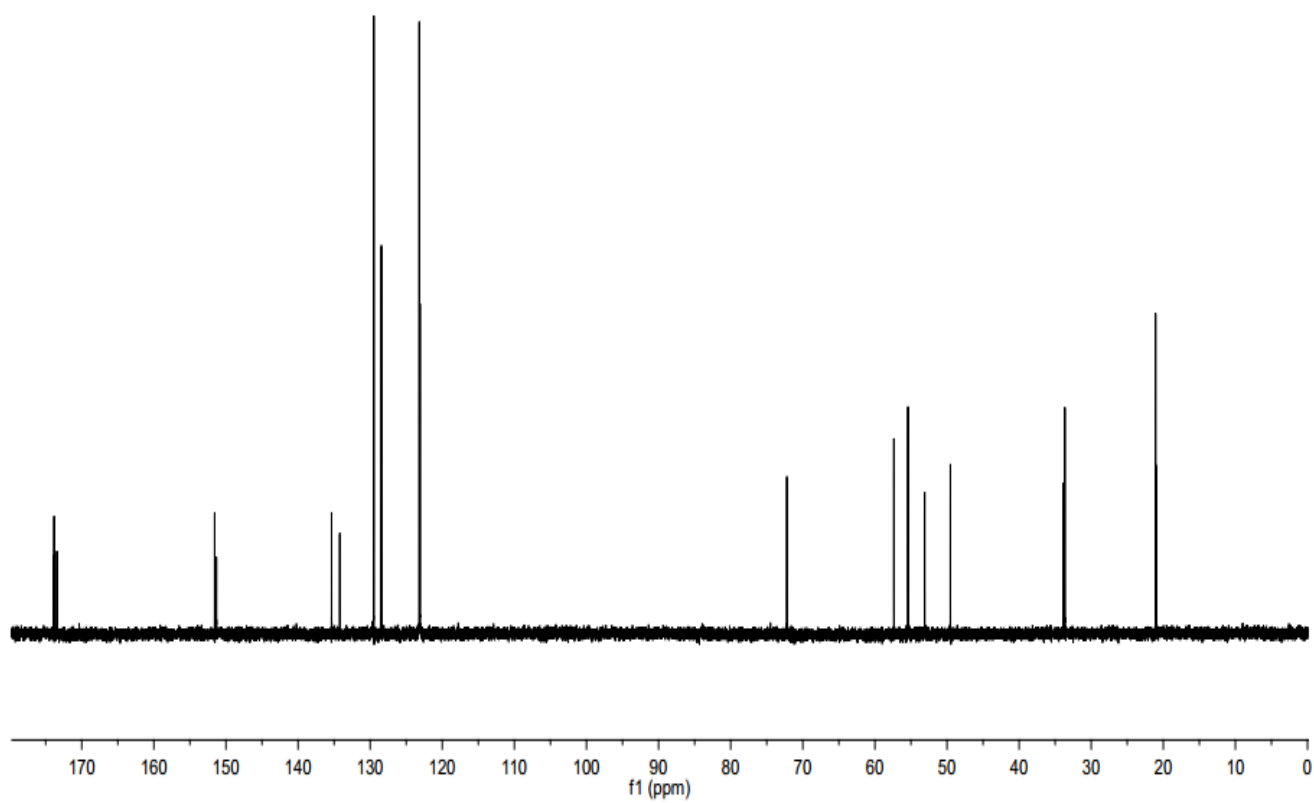


Figure 32. ^{13}C -NMR analysis of synthesized CpDA.

3.3.3.3 Screen for biological activity of CpDA

The effects of CpDA on the spectral properties of partially purified CYP11B1 from ovine adrenals were used to screen for biological activity of CpDA. The cytochrome P450 activity assay and the DOC/inhibitor-induced difference spectra were performed in triplicate and the spectral assays are presented as the mathematical mean.

3.3.3.3.1 Cytochrome P450 activity assay

A cytochrome P450 activity assay was performed to determine the concentration and the activity of cytochrome P450 enzymes in the mitochondrial preparation. The crude enzyme preparation was active and free from cytochrome P420 enzyme (no peak was evident at 420 nm), as shown in **Figure 33**. A maximum peak at 450 nm was observed, with a deep trough 408 nm and a smaller trough at approximately 480 nm. Therefore, the P450-enriched mitochondrial powder could be used to screen for biological activity of the inhibitors. The cytochrome P450 concentration of a 2 mg/mL mitochondrial preparation was 0.686 nmol P450/ mg protein.

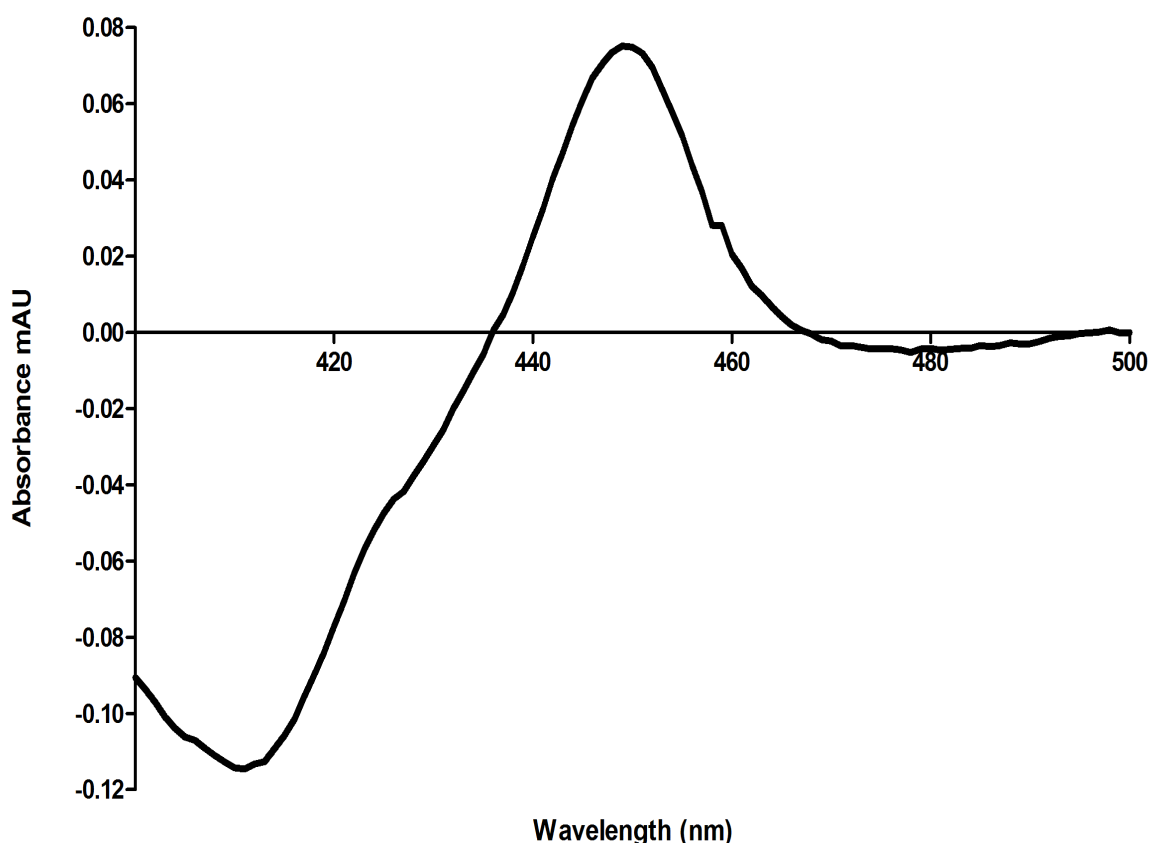


Figure 33. CO-induced difference spectrum of a crude mitochondrial-acetone preparation, 2 mg/mL, in 0.1 M phosphate buffer, containing 10% ethylene glycol. [P450], 0.686 nmol P450/mg protein.

3.3.3.3.2 Difference spectra

The influence of various concentrations of CpDA (ranging from 250 μM , 500 μM , 750 μM and 1000 μM), dissolved in dH_2O , is shown in **Figure 34**, and the ability of CpDA to induce a difference spectrum on its own is shown in **Figure 35**.

The different concentrations (250 μM – 1000 μM) of CpDA inhibited the Type I DOC-induced difference spectra in a concentration dependent manner as a decrease shift in absorbance maxima and an increase shift of absorbance minima were detected at 420 and 390, respectively. The different concentrations of CpDA, 250 μM , 500 μM , 750 μM and 1000 μM , inhibited the Type I difference spectra by 16.85%, 30.84%, 50.30% and 64.53%, respectively. Furthermore, CpDA (200 μM) induced a Type II difference spectrum on its own with an absorbance minimum at 412 nm and maximum at 430 nm.

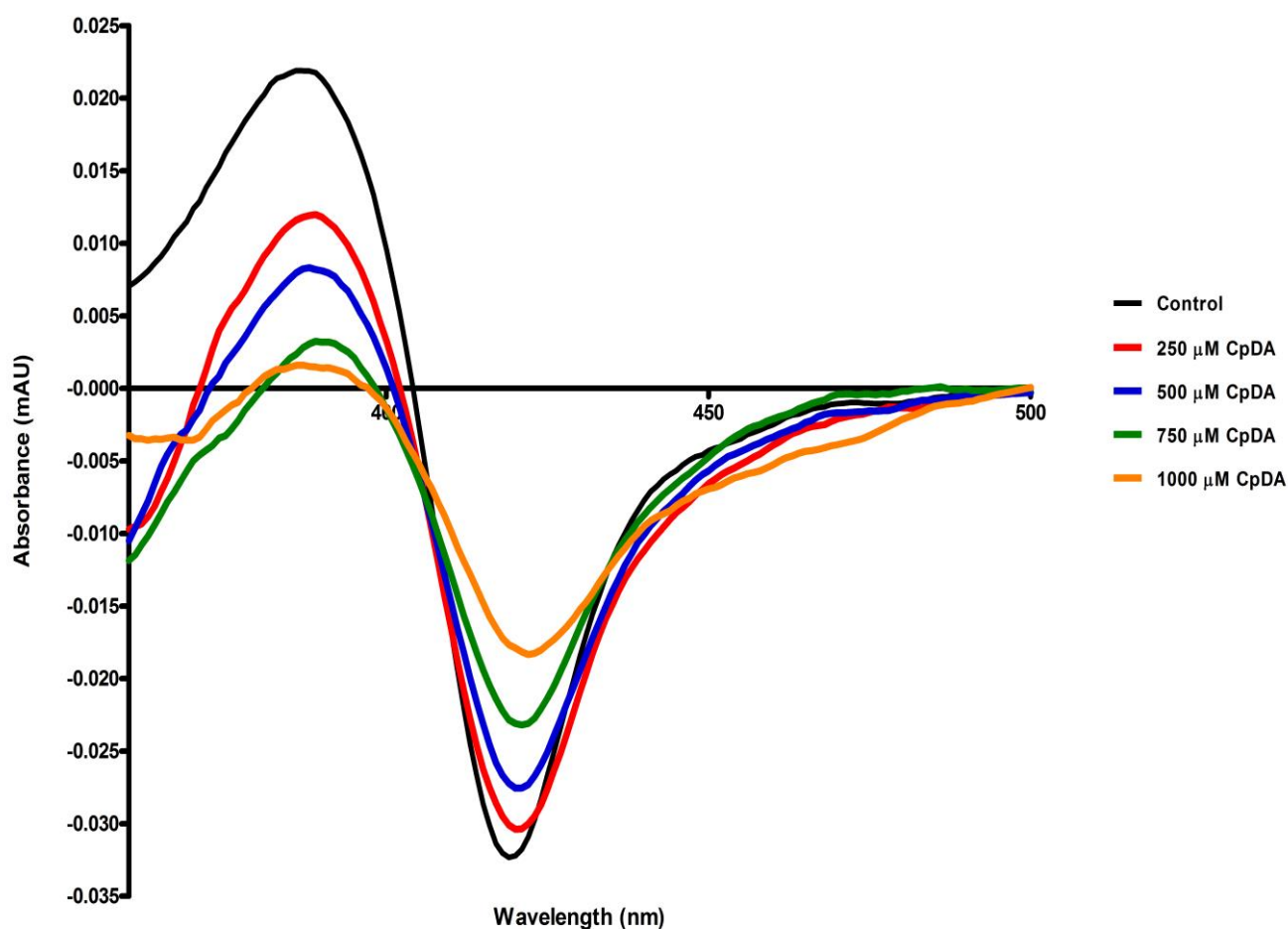


Figure 34. Influence of CpDA on the DOC-induced difference spectrum of a mitochondrial suspension, 2 mg/mL, in 0.1 M phosphate buffer, containing 10% ethylene glycol. [P450], 0.686 nmol P450/mg protein; [DOC], 3.21 μM ; % inhibition of CpDA at 250 μM , 16.85%; 500 μM , 30.84%; 750 μM , 50,30%; and 1000 μM , 64.53%.

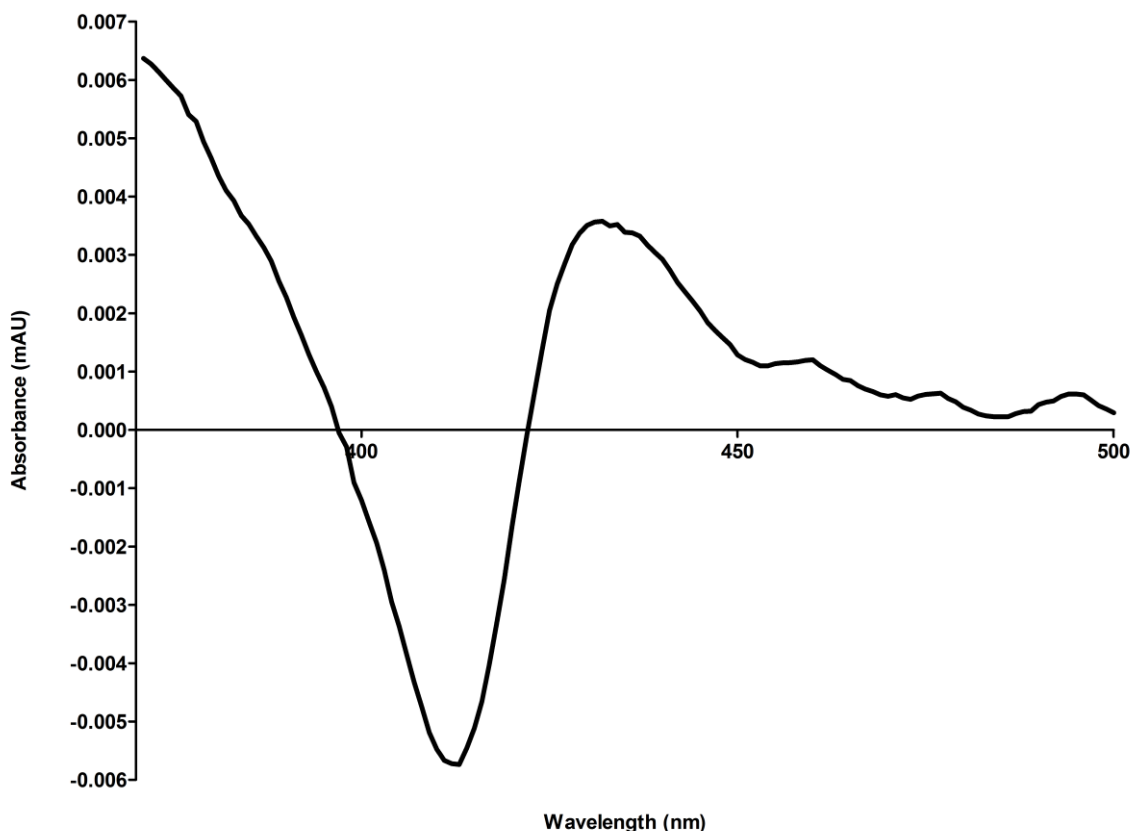


Figure 35. Type II-induced difference spectrum of CpDA (200 μM). [P450], 0.686 nmol P450/mg protein.

The results obtained from these spectral assays confirm that CpDA is biologically active as it inhibited the binding of DOC to partially purified CYP11B1 and it stabilized the low spin state of the iron in the absence of substrate. These results were comparable with work previously published (27, 28). The results furthermore confirmed that the bioactivity of the racemic mixture of CpDA could be used to assess the activity of the individual enantiomers of the *R*- and *S*-enantiomers of CpDA.

3.3.3.3 Screen for biological activity of synephrine and tartaric acid

As synephrine is the precursor of CpDA and tartaric acid is used as the resolving agent during the chiral resolution of the *R*- and *S*-enantiomer of CpDA, spectral assays were performed to determine whether these compounds could potentially influence the results. As shown in **Figure 36 A** synephrine (500 μM) and tartaric acid (500 μM) did not inhibit the Type I DOC-induced difference spectrum. It did, however, appear that synephrine (200 μM) in **Figure 36 B** induced a highly distorted Type II difference spectrum on its own as a minimum absorbance was detected at 419 nm and an absorbance maximum was detected at \pm 446 nm. As synephrine is the precursor of CpDA it is possible for synephrine to stabilize the low spin state of the iron and still remain biologically inactive. Tartaric acid (200 μM), however, did not induce a Type II difference spectrum as no definite absorbance maximum or minimum were detected.

Taken together, these results indicate that neither synephrine nor tartaric acid interferes with the binding of DOC to CYP11B1, therefore these compounds would not influence the results.

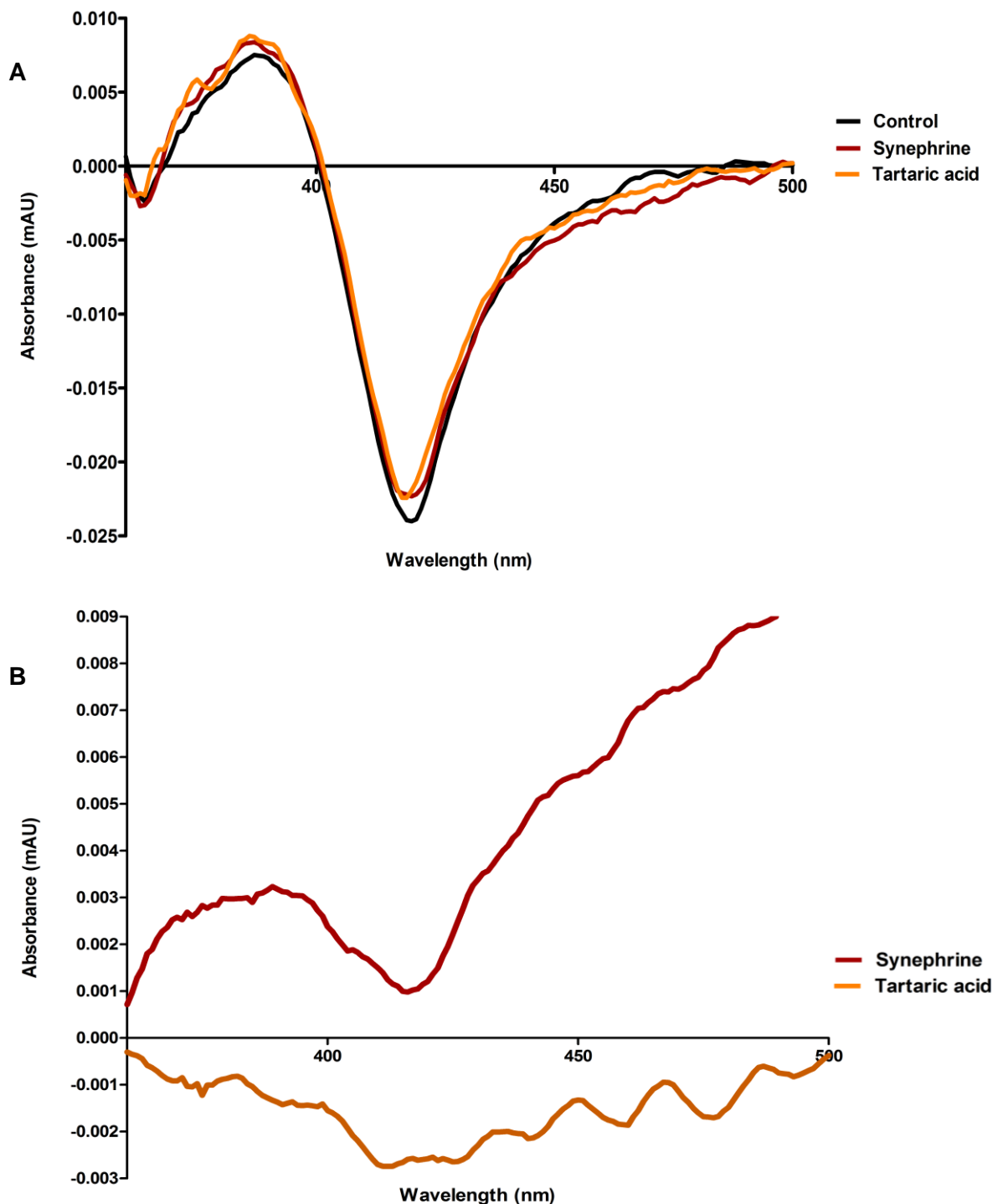


Figure 36. Screen for biological activity of synephrine and tartaric acid. **(A)**, Influence of synephrine (500 μM) and tartaric acid (500 μM) on the DOC-induced difference spectrum of a mitochondrial suspension, 2 mg/mL, in 0.1 M phosphate buffer, containing 10% ethylene glycol. [P450], 0.686 nmol P450/mg protein; [DOC] = 3.21 μM; no inhibition was observed. **(B)** Type II-induced difference spectrum of synephrine (200 μM) and tartaric acid (200 μM). [P450], 0.686 nmol P450/mg protein.

3.3.2 Separation of the *R*- and *S*-enantiomers of CpDA

Diastereomeric salt crystallization was used in an attempt to separate the *R*- and *S*-enantiomers of CpDA. This approach involved mixing a racemic mixture of CpDA with optically pure L-(+)-tartaric acid to produce diastereomeric salts, which were separated by selective crystallization using methanol as solvent. The salts were converted to the pure enantiomers by treatment with HCl. The change in pH protonated the tartaric acid, making it less soluble in the acidic solution, which allowed extraction with ether.

The ratio of tartaric acid to 1-phenylethylamine in Ault's experiment (86) was down-scaled in this study to determine whether this approach could be used to separate the enantiomers. Due to the labile nature of CpDA, precautions had to be implemented, which involved working in the dark in an acidic environment with minimum exposure to oxygen, to prevent the cyclisation of the open-ring aziridine structure of CpDA.

On a micro-scale, this approach was suitable for separating the enantiomers. However, difficulties were experienced when applying the protocol to a preparative large scale preparation.

3.3.2.1 Mass spectrometry of the *R*- and *S*-enantiomers of CpDA

An overlay of the Q-ToF MS analysis of the *R*- and *S*-enantiomers of CpDA are shown in **Figure 37**. As depicted in the overlay of the total ion chromatogram using MS of the *R*- and *S*-enantiomers, five major peaks were seen for the *R*-enantiomer at 1.18, 2.17, 2.54, 2.93 and 3.44 minutes and for the *S*-enantiomer at 1.18, 2.23, 2.54, 2.95 and 3.44 minutes. Each respective peak of both the *R*- and *S*-enantiomers was further analysed and the ESI-MS results are shown in **Figure 38**, **Figure 39** and **Figure 40**.

Figure 38 (A and B) represents the ESI-MS of the *R*- and *S*-enantiomers at 1.18 minutes whereas **Figure 38 (C and D)** depicts that of the *R*- and *S*-enantiomers at 2.17 and 2.23 minutes, respectively.

- The results from **Figure 38 (A and B)** shows a $[M+H]^+$ peak at (m/z) at 150 and 168, respectively. Tartaric acid also has a molecular mass of 150.087 g/mol. However, as ESI-MS is performed in positive mode, and tartaric acid is fully protonated, it is not possible to see tartaric acid in the mass spectrum. The $[M+H]^+$ peak at (m/z) = 150, therefore, more likely represents 2-(4-hydroxyphenyl)-1-methylaziridine (structure depicted in **Figure 38 A**), whereas the peak at (m/z) = 168 is unequivocally identified as synephrine.
- The results from **Figure 38 (C and D)** show a $[M+H]^+$ peak at (m/z) at 150 and 182, respectively. Similarly, to the results shown in **Figure 38 (A and B)**, the $[M+H]^+$ peak

at (m/z) = 150, represents 2-(4-hydroxyphenyl)-1-methylaziridine. The $[M+H]^+$ peak at (m/z) = 182 could not be identified. However, it is possible that the molecular ion and its fragmentation pattern is the result of contamination. It was interesting to see that the *S*-enantiomer had a bigger peak at 2.20 minutes in the time-of-flight mass spectrum (**Figure 37**), suggesting that the *S*-enantiomer is more labile than the *R*-enantiomer as more of the *S*-enantiomer cyclizes into the 2-(4-hydroxyphenyl)-1-methylaziridine than the *R*-enantiomer.

Figure 39 (A and B) represents the ESI-MS of the *R*- and *S*-enantiomers at 2.54 minutes whereas **Figure 39 (C and D)** denotes ESI-MS of the *R*- and *S*-enantiomers at 2.93 and 2.95 minutes, respectively.

- Three major peaks were seen in **Figure 39 (A and B)** at a (m/z) of 150, 192 and 210, which were representative of 2-(4-hydroxyphenyl)-1-methylaziridine, 2-(4-acetoxyphenyl)-1-methylaziridine (inactive form of CpDA) and 2-(4-acetoxyphenyl)-2-hydroxy-*N*-methylethanamine, respectively. In contrast to the mass spectrum of the *R*-enantiomer in **Figure 39 (A)**, the mass spectrum of the *S*-enantiomer of **Figure 39 (B)** had more fragmentation, suggesting that the *S*-enantiomer contained more impurities than the *R*-enantiomer.
- The results from **Figure 39 (C and D)** show $[M+H]^+$ peaks at (m/z) at 150, 192, 228 and 252 which denotes 2-(4-hydroxyphenyl)-1-methylaziridine, 2-(4-acetoxyphenyl)-1-methylaziridine, CpDA and an unidentified compound, respectively.

Figure 40 (A and B) represents the ESI-MS of the *R*- and *S*-enantiomers at 3.44 minutes.

- Three major $[M+H]^+$ peaks were seen at a (m/z) of 150, 192 and 224. The fragmentation pattern of (m/z) = 150 and 192 is consistent with 2-(4-hydroxyphenyl)-1-methylaziridine and 2-(4-acetoxyphenyl)-1-methylaziridine. However, the $[M+H]^+$ peak at (m/z) = 224 could not be identified to a specific compound, and therefore it is possible that this fragment is an impurity.

Taken together, these results suggest the successful separation of the *R*- and *S*-enantiomers of CpDA as comparable mass spectra were seen in both the Q-ToF MS (**Figure 37**) and the ESI-MS analysis (**Figure 38**, **Figure 39** and **Figure 40**). However, the ESI-MS analysis suggests that the *R*- and *S*-enantiomer cyclizes into 2-(4-hydroxyphenyl)-1-methylaziridine and the inactive form of CpDA, suggesting that the separation of the enantiomers influences the stability and therefore the activity of the *R*- and *S*-enantiomers.

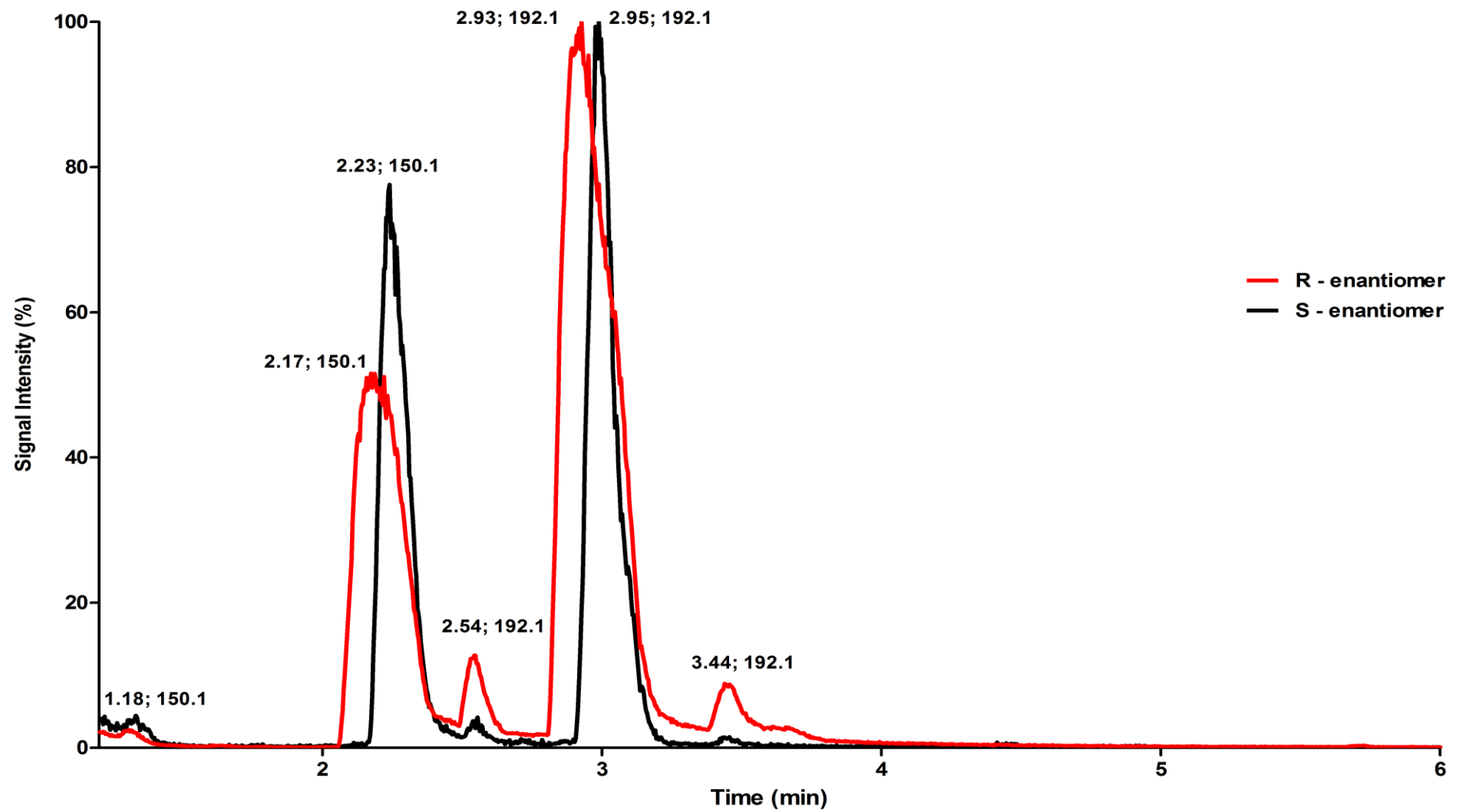


Figure 37. Q-ToF MS of the R- and S-enantiomers (1 mg/mL) of CpDA prepared in deionised water.

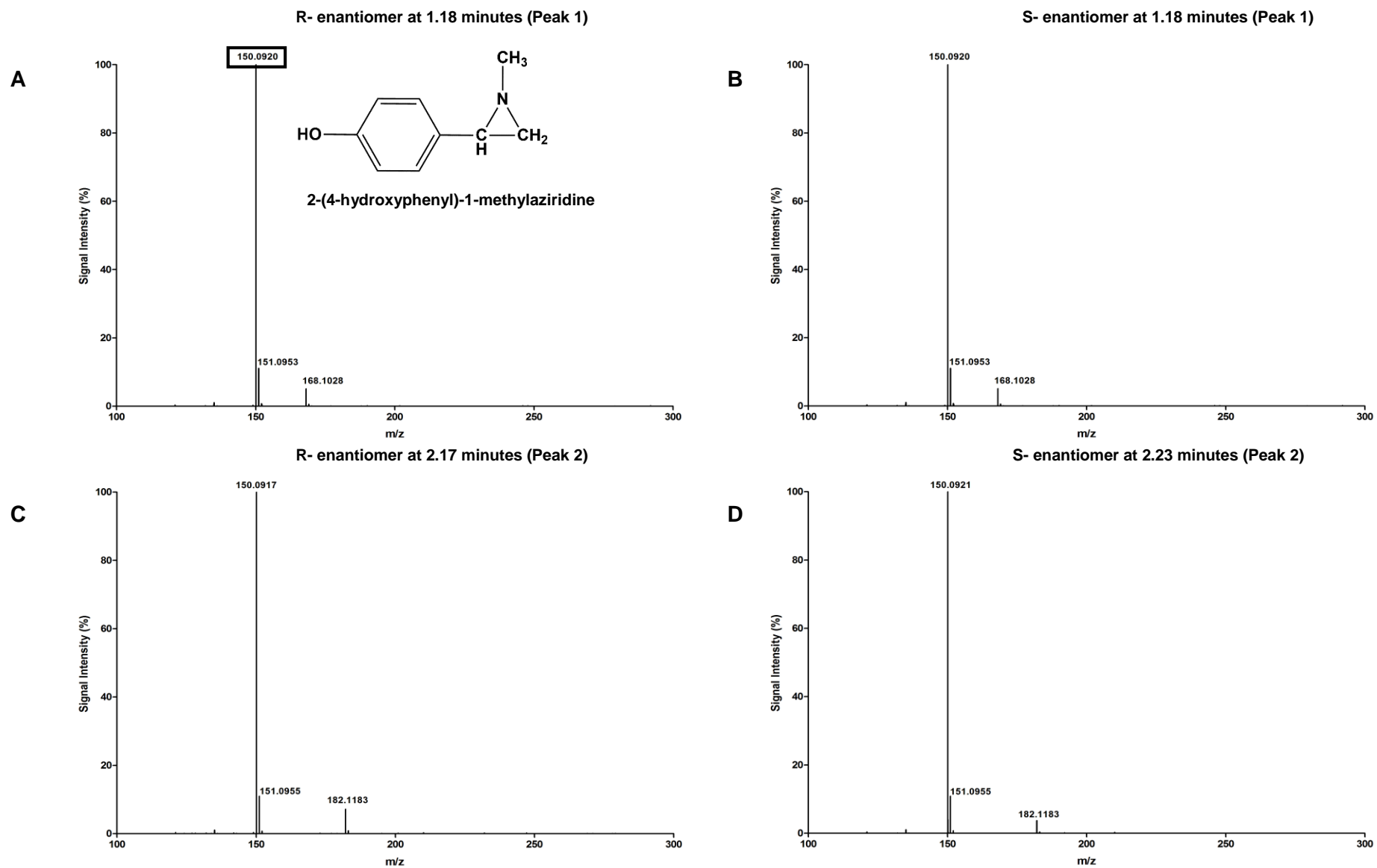


Figure 38. ESI-MS spectra of the Q-ToF MS spectrum of CpDA enantiomers. (A) R-enantiomer and (B) S-enantiomer at 1.18 minutes (Peak 1); (C) R-enantiomer at 2.17 minutes and (D) S-enantiomer at 2.23 minutes (Peak 2).

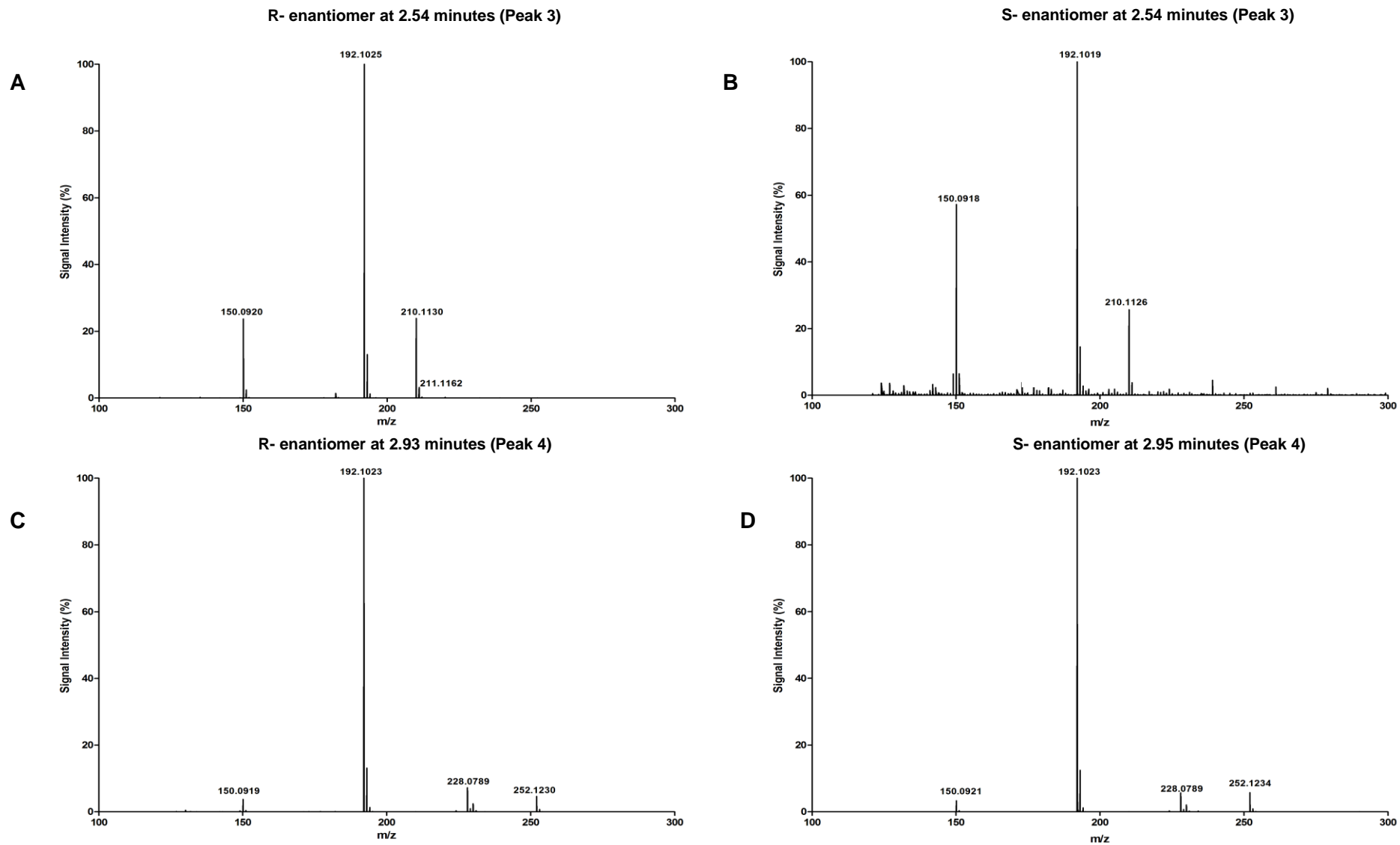


Figure 39. ESI-MS spectra of the Q-ToF MS spectrum of CpDA enantiomers. (A) *R*-enantiomer and (B) *S*-enantiomer at 2.54 minutes (Peak 3); (C) *R*-enantiomer at 2.93 minutes and (D) *S*-enantiomer at 2.95 minutes (Peak 4).

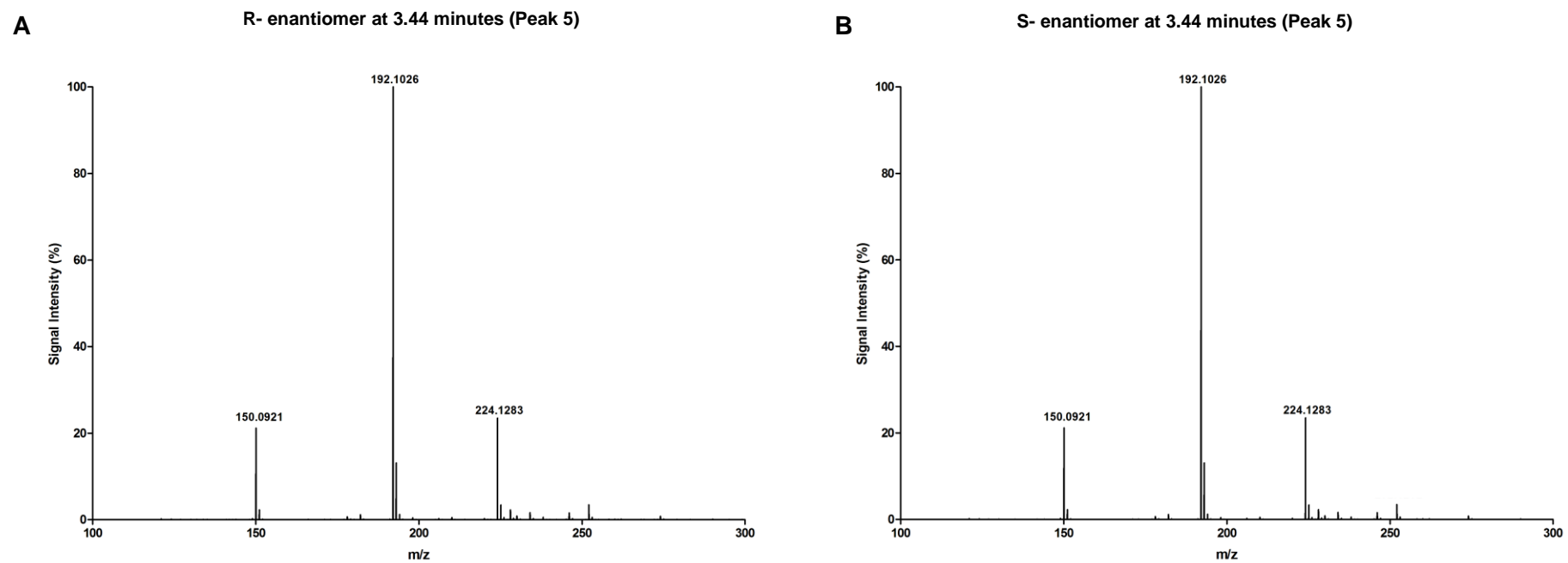


Figure 40. ESI-MS spectra of the Q-ToF MS spectrum of CpDA enantiomers. (A) R-enantiomer and (B) S-enantiomer at 3.44 minutes (Peak 5);

3.3.2.2 NMR analysis of the *R*- and *S*-enantiomers of CpDA

As enantiomers are structurally identical, they will have a similar proton and carbon NMR spectrum. However, due to the low yield of the *S*-enantiomer, only a proton spectrum of the *R*- and *S*-enantiomers were completed. The proton spectrum of the *R*- and *S*-enantiomers, as shown in **Figure 41**, are stacked above each other to demonstrate the similarity in the ^1H -NMR analysis of the enantiomers. There are, however, some differences in the proton spectra as the *R*-enantiomer has an additional proton peak at approximately 3.4 and 3.7 ppm, whilst the *S*-enantiomer has an additional proton peak at 2.1 ppm. Because the racemic mixture of CpDA already contained impurities, it was expected that the enantiomers would also contain some impurities. The proton spectra of the *R*- and *S*-enantiomers of CpDA nevertheless show significant similarity, indicating that they are indeed the *R*- and *S*-enantiomers of CpDA.

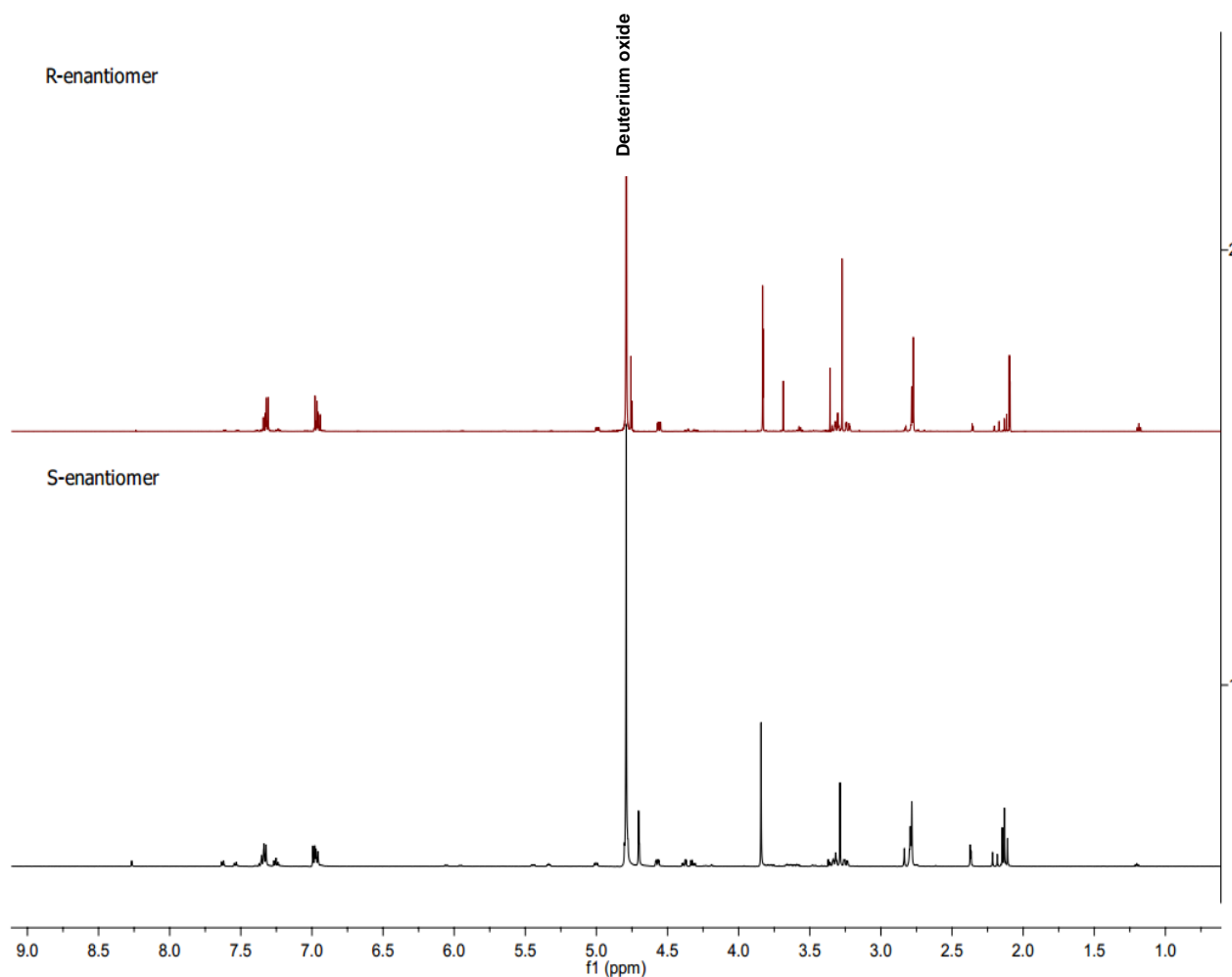


Figure 41. Stacked ^1H -NMR spectra of the *R*- and *S*-enantiomers of CpDA.

3.3.2.3 Biological activity of the *R*- and *S*-enantiomers of CpDA

Spectral assay A (DOC-induced difference spectrum) and Spectral assay B (Inhibitor-induced difference spectrum) were used to determine the biological activity of the *R*- and *S*-enantiomers. The influence of the *R*- and *S*-enantiomers on the DOC-induced difference spectrum is shown in **Figure 42 A**. As CpDA (750 μ M) inhibited \pm 50% on the Type I-induced difference spectrum (**Figure 34**), this concentration was chosen as the standard to compare the inhibitory potential of the *R*-enantiomer and the *S*-enantiomer.

As shown in **Figure 42 A**, the three test compounds inhibited the DOC-induced Type I difference spectrum, with the inhibition of CpDA (750 μ M), being 51.05% and the *R*- and *S*-enantiomers (750 μ M) 18.96% and 31.54%, respectively.

Furthermore, both the *R*-enantiomer (200 μ M) and the *S*-enantiomer (200 μ M) had the ability to induce a Type II difference spectrum (**Figure 42 B**). It is, however, interesting to note that the *R*- and *S*-enantiomers induced different Type II difference spectra. The *R*-enantiomer had an absorbance minimum and maximum at approximately 412 nm and 430 nm, respectively, which was comparable with the Type II difference spectrum induced by CpDA (**Figure 35**). The *S*-enantiomer, however, induced an absorbance minimum at 402 nm and an absorbance maximum at 440 nm.

Taken together, these results clearly show that the *R*- and *S*-enantiomers are biologically active, as they inhibited the DOC-induced Type I difference spectrum and induced a Type II difference spectrum in the absence of substrate. It was interesting to note the *S*-enantiomer was biologically more active than the *R*-enantiomer, even though there were more impurities in the *S*-enantiomer. In addition, the Type II difference spectrum induced by the *S*-enantiomer was different to that of both CpDA and the *R*-enantiomer, suggesting that the enantiomers interact differently with the enzymes in the P450-enriched mitochondrial preparation. The mechanism of action of the *R*- and *S*-enantiomers of CpDA could, however, only be explained by investigating the effects of each enantiomer with purified CYP11B1 from ovine adrenals.

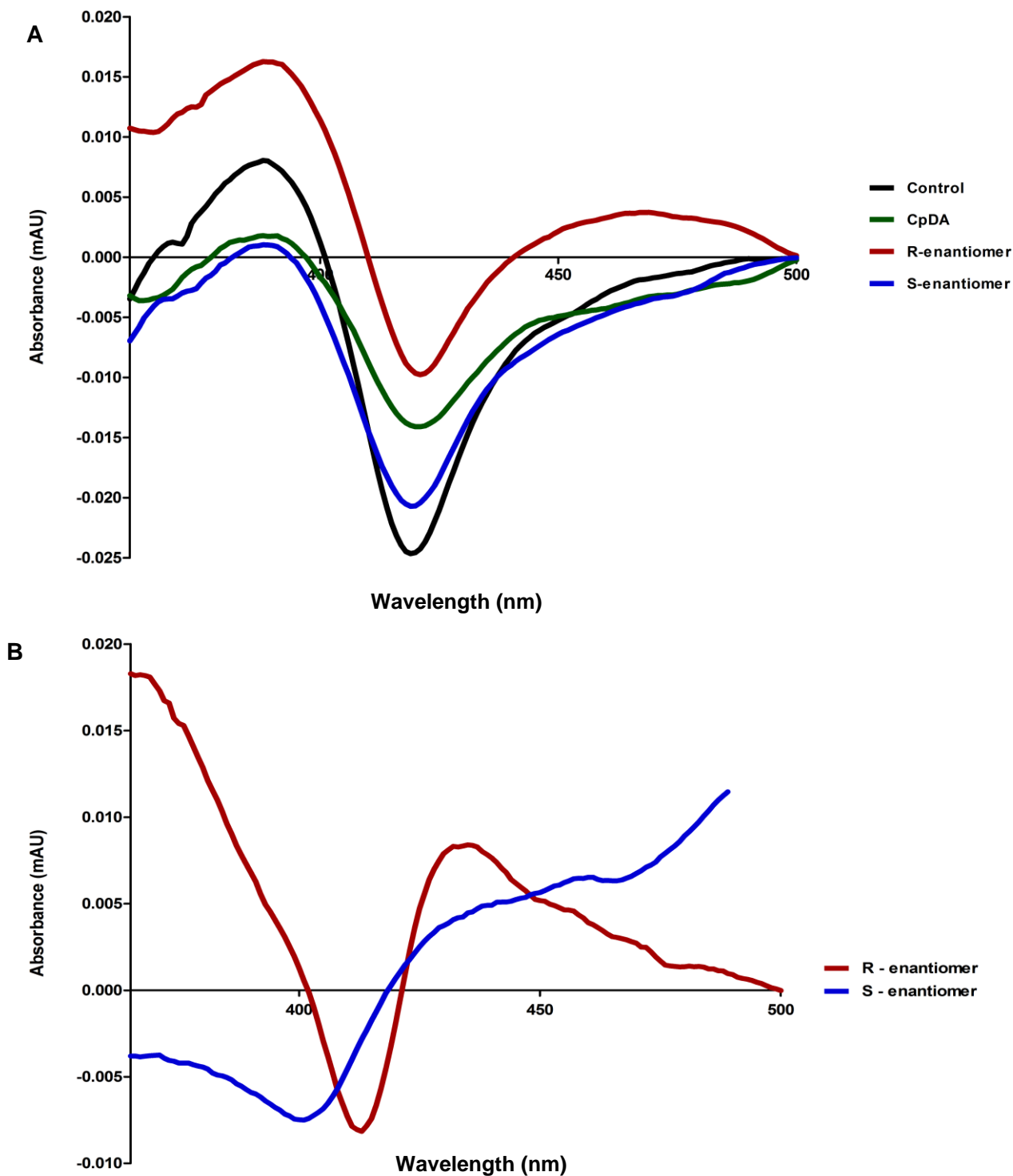


Figure 42. (A) Influence of CpDA (750 μ M) and the R-enantiomer (750 μ M) and the S-enantiomer (750 μ M) on the DOC-induced difference spectrum of a mitochondrial suspension, 2 mg/mL, in 0.1 M phosphate buffer, containing 10% ethylene glycol. [P450], 0.686 nmol/mg protein; [DOC], .3.21 μ M; % inhibition of CpDA and the R- and S-enantiomers of CpDA was 51.05%, 18.96 % and 31.54%, respectively (B) Type II-induced difference spectrum of the R-enantiomer in red (200 μ M) and S-enantiomer in blue (200 μ M) of CpDA. [P450], 0.686 nmol P450/mg protein.

3.4 Conclusion

The work described in this chapter included the synthesis of a racemic mixture of CpDA, the separation of the *R*- and *S*-enantiomers of the racemic mixture of CpDA and the determination of the biological activity of the racemic mixture and each enantiomer.

Q-ToF/ESI-MS, ¹H-NMR, ¹³C-NMR and biological studies confirmed the successful synthesis of a racemic mixture of CpDA. Data obtained by MS and NMR, however, showed that there were impurities in the synthesized sample, which were attributed to formation of 2-(4-acetoxyphenyl)-2-hydroxy-*N*-methylethanamine and tri-acetylated synephrine. In addition, MS also indicated that a large portion of the ring-opened form of CpDA cyclises into the inactive aziridine, demonstrating the unstable nature of CpDA. However, the conversion from the active to the inactive form during MS analyses could be attributed to the instrumental set up as a high cone voltage and source temperature may influence the structure of CpDA. Spectral studies with CpDA and CYP11B1 confirmed that it was biologically active. The CYP11B1 spectral assays further confirmed that synephrine and tartaric acid were not biologically active and as such would therefore not influence the activity studies with the enantiomers.

The enantiomers of CpDA were separated via diastereomeric salt crystallization by reacting it with an optically pure resolving agent (L-(+)-tartaric acid). A micro-separation was first carried in which the reaction was scaled down (\pm 30-fold), to assess the viability of the salt crystallization protocol. Although the separation of the enantiomers was successful the *R*- and *S*-enantiomers were not completely pure, as indicated in the LC-Q-ToF MS and NMR analysis. Spectral studies with a P450-containing mitochondrial powder, nevertheless showed that the enantiomers were biologically active even in the presence of impurities introduced in the separation and in the synthesis of CpDA. Interestingly, the two compounds acted differently in a biological environment, with the *S*-enantiomer inducing a greater inhibitory effect on the binding of DOC to CYP11B1 than the *R*-enantiomer. The *R*-enantiomer, however, induced a distinct Type II difference spectrum, similar to the racemic mixture of CpDA, while the *S*-enantiomer did not induce a typical difference spectrum of any kind.

Unfortunately, due to the impurities, the optical rotation of the respective enantiomers could not be determined, as a pure sample (\geq 95%) is required for both a polarimeter and circular dichroism to produce accurate interpretations. However, as Ault used a compound (86) structurally similar to CpDA, it is assumed that the respective enantiomers allocated in this study were the *R*- and *S*-enantiomers of CpDA.

As part of this study, it was important to scale the micro-separation protocol up to a preparative protocol to allow the separation and purification of the two enantiomers. It was, however, a tremendous challenge as LC-Q-ToF MS analyses revealed the complete conversion of the

active form of CpDA to the inactive form. Spectral studies further confirmed that the enantiomers that were separated on a preparative-scale were biologically inactive. For future studies the diastereomeric salt crystallization for the separation of the *R*- and *S*-enantiomers of CpDA on a preparative scale will have to be refined and adapted in order to yield sufficient material to fully characterise the enantiomers.

To conclude, CpDA was successfully synthesised and its enantiomers separated by using diastereomeric salt crystallization. In Chapter 4, the interaction of the enantiomers and the racemic mixture of CpDA with highly purified CYP11B1 will be described.

CHAPTER 4

The interaction of CpDA and its enantiomers with purified ovine adrenal cytochrome P450 11 β -hydroxylase and adrenal mitochondrial electron transport

4.1 Introduction

In Chapter 3, the interaction of partially purified CYP11B1 with CpDA and its enantiomers were described. Previous studies with purified CYP11B1 from ovine adrenals indicated that CpDA is a mixed inhibitor of CYP11B1, with both a competitive ($K_{ic} = 106\text{-}110\ \mu\text{M}$) and uncompetitive element ($K_{iu} = 667\text{-}737\ \mu\text{M}$) (27). The fact that CpDA is a chiral compound (24, 30) can contribute to the mixed inhibitory effects observed. It was therefore decided to investigate the enzyme-substrate and enzyme-inhibitor interaction of CpDA and the *R*- and *S*-enantiomers with fully purified ovine CYP11B1.

As discussed in Chapter 2, the spectral properties of cytochrome P450 enzymes are influenced by a range of factors, such as temperature, pH, ionic strength, the presence of a substrate or inhibitor, as well as the purity of the preparation. The crude mitochondrial preparation used in the spectral assays contained a mixture of endogenous cholesterol, cytochrome c, ADXR, ADX, as well as CYP11A1, CYP11B1 and CYP11B2. Even though the two mitochondrial enzymes are substrate specific, CYP11A1 could influence results and interpretations of the spectral assays. The spectral properties of CYP11B1 can also be influenced by the contaminating components, such as the endogenous cholesterol and the various cellular proteins in the crude mitochondrial extract (7, 18, 70). Spectral assays with purified CYP11B1 therefore provided a more comprehensive understanding of the mechanism of action of the *R*- and *S*-enantiomers of CpDA.

The adrenal mitochondrial steroid hydroxylation system is dependent on a short but highly specific electron transport chain (79, 88). NADPH reduces ADXR which subsequently transfers a single electron to ADX, which in turn supplies electrons to the mitochondrial cytochrome P450 enzymes (7, 18, 89). It was therefore deemed necessary to also investigate the influence of CpDA and the *R*- and *S*-enantiomers of CpDA on the adrenal mitochondrial electron transport system. As purified CYP11B1 is extremely unstable, commercially available

cytochrome c was used in the place of CYP11B1 as the terminal electron acceptor in this study (7, 18, 90).

The study described in this chapter investigated the influence of the racemic mixture as well as the two enantiomers of CpDA on purified ovine mitochondrial CYP11B1 using difference spectroscopy. The influence of the same compounds on ovine adrenal mitochondrial electron transport was investigated using a partially purified ADXR/ADX preparation and cytochrome c as terminal electron acceptor.

4.2 Experimental

4.2.1 Materials and reagents

Fresh ovine adrenals were collected from Tomis Abattoir & Fresh Meats Wholesalers (Hermon, South Africa). Centrifugation was performed on a Beckman Coulter Avanti[®] J-E centrifuge, whilst the Beckman Optima[™] L-80 XP model was used for ultracentrifugation. Sonication was done with a Branson B12 sonifier. Spectral assays were recorded on a Spark[™] 10M multimode microplate reader from Tecan (Männedorf, Switzerland). Lyophilisation was done with a VirTis[®] BenchTop[™] K freeze dryer from United Scientific (South Africa). The Pierce bicinchoninic acid (BSA) protein quantification kit was acquired from Thermo Fisher Scientific (Rockford III, USA). Polyethylene glycol (PEG) 35 000 and the molecular sieve beads (0.3 Å) were purchased from Merck Millipore (South Africa). The primary antibodies, rabbit anti-sheep IgG against CYP11B1, rabbit anti-sheep IgG ADX and rabbit anti-sheep IgG against ADXR, were in-house antibodies part of previous projects, available in the cytochrome P450 laboratory. Anti-Rabbit goat IgG-peroxidase secondary antibody, glucose-6-phosphate, glucose-6-phosphate dehydrogenase, Phenyl-Sepharose CL-4B resin, sodium dithionite and Tween[®]₂₀ were purchased from Sigma-Aldrich Chemical Co. (St. Louis, MO, USA). Spectra/Por[®] 4 dialysis membrane tubing (MWCO, 3.5 kDa) was obtained from Spectrum labs (South Africa). Purification was performed using the Bio-Rad NGC chromatography system and fractions collected using a BioFrac[™] fraction collector (California, USA). The electrophoresis chamber, Mini-PROTEAN[®] Tetra Hand cast System, Kaleidoscope marker, Precision Plus Protein[™] Kaleidoscope[™] Pre-stained Protein Standard, and the Clarity Western[™] ECL Chemiluminescent Blotting Substrate were purchased from Bio-Rad (California, USA). Bio-Trace NT pure nitrocellulose blotting membranes were purchased from Pall Life Sciences (South Africa).

4.2.2 Methods

4.2.2.1 The preparation of a P450-containing mitochondrial acetone powder from ovine adrenals

P450-enriched adrenal mitochondrial-acetone powder from ovine adrenals was prepared as described in Section 3.2.2.5. The powder was used to isolate and purify CYP11B1 and to isolate a partially purified ADX/ADXR preparation.

4.2.2.2 The preparation of ADXR/ADX from ovine adrenal mitochondrial powder

All steps in the isolation of ADX and ADXR were performed at 4°C according to a previously reported method (7, 14, 90). Crude mitochondrial powder (2 g) was resuspended in a 0.1 M Tris buffer (100 mL, pH 7.4) and sonicated on ice for 10 minutes at 60 Watts, to disrupt the mitochondrial membrane. One-minute interval was allocated between every minute of sonication to prevent overheating of the mitochondrial preparation. The mitochondrial sonicate was ultra-centrifuged at 150 000 x g for 100 minutes. The supernatant contained crude ADX and ADXR, and the pellet insoluble cytochrome P450 mitochondrial enzymes, which could be used to isolate pure substrate-free CYP11B1. The ADX and ADXR protein solution was concentrated in a protein concentrator specifically designed for this purpose (7, 91). The method is based on the osmotic transfer of water to a hydrophilic polymer solution, PEG 35 000 20% (w/v), through a dialysis membrane (MWCO: 3.5 kDa). The 50 mL volume of ADX and ADXR protein solution (supernatant) was concentrated to 6 mL within 3 hours, without loss of biological activity. The concentrated ADX and ADXR solution was stable for a month at -80°C.

4.2.2.3 BCA protein determination assay

The protein concentration of the crude mitochondrial powder and purified CYP11B1 were determined by following the instruction manual of the BCA Protein Assay Kit, as described in Section 3.2.2.6.

4.2.2.4 Cytochrome P450 activity assay

Cytochrome P450 activity assays were performed during each purification step of CYP11B1 to verify that the enzyme remained active and to determine the concentration of CYP11B1 after each purification step. Due to restricted amount of purified enzyme available, the cytochrome P450 activity assay had to be adapted to a 96-well micro-titre plate assay to preserve enzyme for further spectral assays. The total volume required to perform this assay was reduced from 3 mL to 300 µL. CO was bubbled through a purified CYP11B1 preparation.

Equal volumes (150 μL) of the CO saturated enzyme were pipetted into two separate wells of a 96 well micro-titre plate. One well served as the reference well and the second well as the sample well. A baseline was recorded between 400-500 nm. After the baseline recording, 10 μL of sodium dithionite dissolved in deionised water (1 mg/mL) was added to the sample well and an equal volume of deionised water to the reference well. A difference spectrum was recorded between 400-500 nm. The cytochrome P450 content was calculated using the wavelength at 450 nm, an extinction coefficient of $91 \text{ cm}^{-1}\text{mM}^{-1}$ (16) and a path length of 0.47983 cm on a flat bottom well plate.

4.2.2.5 Isolation and purification of substrate bound ovine CYP11B1

The isolation and purification of CYP11B1 from the P450-containing mitochondrial-acetone powder was carried out at 4°C to preserve enzyme activity. All of the isolation and purification buffers contained DOC, to stabilize the enzyme. The purification of CYP11B1 was modified from methods previously published (7, 18, 92).

4.2.2.5.1 Isolation of CYP11B1 from a crude mitochondrial powder

The mitochondrial acetone powder (4 g, 2376 mg protein), was resuspended in 110 mL standard buffer (50 mM potassium phosphate, 100 μM EDTA, 100 μM DTT, and 10 μM DOC, pH 7.4). The mitochondrial suspension was supplemented with Tween₂₀ (0.3%, (v/v)), followed by sonication of the suspension for 30 minutes at 60 Watts on ice. One minute intervals were prescribed between every minute of sonication to prevent the loss of protein activity. The protein concentration of the sonicate was adjusted to 20 mg/mL using the standard buffer. CYP11B1 was extracted from the P450-enriched sonicate by the dropwise addition of 10% sodium cholate to yield a final concentration of 1% sodium cholate. The mixture was stirred for one hour and thereafter subjected to ultra-centrifugation at $105\,000 \times g$ for 104 minutes at 4°C . The resulting supernatant was retained and fractionated with ammonium sulphate. The ammonium sulphate concentration required to fractionate CYP11B1 was between 0 – 32% saturation. The CYP11B1-containing precipitate was stirred for one minute and centrifuged at $12\,000 \times g$ for 15 minutes at 4°C . The resulting pellet was resuspended in standard buffer, containing 1% sodium cholate and 1 M KCl (20 mL) pH 7.4. Alumina γ C gel (380 mg/g mitochondrial pellet) was added to the suspension and stirred for 30 minutes on ice. After the 30 minutes, the Alumina γ C was removed by centrifugation at $12\,000 \times g$ for 10 minutes at 4°C . The resulting supernatant (20 mL) was retained and dialyzed overnight against 2 L standard buffer.

4.2.2.5.2 Purification of CYP11B1

The dialysate which contained precipitated CYP11B1, was collected and subjected to ultra-centrifugation at 100 000 x g for 100 minutes at 4°C. The resulting pellet was resuspended in 8 mL equilibration buffer (standard buffer containing 0.7 % sodium cholate and 200 mM KCl, pH7.4) and stirred for 10 minutes to yield a homogenous sample. As the volume of the sample was small and too sensitive to filter, it was centrifuged at 3000 x g for 5 minutes at 4°C. The supernatant was decanted and used to purify CYP11B1 using HIC on a Phenyl-Sepharose CL-4B column. Phenyl-Sepharose CL-4B resin was prepared according to the instruction manual and packed in an 8 cm x 1 cm column¹. The supernatant (7 mL) was applied onto the resin using a Finnigan Surveyor Auto sampler-plus fitted with a 10 mL sample loop. The column was equilibrated with the equilibration buffer (2 x column volume), or until a stable baseline was obtained. The Bio-Rad NGC chromatographic system was set to measure the absorbance at 280 mAU during the run, at a flow rate of 1 mL/min by using a linear gradient. CYP11B1 was eluted with an elution buffer (standard buffer containing 0.5 % sodium cholate, 500 mM KCl, 0.5 % Tween₂₀ pH7.4). The elution profile of CYP11B1 is summarized in **Table 3**.

Table 3. Chromatographic elution profile for CYP11B1

	Time (minutes)	Flow (mL/min)	% Washing buffer	% Elution buffer
1	0.01	1	100	0
2	12	1	0	100
3	62	1	100	100
4	72	1	100	0
5	90	1	0	0

Cytochrome P450 activity assays were performed on all the fractions and only the active fractions were collected (20 mL) and re-concentrated with ammonium sulphate (0-32%) for four hours. The precipitate was centrifuged at 12 000 x g for 10 minutes and the resulting pellet resuspended in 5 mL dialyzing buffer (standard buffer, containing 0.3 % sodium cholate, 0.3 % Tween₂₀, pH 7.4). The purified substrate-bound CYP11B1 was dialyzed against 1 L dialyzing buffer for 5 hours and subsequently used to prepare a substrate-free CYP11B1

¹ This commercially available resin replaced the aniline-Sepharose CL-4B resin previously used for the purification of CYP11B1. Aniline Sepharose CL-4B is not commercially available and had to be prepared using highly toxic cyanogen bromide (CNBr) to activate Sepharose CL-4B prior to aniline coupling (92).

preparation. The substrate-bound CYP11B1 preparation (5 mL) contained 11.563 nmol P450/mg protein.

4.2.2.6 SDS-PAGE analyses of purified CYP11B1 and ADX/ADXR

SDS-PAGE analyses of the purified substrate-bound CYP11B1 and the crude ADX/ADXR preparation were performed as previously published (93). Briefly, protein samples (25 μ L) were electrophoresed using 12% polyacrylamide gels for 40 minutes at 4°C and 200 V. Precision Plus Protein™ Kaleidoscope™ Standard marker (10-250 kDa) was used to monitor protein separation. After the electrophoretic separation of the protein samples, the individual gels were placed in separate holders and stained for 60 minutes with Coomassie Brilliant Blue R-250 staining solution (3 mM Coomassie R-250, in 10% acetic acid and 45% methanol). The staining solution was decanted and the gels placed in 30 mL destain 1 solution ((50% (v/v) methanol, 10% (v/v) acetic acid) for 60 minutes. After 60 minutes destain 1 solution was replaced with 30 mL destain 2 solution (20% (v/v) methanol, 7% (v/v) acetic acid), overnight after which the protein bands were visualised and photographed.

4.2.2.7 Western Blot analysis of CYP11B1 and ADX/ADXR

Western blot analyses were performed after the separated protein samples were transferred from the SDS-PAGE gels to Bio-Trace NT pure nitrocellulose blotting membranes (93). After the 90-minute transfer step at 4°C, 110 V, the surface of the nitrocellulose membranes was blocked, by gently agitating the membranes with 20 mL casein buffer (10 mM Tris, pH 7.6, 0.15 M NaCl, 0.5% (*m/v*) casein) for 30 minutes at 37°C. Thereafter, the casein buffer was replaced with fresh casein buffer (20 mL) and the membrane incubated with the respective primary anti-bodies for 60 minutes at 37°C. Rabbit anti-sheep against CYP11B1 (1:4000), rabbit anti-sheep against adrenodoxin (1:6000) and rabbit anti-sheep against ADXR (1:6000) were used as the primary antibodies for the detection of CYP11B1 and ADX/ADXR, respectively. After the 60 minutes, the casein buffer was decanted and the membranes washed 4 times with a 0.5% Tween₂₀-PBS solution. Each washing step was carried out for four minutes. Each membrane was subsequently incubated with goat-anti-rabbit secondary antibody (1:20 000 in casein buffer) for 60 minutes at 37°C after which the membranes were washed 4 times as described. Each membrane was incubated with a 1:1 ratio of Pierce ECL Western Blotting chemiluminescent substrate reagent for one minute. The chemiluminescent substrate reagent was decanted and the individual blots developed using Fuji medical X-ray film (Fuji Photo Film Co.) with an exposure time ranging from 5-10 seconds.

4.2.2.8 Preparation of substrate-free CYP11B1

As previously mentioned, CYP11B1 is extremely unstable when released from its membrane and substrate and readily converts to its inactive P420 form within one hour. Therefore, during the purification, an excess of DOC is added to all buffers to stabilize the enzyme and preserve activity. However, the mechanism of action of the *R*- and *S*-enantiomers of CpDA can only be determined when the substrate is removed and the heme-iron converts back into the low-spin state. Therefore, substrate-free CYP11B1 was prepared with the aid of dextran coated charcoal (DCC) as previously described (13, 18, 26). All experimental procedures were carried out at 4°C.

4.2.2.8.1 Preparation of dextran-coated charcoal (DCC)

Dextran T70 (0.1 g) was dissolved in 200 mL Tris-buffer (10 mM, pH 8) containing EDTA (1 mM) and NaCl (150 mM) and stirred for 10 minutes, until a homogenous solution was obtained. Norit A charcoal (1 g) was added to the homogenous solution and stirred for four hours at 25°C. Three millilitre of the resulting DCC suspension was centrifuged at 12 000 x g for 10 minutes. The pellet was washed three times by resuspension in standard buffer and centrifugation at 12 000 x g. After the final wash, the DCC pellet was resuspended in standard buffer (1 mL).

4.2.2.8.2 Preparation of substrate-free CYP11B1 with the aid of DCC

The DCC-suspension (100 µL) was added to the purified substrate-bound CYP11B1 (1 mL). The resulting mixture was stirred for 15 minutes, after which the mixture was placed in a specially designed centrifuge tube into which a 0.45 µm filter membrane was fitted (**Figure 43**). With the aid of centrifugation at 3000 x g for 3 minutes, the substrate-free enzyme mixture was filtered through to the sample collection chamber. To ensure that all the steroid was removed from the enzyme, the DCC-suspension (100 µL) was added to the filtrate, containing substrate-free CYP11B1, and the same process was repeated. As the substrate-free CYP11B1 remained active for one hour after the removal of the steroid, all spectral assays therefore had to be carried out within that time-frame.

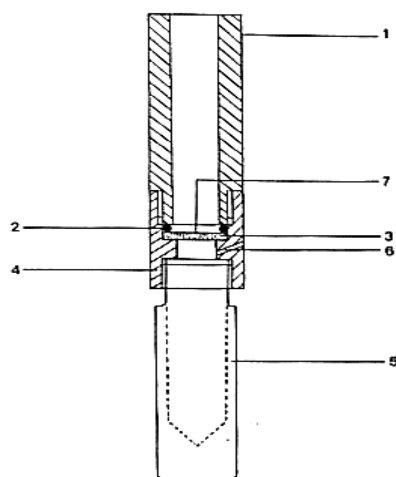


Figure 43. Schematic representation of the specially designed centrifuge tube. The sample application chamber (1) is connected to a 1 mL reactivial sample collector chamber (5), screwed into one another by the membrane support holder (4). The 0.4 µm filter membrane (7), cut to the right size using a punch, is supported by a porous poly-ethylene membrane support (3) and sealed by an O-ring (2). An air vent placed at a 65° angle on the sample application chamber prevents air trapping in the system. Redrawn from (18).

4.2.2.9 Spectral assays

The influence of the *R*- and *S*-enantiomers of CpDA on the spectroscopic properties of purified CYP11B1 was investigated using a modified previously reported method (7, 18, 87). Due to the limited volume of purified substrate-free CYP11B1 the spectral assays were not recorded on a Cary UV-100 spectrophotometer in 1.5 mL cuvettes as previously published, but on a Spark™ 10M multimode microplate reader (96-well micro-titre plates). As discussed in Chapter 2, only a specialized spectrophotometer can be used to record the difference spectra of turbid samples. Therefore, before any spectral assays were performed with the purified enzyme, this method was optimized for the microplate reader using partially purified CYP11B1. A similar inhibitory profile was obtained in both the Cary 100 UV spectrophotometer and the multimode microplate reader, therefore the modified method could be used to determine the mechanism of interaction of the *R*- and *S*-enantiomers of CpDA with purified CYP11B1. Due to the labile nature of the substrate-free enzyme, the amount needed for each experiment was freshly prepared prior to each experiment.

4.2.2.9.1 Spectral Assay A - DOC-induced difference spectra

The design setup for the DOC-induced difference spectrum is shown in **Table 4**. The buffer used for Well 1 and Well 2 (control) was standard buffer (without DOC). The final concentration of inhibitor (CpDA, and the *R*- and *S*-enantiomers of CpDA, respectively) in Well 3 and Well 4 was 750 μM . The DOC concentration was increased from 3.21 μM to 10 μM to give a better response.

Table 4. Design protocol for Spectral Assay A.

Baseline recording				Add substrate and record
Control	Well 1	196 μL purified substrate-free CYP11B1	4 μL buffer	2 μL ethanol
	Well 2	196 μL purified substrate-free CYP11B1	4 μL buffer	2 μL DOC (10 μM)
Inhibitor	Well 3	196 μL purified substrate-free CYP11B1	4 μL of Inhibitor (750 μM)	2 μL ethanol
	Well 4	196 μL purified substrate-free CYP11B1	4 μL of Inhibitor (750 μM)	2 μL DOC (10 μM)

Control

A baseline was recorded between 360-500 nm for both Wells 1 and 2. Ethanol was added to Well 1 and the DOC solution was added to Well 2 and a spectrum recorded between 360-500 nm for each well. After baseline correction, for both Wells 1 and 2, the absorbance values of the ethanol containing well (Well 1) was subtracted from the absorbance values from the DOC containing well (Well 2) to obtain a difference spectrum.

Inhibitor

The same protocol as described under control was carried for each respective inhibitor (CpDA, the *R*-enantiomer, and the *S*-enantiomer) in Wells 3 and 4. The percentage inhibition was calculated by using the equation presented in Section 3.2.2.8.1.

4.2.2.9.2 Spectral Assay B – inhibitor-induced difference spectrum

The design setup for the inhibitor-induced difference spectrum is shown in **Table 5**.

Table 5 . Design protocol for Spectral Assay B

Baseline recording			Add inhibitor and record
CpDA	Well 1	196 μ L purified substrate-free CYP11B1	4 μ L dH ₂ O
	Well 2	196 μ L purified substrate-free CYP11B1	4 μ L CpDA (200 μ M)
R-enantiomer	Well 3	196 μ L purified substrate-free CYP11B1	4 μ L dH ₂ O
	Well 4	196 μ L purified substrate-free CYP11B1	4 μ L R-enantiomer (200 μ M)
S-enantiomer	Well 5	196 μ L purified substrate-free CYP11B1	4 μ L dH ₂ O
	Well 6	196 μ L purified substrate-free CYP11B1	4 μ L S-enantiomer (200 μ M)

A baseline was recorded between 360-500 nm for both wells for each respective inhibitor (CpDA, *R*- and *S*-enantiomer). Distilled water was added to the reference wells (1, 3 and 5) whereas the respective inhibitor was added to the sample wells (2, 4 and 6) and a spectrum recorded between 360-500 nm for each well. After baseline correction, for all the reference and sample wells of the respective inhibitors, the absorbance values of the reference wells (1, 3 and 5) was subtracted from the absorbance values from the inhibitor containing wells (2, 4 and 6) to obtain a difference spectrum.

4.2.2.10 Influence of the CpDA and the *R*- and *S*-enantiomers on the partially purified ADX/ADXR electron transport system

The activity of the crude mixture of ADX/ADXR electron transport system was determined by a modification of a previously published method (7, 14, 90). This method was modified to use a 96-well micro-titre plate instead of 2.5 mL quart cuvettes. All reagents were dissolved in a phosphate buffer (0.02 M, pH 7.4). In order to test the activity of the electron transport reductase system, cytochrome c was used as the electron acceptor. The reaction was initiated by the addition of NADPH (1 mM, 4 μ L) to the reaction mixture.

Reference well

- The incubation mixture of the reference well comprised of cytochrome c (50 nmol, 50 μ L), 50 μ L of a phosphate buffer (0.02 M, pH 7.4), glucose-6-phosphate (G6P) (1 μ mol, 50 μ L) and glucose-6-phosphate dehydrogenase (G6PD) (0.32 U, 50 μ L).

Sample well

- The incubation mixture of the sample well comprised of the same incubation mixture except for the phosphate buffer which was replaced with the ADX/ADXR solution (50 μ L).

Sample well with inhibitor

- The influence of an inhibitor on the reduction of cytochrome c was tested by adding 5 μ L of the inhibitor into the incubation mixture. The incubation mixture comprised of cytochrome c (50 nmol, 50 μ L), 45 μ L of ADX/ADXR solution, 5 μ L of inhibitor with two concentrations (750 μ M and 375 μ M), G6P (1 μ mol, 50 μ L) and G6PD (0.32 U, 50 μ L).

After pre-incubating the reaction mixtures for 5 minutes at 25°C, NADPH (0.04 M, 4 μ L) was added to initiate the reaction. The total volume in each well was 204 μ L. The reduction of cytochrome c was monitored at 550 nm. The reduction of cytochrome c was calculated by using an extinction coefficient of 29.5 $\text{cm}^{-1}\text{mM}^{-1}$ and a path length of 0.60561 cm (90).

4.3 Results and discussion

4.3.1 Isolation and purification of purified substrate-free CYP11B1

The present study involved the isolation and purification of substrate-free CYP11B1. The unique spectroscopic properties of the highly purified enzyme were used to investigate the influence (inhibition) of the CpDA enantiomers on the DOC-induced difference spectrum and their ability to bind CYP11B1 in the absence of substrate and induce a Type II difference spectrum (inhibitor-induced difference spectrum). The results of the spectral assay of the enantiomers were compared to the racemic mixture of CpDA. In the second part of this study, the influence of the inhibitors on the reduction of cytochrome c by the ADX/ADXR electron transport system was investigated, since the compounds may also inhibit the enzyme by interfering with the transfer of electrons.

4.3.1.1 Cytochrome P450 activity assay of partially purified CYP11B1

Prior to the isolation and purification of substrate-bound CYP11B1, a cytochrome P450 activity assay was undertaken to determine both the concentration and the activity of the P450-enriched mitochondrial preparation. The results from this assay, depicted in **Figure 44**, show a maximum peak at 450 nm, with a deep trough at approximately 405 nm and a shallow trough starting at 480 nm. The P450-enriched mitochondrial preparation was free from P420 and could therefore be subjected to the next step in the isolation and purification of CYP11B1. The cytochrome P450 concentration was calculated to be 2.350 nmol/mg protein.

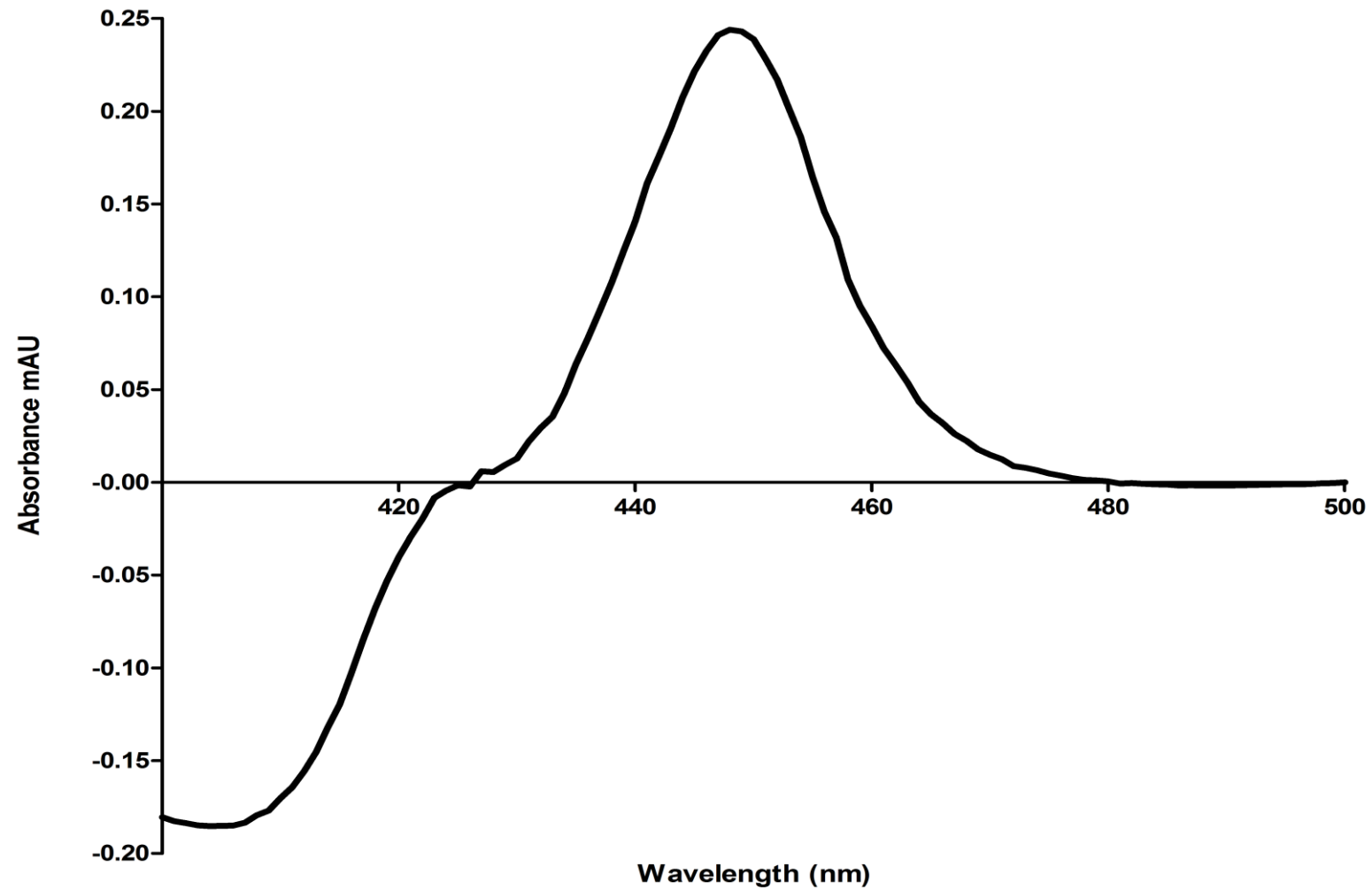


Figure 44. CO-induced difference spectrum of mitochondrial preparation containing CYP11B1. Mitochondrial preparation, 20 mg/mL standard buffer; [P450], 2.350 nmol P450/mg protein.

4.3.1.2 Elution profile of purified substrate-bound CYP11B1 from ovine adrenal

CYP11B1 was purified by using preparative HIC on a Phenyl-Sepharose column at 4°C. The elution profile of purified substrate-bound CYP11B1 is shown in **Figure 45**. Two peaks (Peak 1 and Peak 2) were eluted during the chromatographic separation. The fractions constituting Peak 1 were eluted with equilibration buffer (standard buffer, supplemented with 0.7 % sodium cholate and 200 mM KCl, pH 7.4), whereas the fractions constituting Peak 2 were eluted with elution buffer (standard buffer, supplemented with 0.5% sodium cholate, 500 mM KCl and 0.5% Tween₂₀, pH 7.4).

To determine whether the fractions from Peak 1 and 2 contained active CYP11B1, a cytochrome P450 activity assay was performed for each fraction from Peak 1 and 2. As shown in **Figure 46** Peak 1 contained only P420. This indicated that the CYP11B1 in this fraction was converted to its inactive form and no further studies could be performed using these fractions. The fractions constituting Peak 2, shown in **Figure 47**, had a maximum absorbance at 450 nm, indicating that these fractions contained active, substrate-bound CYP11B1. Fractions 13 and 14, however, had a small trough at 420 nm, therefore to preserve activity, Fractions 13 and 14 were excluded from further purification procedures, whereas fraction 15-18 were collected and concentrated with ammonium sulphate and dialysed. The CYP11B1 concentration of the pooled fraction was 8.327 nmol/mg protein.

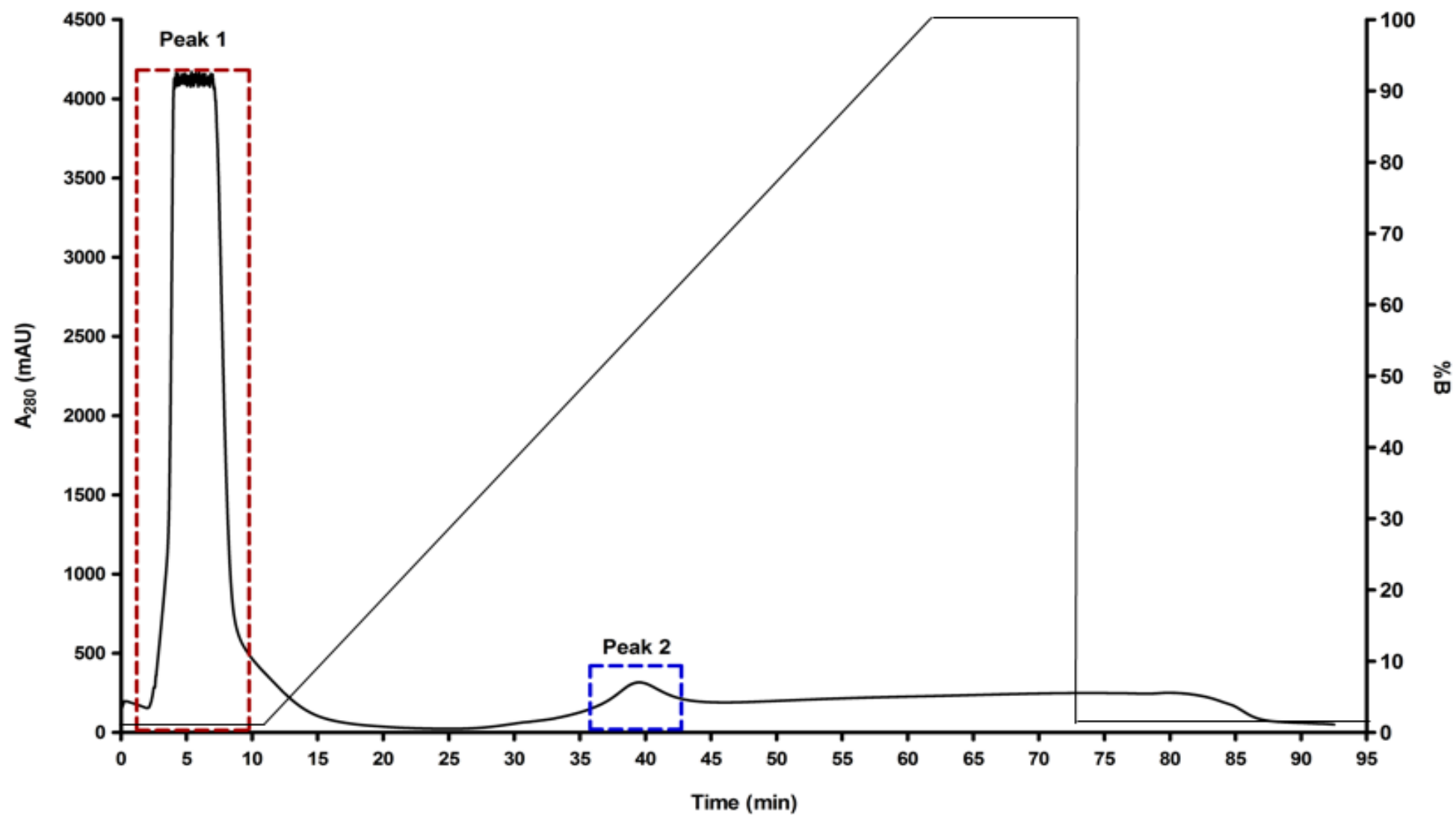


Figure 45. Elution profile of substrate-bound CYP11B1. The dialysed CYP11B1 was applied to an equilibrated Phenyl-Sepharose CL-4B column (8 cm x 1 cm), washed with equilibration buffer, and eluted at 1 mL per minute, with an elution buffer.

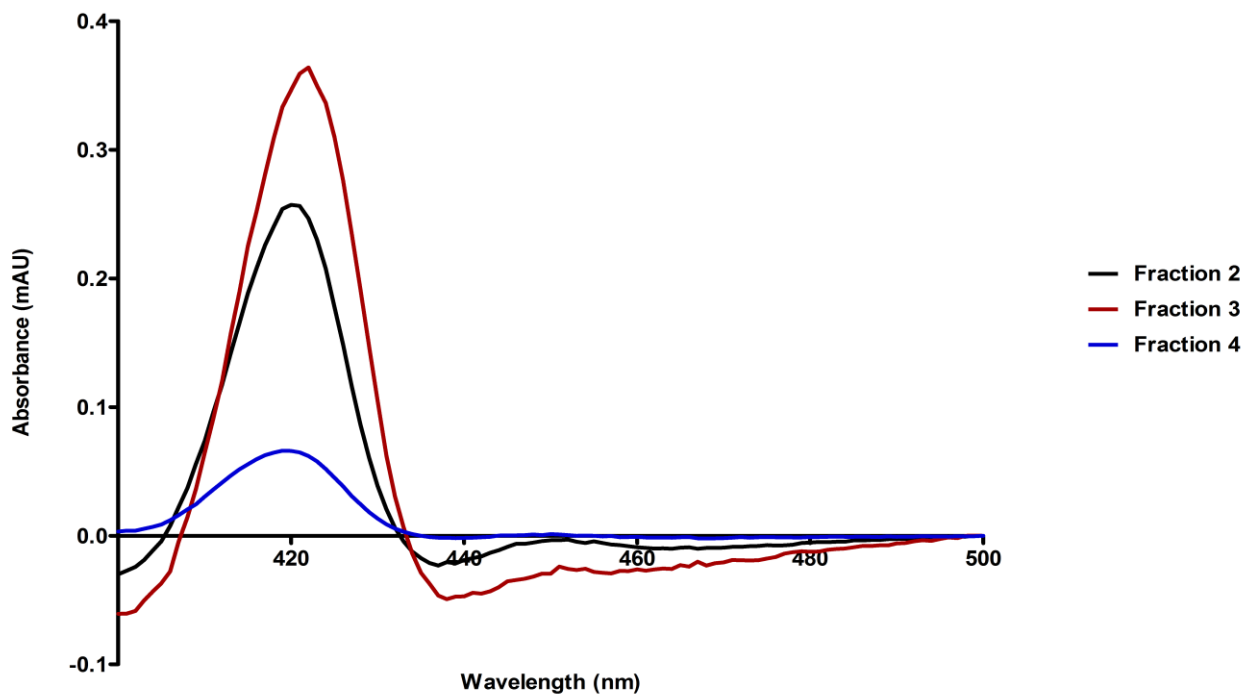


Figure 46. CO-induced difference spectrum of collected Fractions 2-4, (Fig 45 peak 1). The maximum at 420 nm represents the inactive form of CYP11B1.

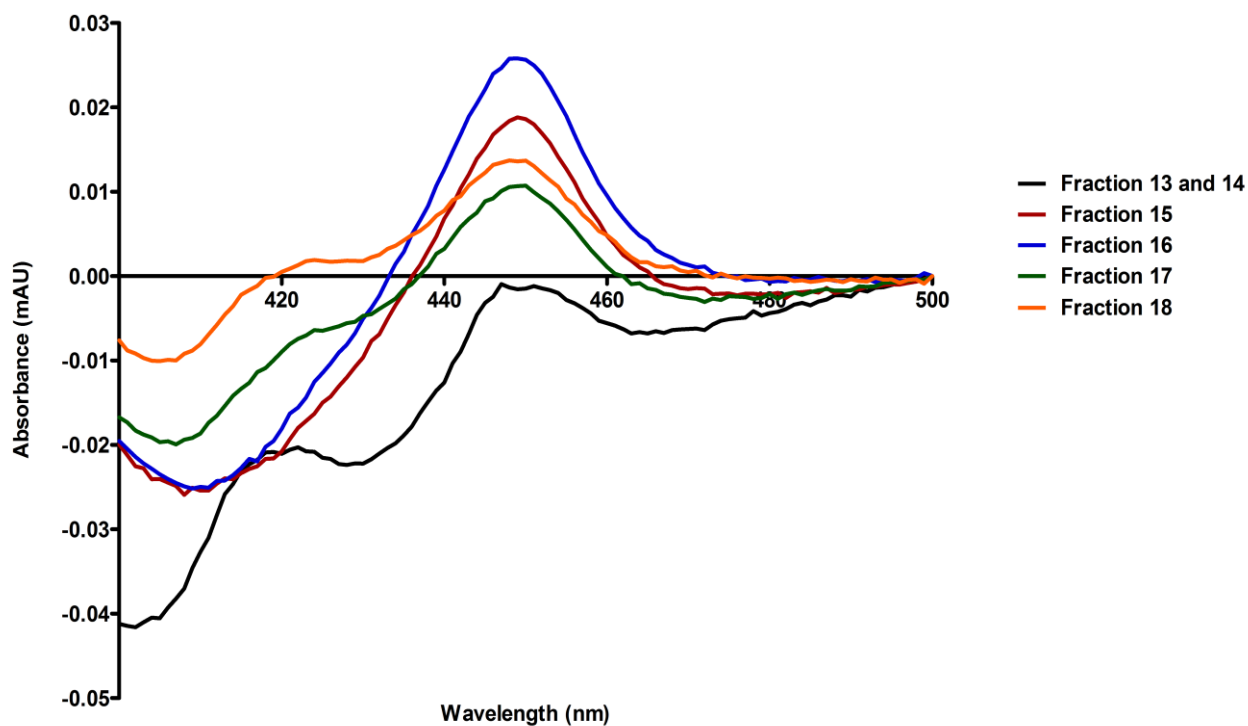


Figure 47. CO-induced difference spectrum of collected Fractions 13-18 (Fig 45 peak 2). The peak at 450 nm represents the active form of CYP11B1. The concentration of the pooled chromatographic fractions was 8.327 nmol/mg protein.

4.3.1.3 SDS-PAGE and Western blot analysis of purified CYP11B1

The purity of CYP11B1 in respective fractions eluted from Peak 1 and Peak 2 was analysed using SDS-PAGE analysis. As shown in **Figure 48 A**, Lanes 2, 3 and 4 represent a 10 x dilution of Fractions 2 (20 µg protein), 3 (25 µg protein) and 4 (7.5 µg protein) collected from Peak 1, while lanes 5, 6 and 7, contain Fractions 16 (15 µg protein), 17 (13 µg protein), 18 (10 µg protein) collected from Peak 2. Lane 8, represents the pooled fractions 15-18 collected from Peak 2 (18 µg protein), depicting the apparent molecular mass of substrate-bound CYP11B1, as previously reported in our laboratory (18). A 30 x dilution (12.30 µg protein) of the crude CYP11B1 preparation prior to HIC, was used as a positive control (Lane 9).

SDS-PAGE analysis revealed that the Phenyl-Sepharose resin successfully separated CYP11B1 from the other mitochondrial proteins, as a single protein band at approximately 46 kDa is shown in Lane 5-8. The protein bands in Lane 2, 3, 4 and 9 indicate the presence of the larger CYP11A1 protein, CYP11B1, CYP11B2, as well as ADX and ADXR.

Although the mitochondrial preparation had been subjected to ultra-centrifugation, with the mitochondrial proteins (CYP11A1, CYP11B1 and CYP11B2) remaining in the pellet and the redox proteins (ADX and ADXR) in the supernatant, it is possible that the redox proteins bound to the mitochondrial proteins' sediment in the pellet. Therefore, it is possible that the faint band visible in Lane 5-8 at ±10 kDa may be residual ADX bound to the enzyme, with the enzyme freed from its redox partner under the denaturing electrophoreses conditions.

A duplicate gel was subjected to Western blot analysis and probed using rabbit anti-sheep CYP11B1 IgG against as primary anti-body and goat anti-rabbit IgG as the secondary anti-body. The immunoblot results are shown in **Figure 48 B**. The antibodies recognised a single band in lanes representing Fractions 16, 17, 18 and the pooled chromatographic fractions.

The purity of CYP11B1 from ovine adrenals was thus confirmed by SDS-PAGE and Western blot analyses.

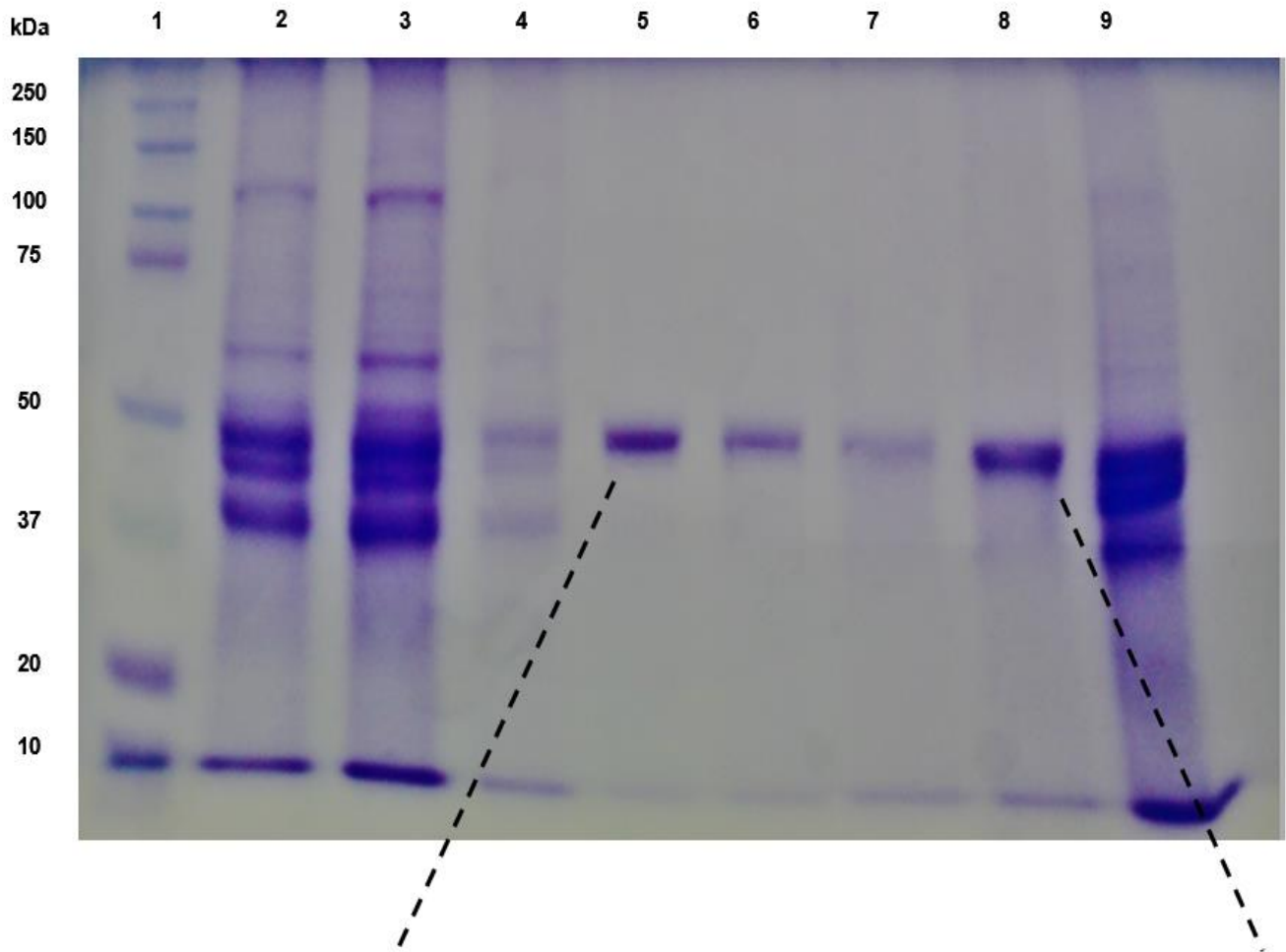
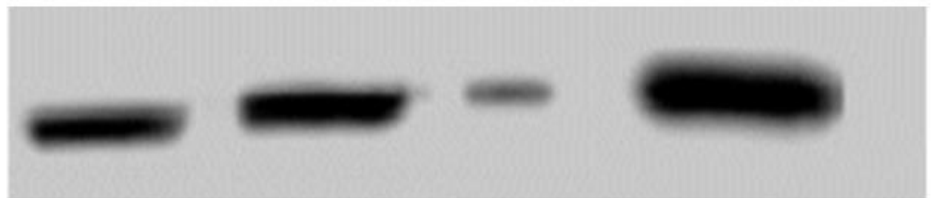
A.**B.**

Figure 48. (A) SDS-PAGE analysis of purified-substrate bound CYP11B1 with apparent molecular mass of 46 kDa. Column eluate samples were separated on a 12% gel. Lane 1: Precision Plus Protein™ Kaleidoscope™ marker (10-250 kDa); Lane 2, fraction 2, 10 x dilution 20 µg protein; Lane 3, fraction 3, 10 x dilution 25 µg protein; Lane 4, Fraction 4, 10 x dilution 7.5 µg protein; Lane 5, Fraction 16, 15 µg protein; Lane 6, Fraction 17, 13 µg protein; Lane 7, Fraction 18, 10 µg protein; Lane 8, pooled chromatographic fractions of 2nd elution peak, 18 µg protein; and Lane 9 partially purified extract, 30 x dilution 12.30 µg protein. (B) Western blot analysis of purified substrate-bound CYP11B1. Lanes 1 – 3, fractions 16, 17 and 18; and Lane 4 pooled chromatographic fractions of 2nd elution peak. CYP11B1 was detected with rabbit anti-sheep IgG against CYP11B1 (1:4000) and goat anti-rabbit IgG (1:20 000) was used as the secondary antibody. Immunoblot bands were visualised by chemiluminescence.

4.3.1.4 Degree of purity of substrate-bound CYP11B1

The degree of purity of the substrate-bound CYP11B1 was determined spectrophotometrically by performing a cytochrome P450 activity assay as well as a protein determination after each major purification step (**Table 6**).

Table 6. Purification table for CYP11B1 isolated from ovine adrenals

Purification step	Volume (mL)	Protein (mg)	Total CYP11B1 (nmol)	Specific activity (nmol/mg)	Purification factor	Yield (%)
Crude extract	118	2376.92	5585.77	2.350	1.00	100
Ammonium sulphate precipitate fraction	105	980.50	3730.33	3.805	1.62	66.78
HIC chromatography on a Phenyl-Sepharose column	20	122.56	1020.60	8.327	3.54	18.27
CYP11B1-reconcentrate with ammonium sulphate	5	16.80	194.26	11.563	4.92	3.48

CYP11B1 was successfully purified using preparative HIC on a Phenyl-Sepharose CL-4B resin. The purity of CYP11B1 was increased 5-fold, which was comparable with results previously reported by our laboratory (18). Loss of enzyme activity was, however, seen after the chromatography step, which can be attributed to the incomplete precipitation after the dialysis step. The final concentration of substrate-bound CYP11B1 was 11.56 nmol/mg protein.

4.3.1.5 Cytochrome P450 activity assay of substrate-free CYP11B1

A cytochrome P450 activity assay was carried out before DOC- or inhibitor-induced difference spectra were performed to establish whether the purified substrate-free enzyme had remained active after the removal of the stabilizing substrate. The result of this cytochrome P450 activity assay is illustrated in **Figure 49**.

A cytochrome P450 activity assay was performed immediately after the filtration process, which is shown in black. A maximum peak at 450 nm was observed with a shallow trough at 480 nm indicating that the substrate-free CYP11B1 was active. The cytochrome P450 concentration of the substrate-free CYP11B1 immediately after the filtration process was 10.950 nmol/mg protein.

To establish the rate of CYP11B1 decay, the enzyme activity was monitored at 5 minute intervals. After 45 minutes a maximum peak at 420 nm was seen, with a small peak visible at 450 nm indicating a $\pm 90\%$ conversion to inactive P420.

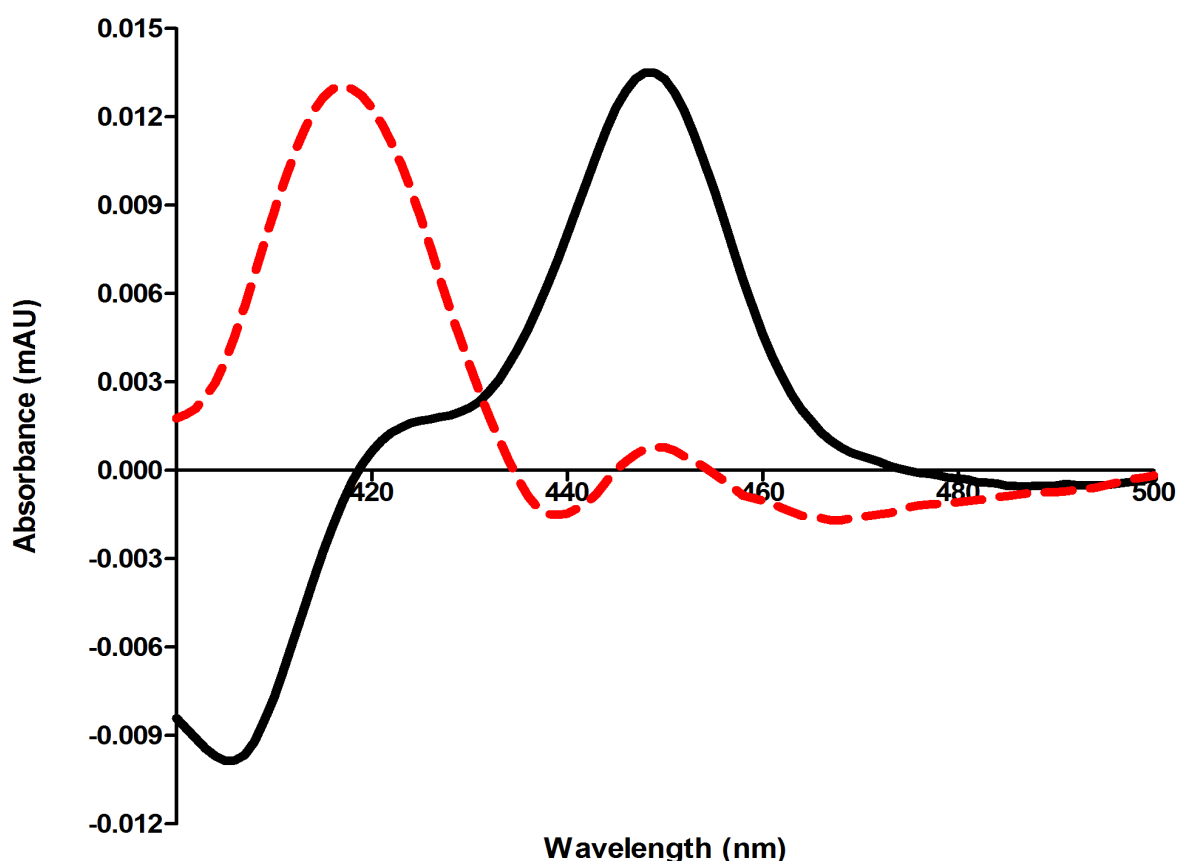


Figure 49. CO-induced difference spectrum of reduced purified substrate-free CYP11B1 in standard buffer. [CYP11B1] = 10.950 nmol P450/mg protein; black trace, CYP11B1 immediately after the filtration process; red trace; CYP11B1 after a 45 minutes;

4.3.1.6 Spectral assays with substrate-free CYP11B1

CYP11B1 was extremely labile when released from DOC, as seen in **Figure 49**. Loss of enzyme activity was therefore expected and thus only a limited time was available to perform spectral assays. Furthermore, due to the total amount of purified enzyme (5 mL) available, careful planning was key to the successful recording of the DOC-induced difference spectra.

4.3.1.6.1 DOC/inhibitor-induced difference spectra with substrate-free CYP11B1

The difference spectra were performed in duplicate by the 96-well micro-titre plate assay and data presented as the mathematical mean. The influence of the racemic mixture of CpDA, and the *R*- and *S*-enantiomers of CpDA on the DOC-induced difference spectrum of purified CYP11B1 is shown in **Figure 50**, **Figure 51** and **Figure 52**, respectively.

As described in Chapter 3, CpDA, at a concentration of 750 μM , inhibited the DOC-induced difference spectra of CYP11B1 by $\pm 50\%$. The same concentration of inhibitor was therefore used as a standard for all substrate-induced difference spectra of purified CYP11B1.

As shown in **Figure 50 A**, the amplitude of the DOC-induced difference spectrum of purified CYP11B1 was reduced significantly with CpDA inhibition of the difference spectrum being 52.30%. Additionally, when CpDA was added to the enzyme in the absence of DOC, a typical Type II difference spectrum was induced, with an absorbance maximum at 430 nm and absorbance minimum at 412 nm (**Figure 50 B**). These results corroborated previous studies which showed that CpDA binds to the active site of CYP11B1 and inhibits the binding of DOC to the enzyme. Furthermore, CpDA (200 μM) was shown to have the ability to induce a Type II difference spectrum as it stabilizes the low-spin state of the iron (27).

In the presence of the *R*-enantiomer, the amplitude of the DOC-induced difference spectrum was also reduced but to a lesser degree compare to the reduction by CpDA (**Figure 51 A**). The *R*-enantiomer inhibited DOC binding by 14.90%, indicating that the *R*-enantiomer was ± 3.5 -fold less effective than racemic CpDA. Furthermore, the addition of the *R*-enantiomer (200 μM) in the absence of DOC to CYP11B1 induced a Type II difference spectrum, with a maximum and minimum at 430 and 412 nm, respectively (**Figure 51 B**). The Type II spectrum induced by the *R*-enantiomer had a similar Type II profile as the spectrum induced by CpDA.

Under the same conditions, the *S*-enantiomer inhibited the DOC-induced difference spectrum by 35.18% (**Figure 52 A**). The *S*-enantiomer was 1.5-fold less effective than the racemic mixture of CpDA. Interestingly, the inhibitory effect of both the *R*- and *S*-enantiomers combined was 50.08%, which is equivalent to the percentage inhibition induced by the racemic mixture of CpDA (52.30%). In a paper by Mentel *et al.* (94) they describe three modes for enantiomers of a chiral compound to bind the active site of a protein: the protein is selective for one

enantiomer in a racemic mixture, the R- and S-enantiomers can bind to the protein individually and both enantiomers can bind to the active site of the protein, simultaneously. This result obtained from the spectral assays could possibly mean that the inhibitory effect induced by the racemic mixture of CpDA could be due to both the enantiomers binding to the active site simultaneously.

Furthermore, when the S-enantiomer (200 μ M) was added to CYP11B1 in the absence of DOC, a Type II difference spectrum was induced (**Figure 52 B**). However, the S-enantiomer induced a distorted Type II profile when compared to CpDA and the R-enantiomer, as two maxima were observed at 445 nm and 470 nm and a minimum absorbance at 408 nm, respectively. As previously mentioned, CpDA is classified as a mixed inhibitor of ovine CYP11B1. CpDA, therefore, has the ability to inhibit the enzyme in a competitive or uncompetitive manner (27). The mixed inhibitory effect of CpDA can therefore be attributed to a manner in which the individual enantiomers bind to the active site of CYP11B1.

The results obtained from the spectral assays revealed that the inhibitory effect induced by the racemic mixture of CpDA is significantly reduced when the enantiomers are separated. Furthermore, the results also suggest that the enantiomers bind simultaneously to the active site of CYP11B1 from ovine adrenals, however further experimental work is required.

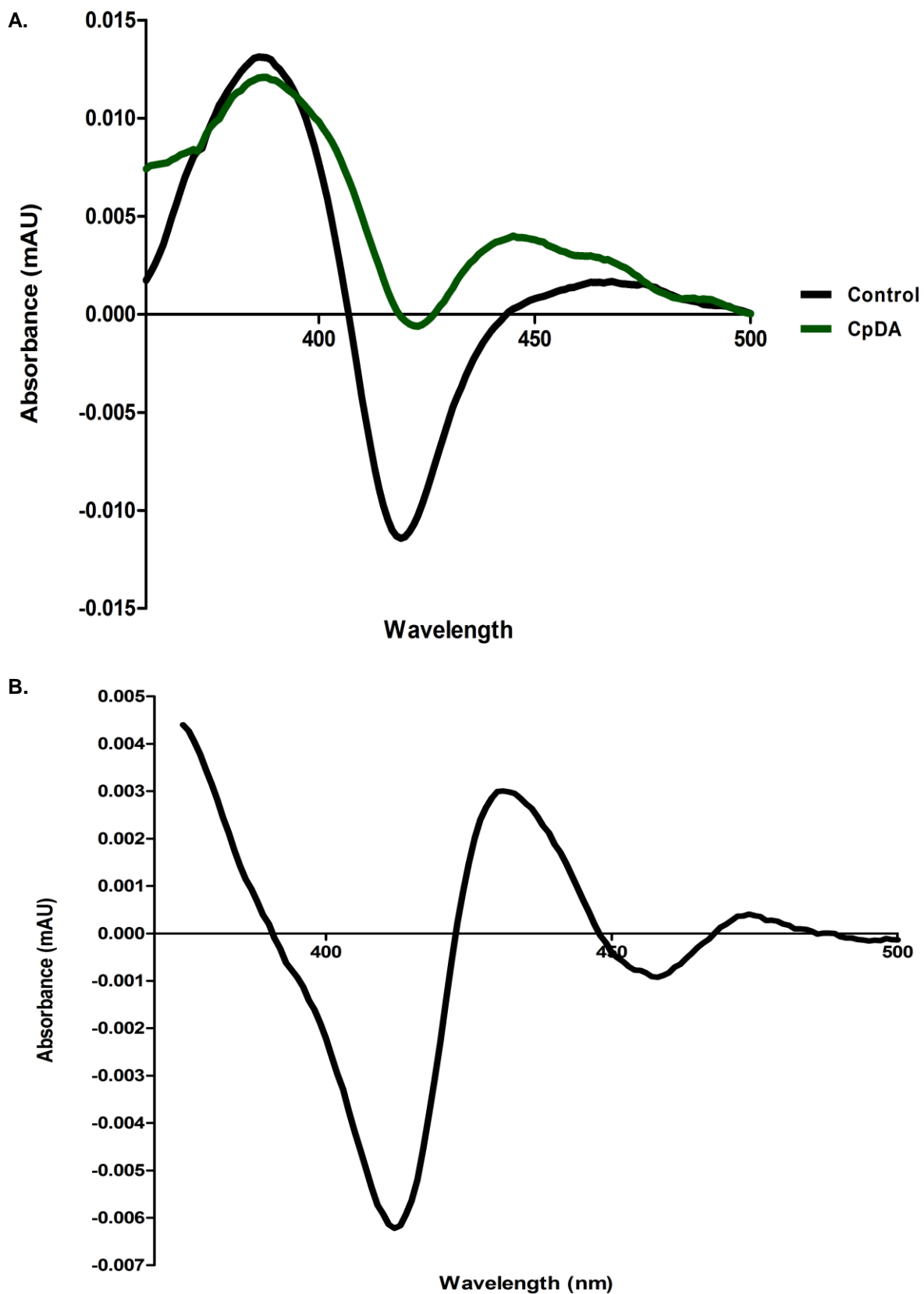


Figure 50. (A) Influence of the racemic mixture of CpDA on the DOC-induced difference spectra with purified CYP11B1. CpDA, 750 μ M, inhibition, 52.30%; [CYP11B1] = 10.950 nmol/mg protein. [DOC] = 10 μ M. (B) CpDA-induced Type II difference spectrum of purified CYP11B1. [CYP11B1] = 10.950 nmol/mg protein. [DOC], 10 μ M; and [CpDA], 200 μ M.

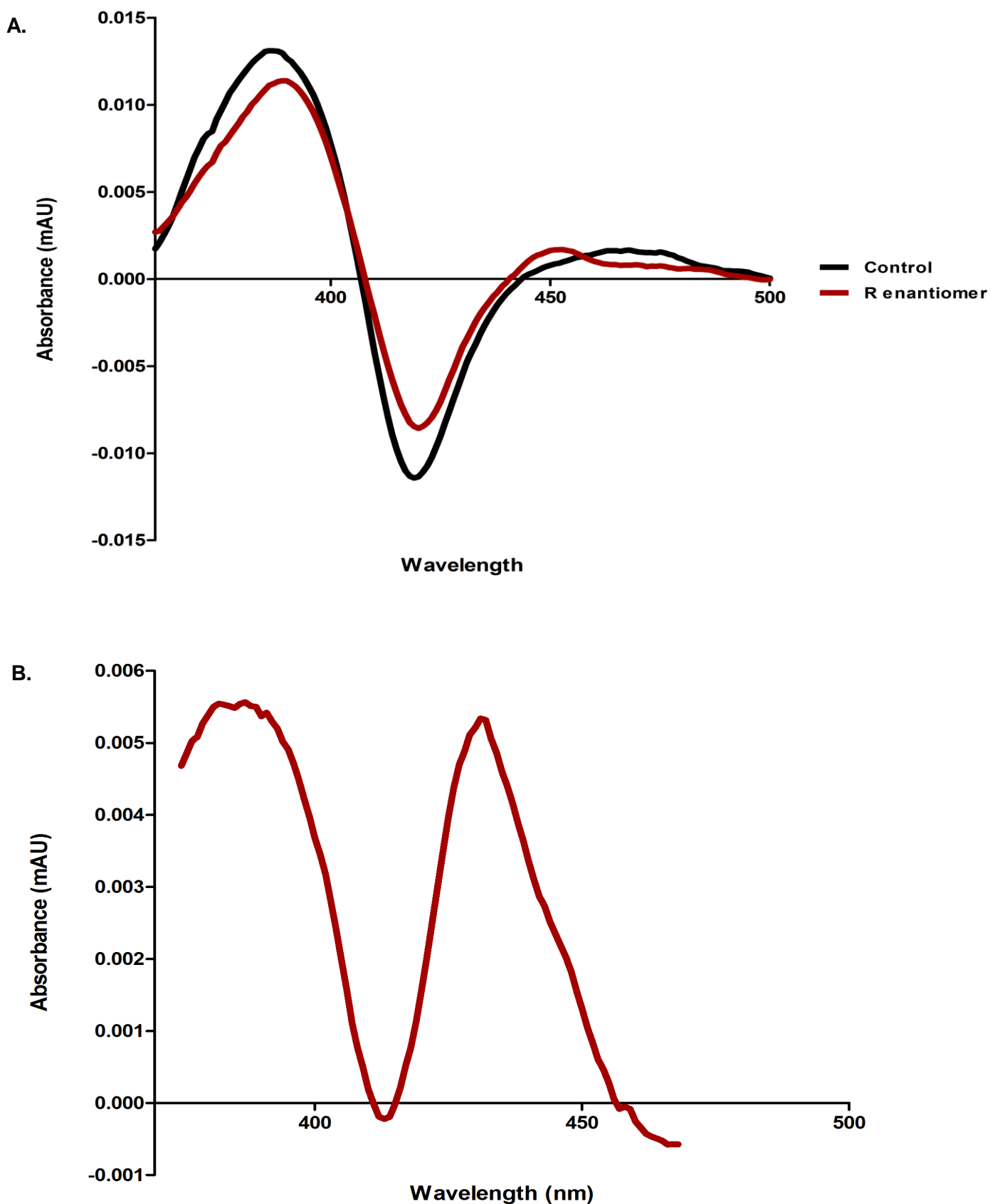


Figure 51. (A) Influence of the *R*-enantiomer of CpDA on the DOC-induced difference spectra with purified CYP11B1. *R*-enantiomer, 750 μ M, inhibition, 14.90%; [CYP11B1] = 10.950 nmol/mg protein. [DOC] = 10 μ M. (B) *R*-enantiomer of CpDA-induced Type II difference spectrum of purified CYP11B1. [CYP11B1] = 10.950 nmol/mg protein. [DOC], 10 μ M; and [CpDA], 200 μ M.

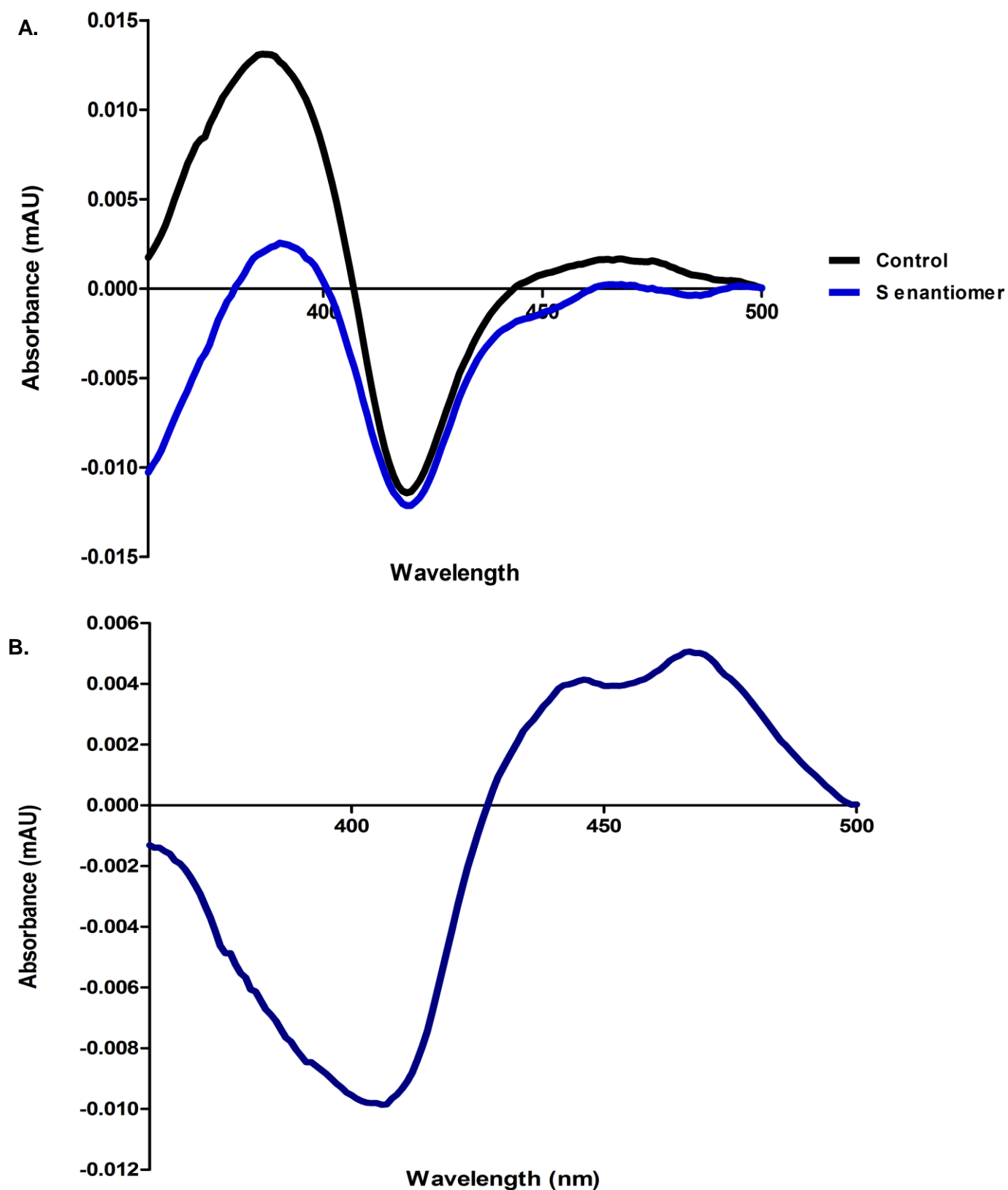


Figure 52. (A) Influence of the S-enantiomer of CpDA on the DOC-induced difference spectra with purified CYP11B1. S-enantiomer, 750 μ M, inhibition, 35.18%; [CYP11B1] = 10.950 nmol/mg protein. [DOC] = 10 μ M. (B) S-enantiomer of CpDA-induced Type II difference spectrum of purified CYP11B1. [CYP11B1] = 10.950 nmol/mg protein. [DOC], 10 μ M; and [CpDA], 200 μ M.

4.3.2 Isolation of the adrenal mitochondrial electron transport chain

ADX and ADXR were prepared to determine whether the *R*- and *S*-enantiomers of CpDA and the racemic mixture of CpDA has an effect on the adrenal mitochondrial steroid electron transport system. Cytochrome *c* was used as the terminal electron acceptor and the reduction of cytochrome *c* was monitored spectrophotometrically by a modification of the method previously published (14, 90).

4.3.2.1 SDS PAGE and Western blot analysis of isolated ADXR/ADX

ADX and ADXR were isolated from partially purified adrenal mitochondria from ovine adrenals and concentrated by using PEG 35 000. Both the crude and concentrated ADXR/ADX solution were subjected to SDS-PAGE and Western blot analysis. The results obtained in the SDS-PAGE analysis (**Figure 53 A**) show distinct bands in both lanes 2 and 3 at \pm 48 kDa and 10 kDa corresponding to the apparent molecular mass of ADXR and of ADX, respectively. Lane 2 represents the crude ADX/ADXR solution, whereas lane 3 represents the concentrated ADXR/ADX solution.

Western blot analysis was carried out to confirm that the distinct bands in the SDS-PAGE gels were ADXR and ADX, shown in **Figure 53 B and C**. Because different primary antibodies were required to identify ADXR and ADX, two separate blots were prepared. A single band was detected in Lane 1 and 2 using rabbit anti-sheep ADX IgG shown in **Figure 53 B**, with Lane 1 representing the crude ADXR/ADX solution and Lane 2 the concentrated ADXR/ADX solution. Shown in **Figure 53 C** is the second immunoblot in which rabbit anti-sheep ADXR IgG was used to detect the ADXR protein band. Lane 1 and 2 of the ADXR blot represents the crude ADXR/ADX solution and concentrated ADXR/AXD solution, respectively.

In both immunoblots, the concentrated ADXR/ADX protein mixture had a more intense signal when compared to the crude ADXR/AXD protein, indicating that ADXR and ADX were indeed concentrated from the crude solution. The presence of ADXR and ADX was therefore confirmed by SDS-PAGE and Western blot analyses.

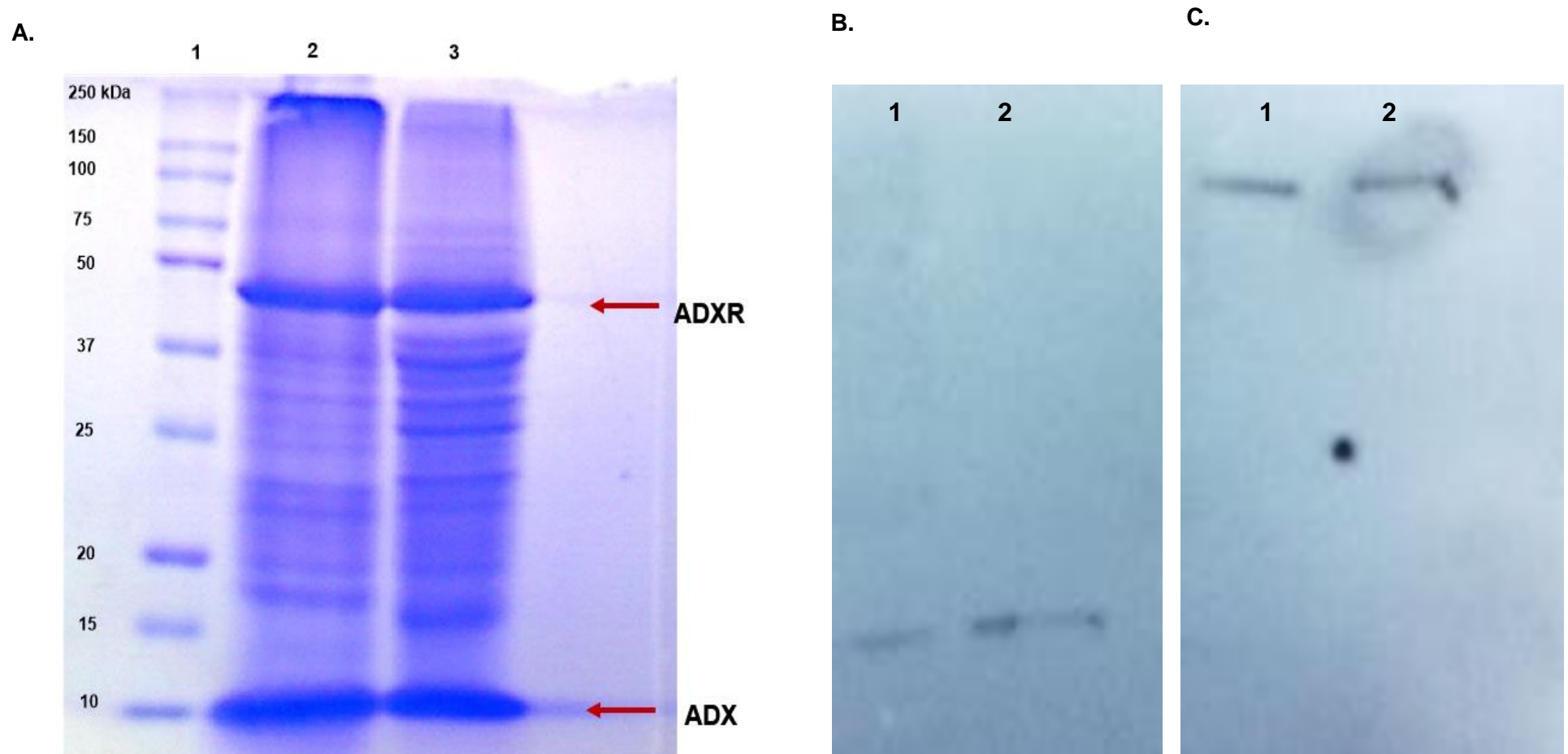


Figure 53. (A) SDS-PAGE of ADX and ADXR. Lane 1, Kaleidoscope protein marker; Lane 2, crude ADXR/ADX preparation; and Lane 3 concentrated ADXR/ADX preparation. In each lane, 20 μ g protein was loaded. (B) Western blot analysis of ADX. Lane 1, crude ADXR/ADX preparation and Lane 2, concentrated ADXR/ADX preparation. In each lane, 20 μ g protein was loaded. Rabbit anti-sheep ADX IgG 1:6000. (C) Western blot analysis of ADXR. Lane 1, crude ADXR/ADX preparation and Lane 2, concentrated ADXR/ADX preparation. In each lane, 20 μ g protein was loaded. Rabbit anti-sheep ADXR IgG, 1:6000; goat anti-rabbit IgG (1:20 000).

4.3.2.2 The influence of CpDA and the enantiomers of CpDA on the reduction of cytochrome c by the ADX/ADXR electron transport system

Before the influence of racemic CpDA and the *R*- and *S*-enantiomers on the reduction of cytochrome c could be determined, the activity of ADX/ADXR needed to be established. The activity of the concentrated ADX/ADXR preparation was therefore monitored spectrophotometrically at 550 nm and was calculated from the amount of cytochrome c (nmol) reduced per second using a millimolar extinction coefficient of reduced cytochrome c, $29.5 \text{ cm}^{-1} \text{ mM}^{-1}$ (90).

After pre-incubation for 5 minutes at 25°C, NADPH was added to both the incubation mixtures in the reference well (without ADX/ADXR) and sample well (with ADX/ADXR) to initiate the reaction. As shown in **Figure 54**, the red trace represents the sample well and the black trace the reference well. In the absence of ADX/ADXR, the reducing equivalents from NADPH could not reduce cytochrome c, therefore the absorbance reading remained constant and a straight line (black trace) was observed at approximately 0.522 mAU. The red curve clearly indicates the increase in the absorbance at 550 nm due to the reduction of cytochrome c. The reduction plateaued at ± 60 seconds and at 100 seconds complete reduction of cytochrome c was reached as the NADPH concentration was not limiting. The amount of cytochrome c reduced was calculated using a millimolar extinction coefficient of $29.5 \text{ cm}^{-1} \text{ mM}^{-1}$ and a path length of 0.60561 cm (90).

The influence of CpDA, at two concentrations, on the reduction of cytochrome c is shown in **Figure 55 A**. The blue curve represents CpDA at 750 μM and the green curve at 375 μM . Data suggested that CpDA inhibited the initial reaction rate when compared to control without the compound (red curve). A plateau is reached after 110 seconds compared to the 100 seconds in the absence of CpDA. The reduction of cytochrome c was analysed by fitting a linear regression model on the linear section of the curve and the results are shown in **Figure 55 B**. The initial rate of cytochrome c reduction by the ADXR/ADX preparation without inhibitor was 0.01008 nmol/sec (0.01 nmol/sec). In the presence of CpDA (750 μM and 375 μM), the rate of cytochrome c reduction was 0.007474 nmol/sec (0.0075 nmol/sec) and 0.007915 nmol/sec (0.008nmol/sec), respectively. As the influence of CpDA on the mitochondrial electron transport chain was not directly concentration dependent, it can be assumed that CpDA does not have a significant influence on the reduction of cytochrome c via the ADX/ADXR electron transport system.

The influence of the *R*-enantiomer and the *S*-enantiomer on the reduction of cytochrome c is shown in **Figure 56 A** and **Figure 57 A**, respectively. In **Figure 56 A**, the orange curve represents the *R*-enantiomer at 750 μM and the light-green curve at 375 μM . The purple curve

in **Figure 57 A** represents the *S*-enantiomer at 750 μM and the light-blue curve at 375 μM . It appears that both the *R*- and *S*-enantiomer behave similarly to CpDA, as the respective enantiomers also inhibit the initial rate when compared to the control. In the absence of inhibitor, the plateau was reached at 100 seconds while the *R*- and *S*-enantiomers of CpDA reached a plateau after 110 seconds, comparable to racemic CpDA.

The reduction of cytochrome *c* was analysed by fitting a linear regression model on the linear section of the curve. The effect of the *R*- and *S*-enantiomers on the reduction of cytochrome *c* are shown in **Figure 56 B** and **Figure 57 B**, respectively. The initial rate cytochrome *c* reduction by the ADXR/ADX preparation without inhibitor (red-curve) in both **Figure 56 B** and **Figure 57 B** was 0.01 nmol/sec. In the presence of the *R*-enantiomer at 750 μM and 375 μM , the rate of cytochrome *c* reduction was 0.0077 nmol/sec and 0.0083 nmol/sec respectively (**Figure 56 B**). In the presence of the *S*-enantiomer, 750 μM and 375 μM , the rate of cytochrome *c* reduction was 0.0077 nmol/sec and 0.0084 nmol/sec respectively (**Figure 57 B**). As the influence of the *R*- and *S*-enantiomers of CpDA on the adrenal mitochondrial electron transport chain was not concentration-dependent, it can be assumed that neither the *R*-enantiomer or the *S*-enantiomer had a significant influence on the reduction of cytochrome *c* by the ADX/ADXR electron transport system.

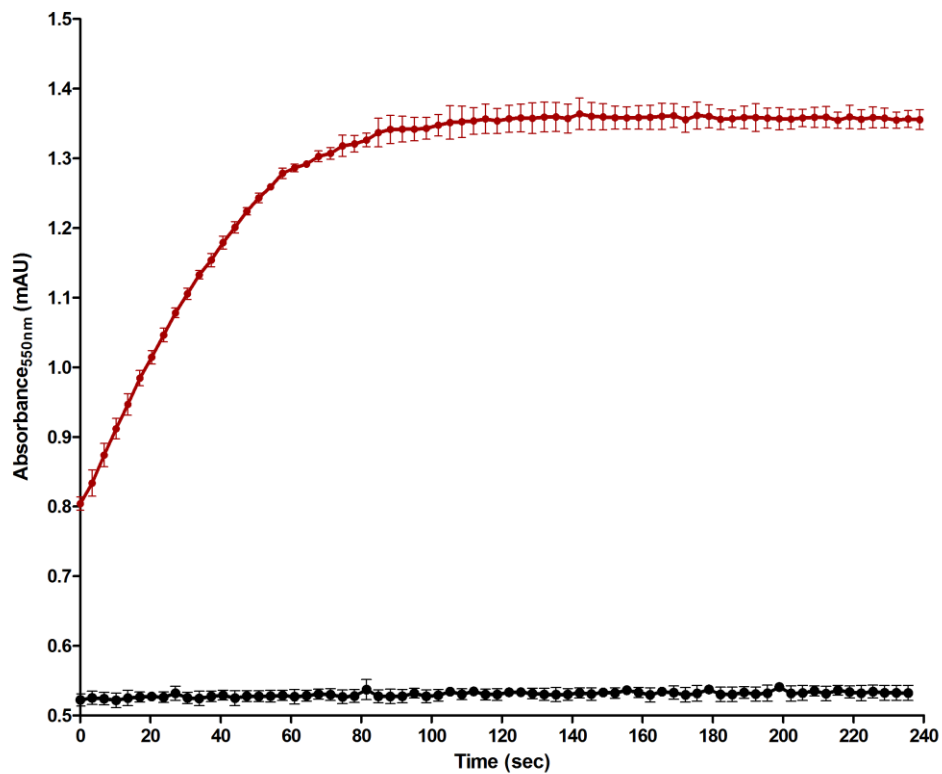


Figure 54. Reduction of cytochrome c by the ADX/ADXR electron transport system. The red curve represents the incubation mixture of the sample well (cytochrome c, ADX/ADXR, G6P and G6PD). The black line represents the incubation mixture of the reference well without the ADX/ADXR preparation.

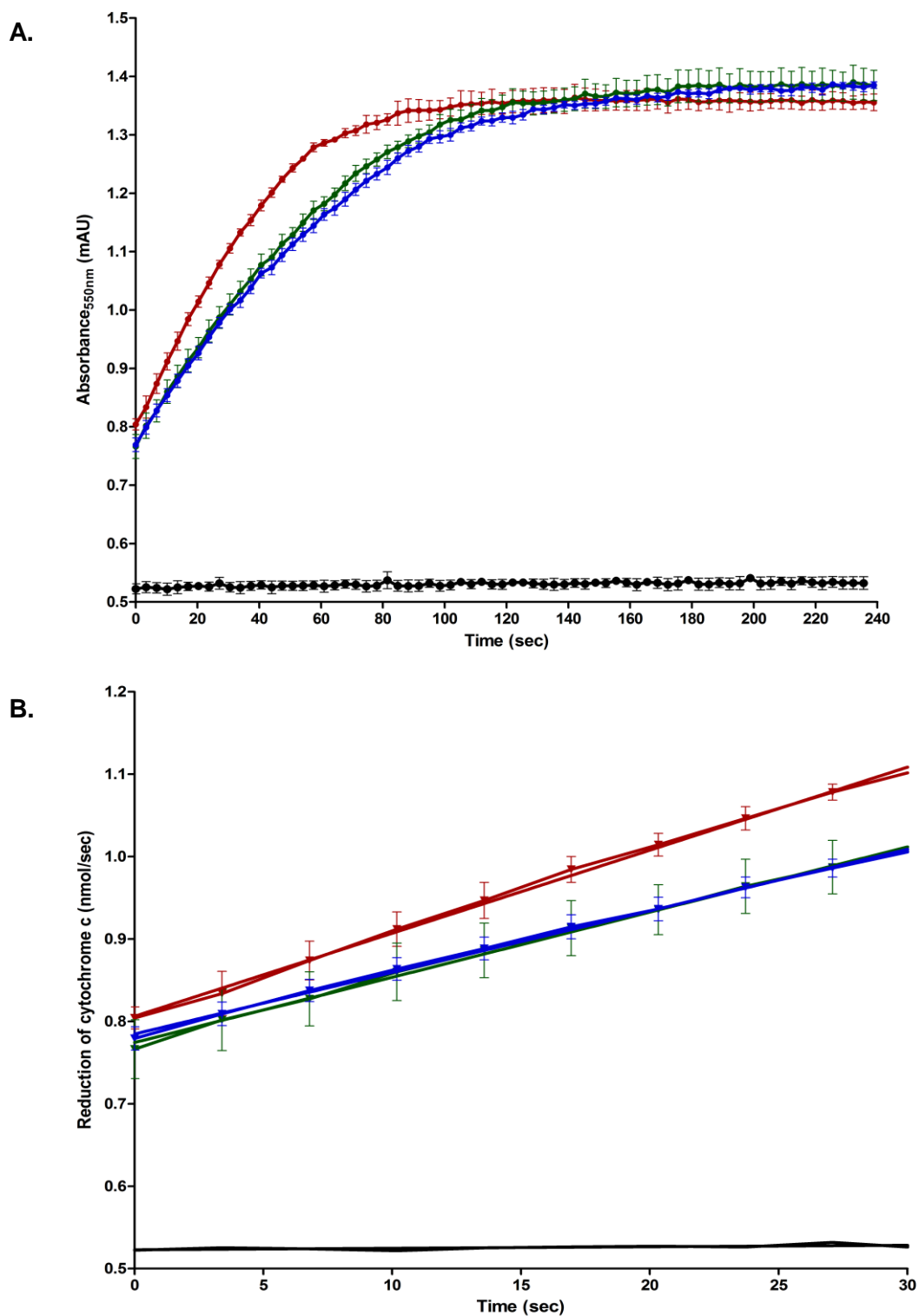


Figure 55. (A) Reduction of cytochrome c by the ADX/ADXR electron transport system. The red curve represents the incubation mixture of the sample well (cytochrome c, ADX/ADXR, G6P and G6PD). The black line represents the incubation mixture of the reference well without the ADX/ADXR preparation. The blue curve represents the incubation mixture with racemic CpDA, 750 μ M, and the green curve the incubation mixture with racemic CpDA, 375 μ M. (B) Linear regression of the first 30 seconds of the curves.

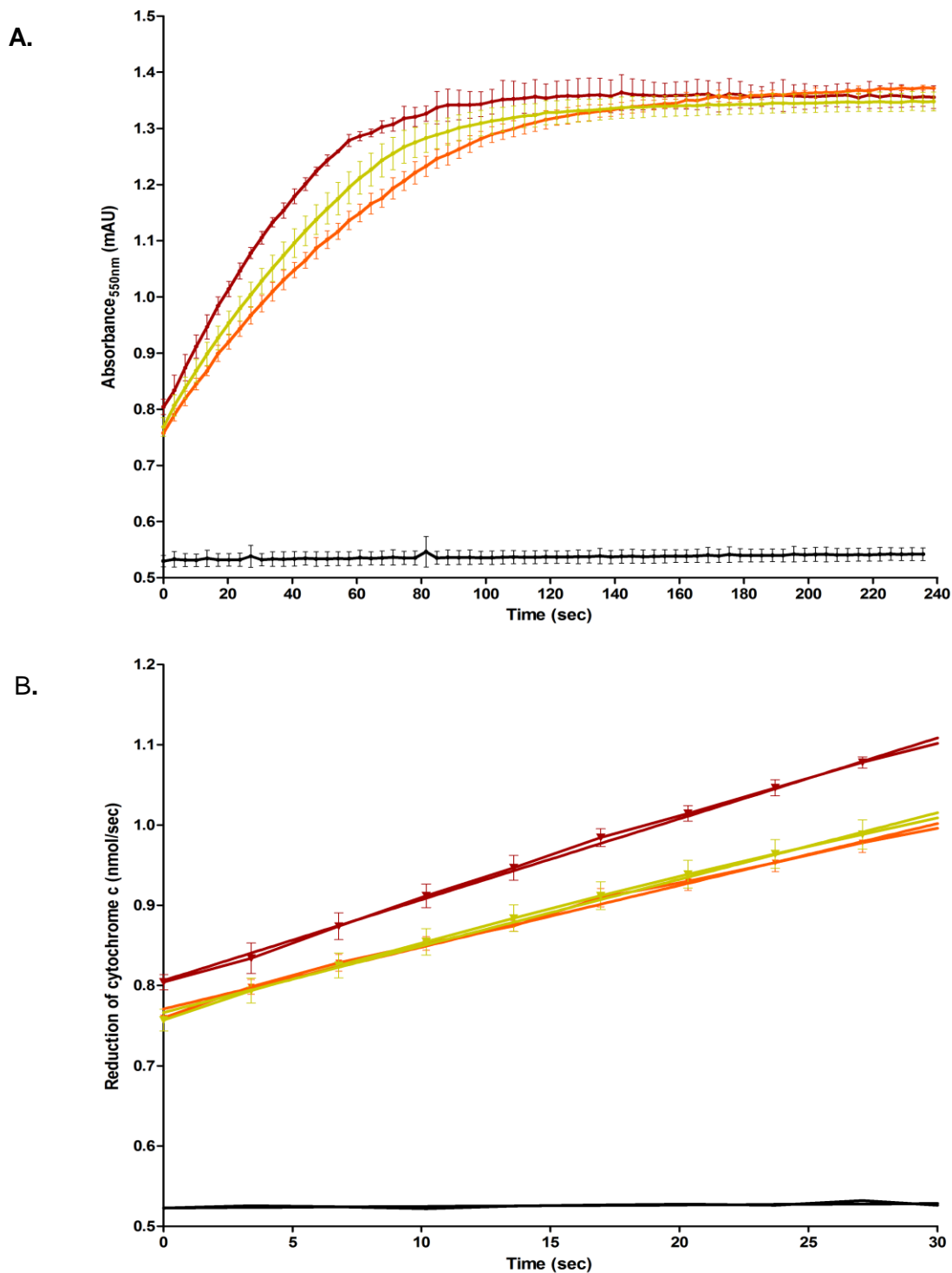


Figure 56. (A) Reduction of cytochrome c by the ADX/ADXR electron transport system. The red curve represents the incubation mixture of the sample well (cytochrome c, ADX/ADXR, G6P and G6PD). The black line represents the incubation mixture of the reference well without the ADX/ADXR preparation. The orange curve represents the incubation mixture with the *R*-enantiomer, 750 μM , and the light green curve the incubation mixture with the *R*-enantiomer, 375 μM . (B) Linear regression of the first 30 seconds of the curves.

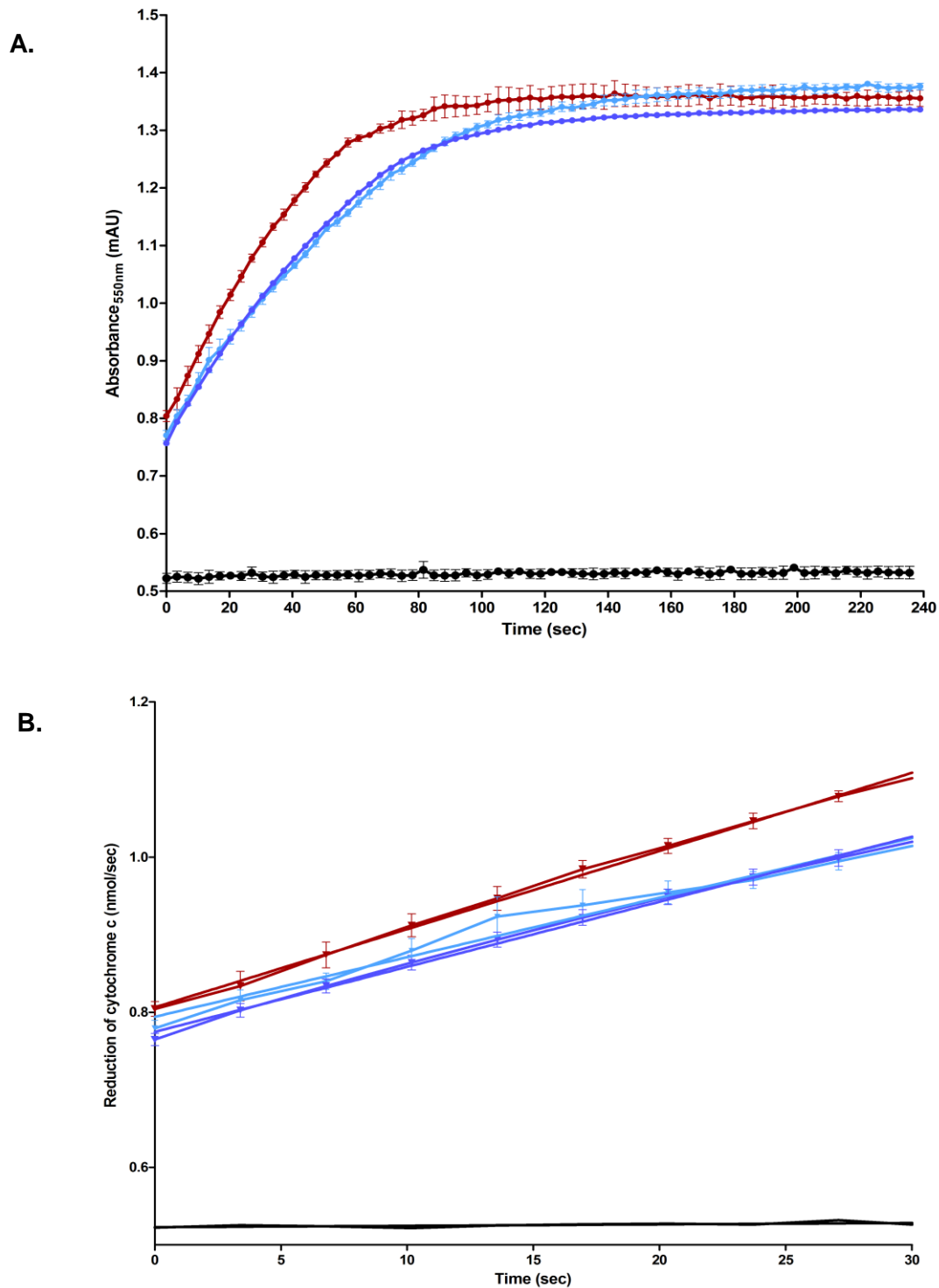


Figure 57. (A) Reduction of cytochrome c by the ADX/ADXR electron transport system. The red curve represents the incubation mixture of the sample well (cytochrome c, ADX/ADXR, G6P and G6PD). The black line represents the incubation mixture of the reference well without the ADX/ADXR preparation. The purple curve represents the incubation mixture with the *S*-enantiomer, 750 μM , and the light blue curve the incubation mixture with the *S*-enantiomer, 375 μM . **(B)** Linear regression of the first 30 seconds of the curves.

4.4 Conclusion

This study aimed to investigate the influence of the *R*- and *S*-enantiomers of CpDA on the spectral properties of CYP11B1 and the adrenal mitochondrial electron transport system.

In our laboratory CYP11B1 was previously isolated and purified from ovine adrenals using preparative HIC on an aniline-Sepharose resin. Aniline-Sepharose is, however, not commercially available and has to be prepared by the CNBr activation of Sepharose CL-4B followed by the coupling of aniline to the activated Sepharose resin. This procedure involves two toxic chemicals, aniline, which has to be distilled prior to use, and CNBr. Due to the toxic nature of these substances, a modified method was employed for the purification of CYP11B1, which involved replacing the aniline-Sepharose resin with commercially available Phenyl-Sepharose CL-4B resin. By employing this modified method, substrate-bound CYP11B1 was successfully purified from a P450-enriched mitochondrial powder from ovine adrenals, resulting in a \pm 5-fold purification, with a recovery yield of 3.5% (**Table 6**). These results were comparable to previous studies in our laboratory (purification fold 5% and recovery yield 2.9%) using the aniline-Sepharose resin (18). The substrate, DOC, was used to stabilize CYP11B1, however, as membrane-bound enzyme are highly labile when released from their membranes, loss of enzyme activity was expected during the purification process. The loss of enzyme activity could be attributed to the incomplete precipitation after the dialysis steps. From this data it can be concluded that the new resin served as a safer and effective alternative to purify CYP11B1.

It has previously been reported in our laboratory that the molecular weight of CYP11B1 from ovine adrenals is 46 kDa (18). SDS-PAGE and Western blot analysis confirmed the presence of CYP11B1, with a prominent single band at approximately 46 kDa, as shown in **Figure 48 A** and **B**. There was, however, a faint protein band visible at \pm 10 kDa in Lane 5-8 of the acrylamide gel, indicating the presence of residual ADX bound to CYP11B1, with the enzyme freed from its redox partner under the denaturing electrophoreses conditions.

DOC stabilises the high spin-state of the heme-iron of CYP11B1 (7, 18, 27). Therefore, before any spectral assays could be completed, the conversion of the heme-iron of CYP11B1 back into the low-spin state form was a prerequisite. This removal of DOC from substrate-bound CYP11B1 was achieved using DCC, to adsorb the steroid, and a combination of filtration and centrifugation to separate the steroid from the substrate-free CYP11B1 solution. After the removal of DOC, the substrate-free CYP11B1 was extremely unstable and complete loss of enzyme activity resulted within one hour (**Figure 49**).

Spectral assays were employed using a modified technique, which involved down-scaling from 1.5 mL quartz cuvettes to a 96-well micro-titre assay. Due to the limited time that the

substrate-free enzyme remained active and the amount of purified enzyme available, the modified technique served as an effective and efficient means to investigate the mechanism of action of the *R*- and *S*-enantiomers of CpDA.

It was previously reported that CpDA inhibits the DOC-induced difference spectrum and also induces a Type II difference spectrum in the absence of substrate in CYP11B1 (27). Results presented in this chapter (**Figure 50 A and B**), confirmed these reports. Furthermore, the results obtained in the spectral assays have revealed that both the *R*- and *S*-enantiomers of CpDA also inhibited the DOC-induced difference spectrum of CYP11B1 and induced Type II difference spectra (**Figure 51 and Figure 52**). Interestingly, it was found that separating the single enantiomers of CpDA did not increase its inhibitory profile. In fact, the results suggest that total inhibitory effect induced by the racemic mixture of CpDA, can be attributed to the combined effect of both the *R*- and the *S*-enantiomers. Furthermore, it was found that the *S*-enantiomer displayed a completely different or distorted Type II difference spectrum when compared to the racemic mixture of CpDA and the *R*-enantiomer.

CpDA was previously reported to act as both a competitive and uncompetitive inhibitor, suggesting that CpDA can bind in a reversible manner to the active site of CYP11B1 and prevent substrate-enzyme complex formation or CpDA can bind to the enzyme-substrate complex and cause structural distortion of the active site (27). Previous results have also suggested that that enantiomers of a chiral compound can bind simultaneously to the active site of an enzyme (94). Results obtained from the spectral assays in this study suggest that the *R*- and *S*-enantiomer bind simultaneously to CYP11B1 but in different regions of the active site of the enzyme to induce an inhibitory response, however further studies would be required to confirm this finding. Furthermore, as shown with the purified substrate-free CYP11B1, the inhibition of the enzyme by CpDA and the *R*- and *S*-enantiomers of CpDA occurs at the enzyme-substrate level as the compounds had no significant effect on the electron transport system confirmed in the unhindered ADXR/ADX-catalysed reduction of cytochrome *c*.

To summarize, whether the initial hypothesis that either the *R*- or *S*-enantiomers of CpDA could be linked specifically to a more effective inhibitory profile remains uncertain. While the *S*-enantiomer exhibits a greater inhibitory effect on substrate binding than the *R*-enantiomer, their combined inhibition reflects that of CpDA. It should however be noted that the enantiomers were not present at the same concentrations in CpDA with the *R*- and *S*-enantiomers being present at $\pm 11.5:1$ in the racemic mixture of the synthesised compound. Given the molar distribution and, together with the fact that the *S*-enantiomer exhibited a greater inhibitory effect on substrate/CYP11B1 binding, it could be concluded that this enantiomer may be the more effective compound in terms of both the *R*-enantiomer as well as CpDA. However, future studies are required to confirm this statement.

CHAPTER 5

General discussion

Since the first study conducted with S2, the natural counterpart from the shrub *Salsola tuberculata* in the early 1960s, our understanding of CpDA has advanced substantially. We now know that, not only does CpDA interfere with the terminal reaction in the adrenal glucocorticoid biosynthesis pathway, but it has also been identified as a non-steroidal multi-target AR and GR modulator, with the potential to treat various inflammatory and auto-immune diseases, as well as certain cancers (30). Because the unique pharmacological properties of CpDA allow it to be a prospective candidate to treat various diseases and clinical conditions associated with AR and GR signalling, it was important to investigate a method whereby its therapeutic range could be improved. Therefore, in an attempt to enhance its pharmacological properties and gain further insight into the mechanism of action of CpDA, this study aimed to separate the enantiomers of CpDA and elucidate the biochemical mechanism of action of the respective enantiomers using the spectroscopic properties of CYP11B1.

The first aim of this study was to synthesize a racemic mixture of CpDA. This racemic mixture was subsequently used to separate the *R*- and *S*-enantiomers from the racemate. It also served as a standard while investigating the mechanism of action of the respective enantiomers. Precautionary steps, such as working in a dark and in an oxygen free environment, were taken to preserve its activity during synthesis. LC-Q-ToF/ESI-MS, ¹H-NMR and ¹³C-NMR spectroscopy confirmed the successful synthesis of CpDA, while CYP11B1 spectral assays confirmed biological activity. Impurities present in the racemic mixture of the compound could not be completely removed. The yield obtained was, however, considered to be sufficient to proceed to the chiral resolution of the *R*- and *S*-enantiomers of CpDA.

Diastereomeric salt crystallisation was chosen to separate the *R*- and *S*-enantiomers of CpDA. Although other methods for the separation of enantiomers are available, diastereomeric salt crystallisation was considered to be the most cost-effective and time efficient method, when compared to other separating procedures (48, 49). A modified approach was employed for the separation of the enantiomers of CpDA. This approach was inspired by the work of Ault, who separated the *R*- and *S*-enantiomers of a structurally similar compound, 1-phenylethylamine (86). The separation of 1-phenylethylamine was achieved by reacting a racemic mixture of 1-phenylethylamine with optically pure (*R,R*)-tartaric acid to produce two diastereomeric salt complexes. The (*R,R*) salt complex and (*S,R*) salt complex could be separated by selective

crystallization from methanol. A similar approach was used to separate the *R*- and *S*-enantiomers of CpDA, with precautionary steps taken to prevent the breakdown of CpDA.

The reaction was scaled down approximately 30-fold and the *R*- and *S*-enantiomers of CpDA were successfully separated in their biologically active form. However, the respective enantiomeric preparations contained impurities which was expected as the starting material of the racemic mixture of CpDA was not chemically pure. As a $\geq 95\%$ enantiomerically pure sample is required for accurate interpretations of the 3D-configuration of the respective enantiomers, the optical rotation of the respective enantiomers could not be determined, due to the presence of impurities. It was assumed that the enantiomers of CpDA separated in this study were correctly denoted as the *R*- and *S*-enantiomers since CpDA is structurally related to 1-phenylethylamine. The instability of CpDA was further highlighted by LC-Q-ToF/ESI-MS analysis. A large portion of the respective enantiomers cyclized into 2-(4-hydroxyphenyl)-1-methylaziridine and 2-(4-acetoxyphenyl)-1-methylaziridine, suggesting that the separated enantiomers are less stable than the racemic mixture and more likely to lose activity under standard laboratory conditions. It is interesting to note that attempts to separate the *R*- and *S*-enantiomers on a preparative-scale resulted in the complete conversion of CpDA to both 2-(4-hydroxyphenyl)-1-methylaziridine and 2-(4-acetoxyphenyl)-1-methylaziridine, with a total loss of biological activity. For future studies the micro-separation approach, described in this study, would need to be refined and optimized to yield sufficient material for the purification of the *R*- and *S*-enantiomers to allow for the comprehensive characterization of the respective enantiomers. Moreover, if the relevant resources were to become available, it would be feasible to explore chiral chromatography as a means of separating the enantiomers of CpDA, since this approach enables high quality separation on a preparative scale (49).

In order to establish the biochemical mechanism of action of the respective enantiomers, the influence of the *R*- and *S*-enantiomers of CpDA was further investigated using the spectroscopic properties of a highly purified substrate-free preparation of ovine CYP11B1. Membrane-bound cytochrome P450 enzymes are highly labile and rapidly denature into the inactive P420 form when removed from the membrane environment. The presence of even trace amounts of P420 is undesirable as it masks the influence of an inhibitor on the DOC-induced difference spectrum (7, 18, 27). Nonetheless, previous studies in our laboratory have reported on the successful isolation and purification of active CYP11B1 by adding an excess amount of DOC substrate to the isolation and purification buffers to stabilize the enzyme (18, 92). A modified method was used for the purification of substrate-bound CYP11B1, which involved replacing the aniline-Sepharose CL-4B resin with commercially available Phenyl-Sepharose CL-4B resin. Substrate-bound CYP11B1 was successfully

purified from a partially purified CYP11B1-containing mitochondrial powder from ovine adrenals and purification was confirmed with SDS-PAGE and Western blot analyses.

Analyses of the acrylamide gel clearly showed that the Phenyl-Sepharose resin separated CYP11B1 from the other mitochondrial proteins. The bands representing these proteins (**Figure 48 A**, Lane 2, 3 and 9), indicate the presence of the larger CYP11A1 protein, and while CYP11B1 and CYP11B2 may be represented as a single band the smaller bands may indicate the presence of ADX and ADXR. It would appear that residual ADX and ADXR may be present in the sample which could be attributed to that small portion of the redox proteins bound to CYP11B1. Although the preparation had been subjected to ultra-centrifugation with the redox proteins remaining in the supernatant and the mitochondrial proteins in the pellet, it is possible that ADX and ADXR bound to CYP11B1 (as well as CYP11B2 and CYP11A1) would sediment in the pellet. It is also possible that the faint band visible in the purified sample at ± 10 kDa may be residual ADX bound to the enzyme, with the enzyme freed from its redox partner under the denaturing electrophoreses conditions.

An essential part of this study was the removal of DOC from the purified enzyme. This was an important step as the substrate stabilized the high spin-state of the heme-iron. The preparation of substrate-free CYP11B1 was achieved by methods previously published (13, 18). It is important to note that, after an hour, substrate free CYP11B1 lost all activity and was fully converted to its inactive form. The classic spectroscopic assays using a double beam spectrophotometer and 1.5 mL quartz cuvettes was modified for use to a 96-well micro-titre plate due to the limited time available before the substrate-free enzyme loses complete activity as well as the limited amount of purified substrate-free CYP11B1 available at any given time. This new approach served as an effective means to investigate the biochemical mechanism of action of the *R*- and *S*-enantiomers of CpDA, as the assay time and the amount of enzyme required for the assay were both significantly reduced.

Difference spectra proved that both the *R*- and the *S*-enantiomers of CpDA inhibit the binding of DOC to the active site of CYP11B1 and have the ability to induce Type II difference spectra. However, compared to CpDA, neither the *R*-enantiomer nor the *S*-enantiomer inhibited the DOC-induced difference spectrum to the same extent as the racemate of CpDA. In fact, the inhibitory effect induced by the racemic mixture of CpDA was equivalent to the sum of the inhibitory effects of both the *R*- and *S*-enantiomers of CpDA. Furthermore, in comparison to the typical Type II difference spectrum, induced by CpDA and the *R*-enantiomer, the *S*-enantiomer induced a distorted Type II difference spectrum with one minimum and two maxima absorbance values. These results suggest that the inhibitory effect induced by CpDA, could be attributed to both enantiomers binding simultaneously to CYP11B1, but in different regions of the active site. It should however be emphasised that the concentration of the

R-enantiomer was approximately 12 x more in the racemic mixture of CpDA than the *S*-enantiomer, suggesting that the *S*-enantiomer has a greater inhibitory profile than that of the *R*-enantiomer and the racemic mixture of CpDA.

The investigation into the ADXR/ADX-catalysed reduction of cytochrome c further revealed that CpDA and the enantiomers of CpDA had no significant effect on the mitochondrial electron transport chain, and that the inhibition induced by CpDA and the respective enantiomers impact only at the enzyme-substrate level, and not the mitochondrial electron transport chain.

The initial hypothesis that either the *R*- or *S*-enantiomers of CpDA may yield a more effective inhibitory profile still remains uncertain. Therefore, future studies require pure *R*- and *S*-enantiomers of CpDA to determine aspects such as the absolute chirality of the respective enantiomers and the inhibition of the catalytic activity of purified CYP11B1 by the respective compounds. This future work, involving the effects on the catalytic activity of the *R*- and *S*-enantiomers of CpDA, could provide a greater understanding of the biological nature of each enantiomer and similarly determine whether the *S*-enantiomer has a greater inhibitory profile than the *R*-enantiomer in terms of catalytic activity.

REFERENCES

1. Botschantzev, V. (1974) A synopsis of *Salsola* (Chenopodiaceae) from South and South-West Africa. *Kew Bullentin.* **29** (3), 597-614.
2. Ploss, H. (1906) *Das Weib in d. Natur- u. Völkerkunde* **1**, 670 as cited by Brondegard, V.J. (1973) Contraceptive plant drugs. *Planta Med.* **23**, 167-172.
3. Maritz, K. (1969) Gannabossie is beter as “die pil”. *Dagbreek en Landstem.* **23**, 33.
4. Swart, P., Swart, A. C., Louw, A. and van der Merwe, K. J. (2003) Biological activities of the shrub *Salsola tuberculatiformis* Botsch.: contraceptive or stress alleviator? *BioEssays.* **25** (6), 612-619.
5. De Lange, M. (1961) Prolonged gestation in karakul ewes in South West Africa. *Proc 4th Int. Cong Anim Reprod., The Hague.* **3**, 590–592.
6. Basson, P. A., Morgenthal, J. C., Bilbrough, R. B., Marais, J. L., Kruger, S. P. and van der Merwe, J. L. (1969) “Grootlamsiekte: a specific syndrome of prolonged gestation in sheep caused by a shrub *Salsola tuberculata* (Fenzl ex MOQ) Schinz var. *Tomentosa* C. A. Smith ex Aellen. *Onderstepoort J Vet Res.* **36** (1), 59-104.
7. Swart, P. (1986) The isolation of a novel inhibitor of adrenal cytochrome P-450 from *Salsola tuberculata*. Ph.D. thesis, Dept. Biochemistry, University of Stellenbosch.
8. Snegovskikh, V., Park, J. S. and Norwitz, E. R. (2006) Endocrinology of parturition. *Endocrinol Metab Clin N Am.* **35**, 173-191.
9. van der Merwe, K.J., Hofmeyr, J.H.S., Swart, P., Parkin, D.P., Rossouw, J. and Hartshorne, J. (1976) Natural products affecting the gestation period of sheep and their mode of action. *S Afr J Sci.* **72**, 184.
10. Wheeler, O.H. (1962) The Girard reagents. *Chem Rev.* **62** (3), 205-221.
11. Williamson, D. G., and O'Donnell, V. J. (1969) The interaction of metopirone with adrenal mitochondrial cytochrome P-450. A mechanism for the inhibition of adrenal steroid 11beta-hydroxylation. *Biochemistry.* **8** (4), 1306-1311.
12. Liggins, G.C., Fairclough, R.J., Grieves, S.A., Kendall, J.Z. and Knox, B. S. (1973) The mechanism of initiation of parturition in the ewe. *Recent Prog Horm Res.* **29**, 11-159.
13. Swart, P., Swart, A.C., Meyer, P.C., Bester, R. and van der Merwe, K. J. (1985) A novel method for the preparation of substrate-free cytochrome P-450_{11β}. *Prep Biochem.* **15** (5), 281-290.

14. Swart, P., Todres, P. C., Swart, A. C. and Van der Merwe, K. J. (1988) Micro-assay for sheep 11 β -hydroxylase activity using high-performance liquid chromatography for steroid analysis. *J Chrom.* **442**, 424-430.
15. Swart, P., van der Merwe, K.J., Swart, A.C., Todres, P. and Hofmeyr, J.H.S. (1993) Inhibition of cytochrome P-450_{11 β} by some naturally occurring acetophenones and plant extracts from the shrub *Salsola tuberculatiformis*. *Planta Med.* **59**, 139-143.
16. Omura, T. and Sato, R. (1964) The carbon monoxide-binding pigment of liver microsomes (I) evidence for its heme protein in nature. *J Biol Chem.* **239**, 2370-2378.
17. Kumaki, K., Sato, M., Kon, H. and Nebert, D. W. (1978) Correlation of type I, type II, and reverse type I difference spectra with absolute changes in spin state of hepatic microsomal cytochrome P-450 iron from five mammalian species. *J Biol Chem.* **253** (4), 1048-1058.
18. Swart, A. C. (1986) A biochemical study of two natural products from *Salsola tuberculata*. M.Sc. thesis, Dept. Biochemistry, University of Stellenbosch.
19. van der Merwe, K. J., de Kock, S. S., Swart, P. and Fourie, L. (1991) The application of mass spectrometry in the study of labile natural products. *Biochem Soc Trans.* **19**, 432S.
20. de Kock, S. S. (1990) Die sintese en gebruik van chemiese merkers vir biogene amienderivate wat oor asiridien verval. M.Sc. thesis, Dept. Biochemistry, University of Stellenbosch.
21. van der Merwe, K. J., de Kock, S. S., Swart, P. and Fourie, L. (1992) The electron impact and fast atom bombardment mass spectrometry of aziridines and their 2-chloroethylamine precursors. *Biol Mass Spec.* **21**, 672-674.
22. Fourie, L., van der Merwe, K. J., Swart, P. and de Kock, S. S. (1993) Application of fast atom bombardment mass spectrometry for the analysis of biologically active compounds. *Anal Chim Acta.* **279**, 163-166.
23. Maritz, M. (1994) A study of labile natural products occurring in *Salsola tuberculatisformis* Botsch. (Boraginaceae). M.Sc. thesis, Dept. Biochemistry, University of Stellenbosch.
24. De Kock, S. S. (1995) A study of phenolic aziridines and their precursors. Ph.D. thesis, Dept. Biochemistry, University of Stellenbosch.
25. Dermer, O.C. and Ham, G. E. (1969) Biological properties and uses of aziridines. In: *Ethylenimine and other aziridines: Chemistry and Application*. Academic Press, New York and London, pp 394-443.

26. Louw, A. and Swart, P. (1999) *Salsola tuberculatiformis* Botschantzev and an aziridine precursor analog mediate the *in vivo* increase in free corticosterone and decrease in corticosteroid-binding globulin in female Wistar rats. *Endocrinology*. **140** (5), 2044-2053.
27. Louw, A., Allie, F., Swart, A.C. and Swart, P. (2000) Inhibition of cytochrome P450c11 by biogenic amines and an aziridine precursor, 2-(4-acetoxyphenyl)-2-chloro-N-methyl-ethylammonium chloride. *Endocrine Research*. **26** (4), 729-736.
28. Louw, A., Swart, P. and de Kock, S. S. (1997) Mechanism for the stabilization *in vivo* of the aziridine precursor 2-(4-acetoxyphenyl)-2-chloro-N-methyl-ethylammonium chloride by serum proteins. *Biochem Pharmacol*. **53**, 189-197.
29. Louw, A., Swart, P. and Allie, F. (2000) Influence of an aziridine precursor on the *in vitro* binding parameters of rat and ovine corticosteroid-binding globulin (CBG). *Biochem Pharmacol*. **59**, 16-175.
30. Lesovaya, E., Yemelyanov, A.I., Swart, A. C., Swart, P., Haegeman, G. and Budunova, I. (2015) Discovery of Compound A - a selective activator of the glucocorticoid receptor with anti-inflammatory and anti-cancer activity. *Oncotarget*. **6** (31), 30730-30744.
31. Yemelyanov, A., Czornog, J., Gera, L., Joshi, S., Chatterton, R. T. and Budunova, I. (2008) Novel steroid receptor phyto-modulator compound a inhibits growth and survival of prostate cancer cells. *Cancer Research*. **68** (12), 4763-4773.
32. Yemelyanov, A., Bhalla, P., Yang, X., Ugolkov, A., Iwadate, K., Karseladze, A., and Budunova, I. (2012) Differential targeting of androgen and glucocorticoid receptors induces ER stress and apoptosis in prostate cancer cells: a novel therapeutic modality. *Cell Cycle*. **11** (2), 395-406.
33. Lesovaya, E., Yemelyanov, A., Kirsanov, K., Popa, A., Belitsky, G., Yakubovskaya, M., Gordon, L.I., Rosen, S.T. and Budunova, I. (2013) Combination of a selective activator of the glucocorticoid receptor Compound A with a proteasome inhibitor as a novel strategy for chemotherapy of hematologic malignancies. *Cell Cycle*. **12** (1), 133-144.
34. De Bosscher, K., van den Berghe, W., Beck, I. M., van Molle, W., Hennuyer, N., Hapgood, J., Libert, C., Staels, B., Louw, A. and Haegeman, G. (2005) A fully dissociated compound of plant origin for inflammatory gene repression. *Proc Natl Acad Sci U S A*. **102** (44), 15827-15832.

35. Dewint, P., Gossye, V., De Bosscher, K., van den Berghe, W., van Beneden, K., Deforce, D., van Calenbergh, S., Müller-Ladner, U., van der Cruyssen, B., Verbruggen, G., Haegeman, G. and Elewaut, D. (2008) A plant-derived ligand favoring monomeric glucocorticoid receptor conformation with impaired transactivation potential attenuates collagen-induced arthritis. *J Immunol.* **180** (4), 2608-2615.
36. van Loo, G., Sze, M., Bougarne, N., Praet, J., Mc Guire, C., Ullrich, A., Haegeman, G., Prinz, M. and Beyaert, R. (2010) Antiinflammatory properties of a plant-derived nonsteroidal, dissociated glucocorticoid receptor modulator in experimental autoimmune encephalomyelitis. *Mol Endocrinol.* **24** (2), 310-322.
37. Wust, S., Tischner, D., John, M., Tuckermann, J. P., Menzfeld, C., Hanisch, U. K., van den Brandt, J., Lühder, F. and Reichardt, H. M. (2009) Therapeutic and adverse effects of a non-steroidal glucocorticoid receptor ligand in a mouse model of multiple sclerosis. *PLoS One.* **4** (12), e8202.
38. Zhang, Z. R., Zhang, Z. Y. and Schluesener, H. J. (2009) Compound A, a plant origin ligand of glucocorticoid receptors, increases regulatory T cells and M2 macrophages to attenuate experimental autoimmune neuritis with reduced side effects. *J Immunol.* **183** (5), 3081-3091.
39. Reber, L. L., Daubeuf, F., Plantinga, M., De Cauwer, L., Gerlo, S., Waelput, W., van Calenbergh, S., Tavernier, J., Haegeman, G., Lambrecht, B. N., Frossard, N. and De Bosscher, K. (2012) A dissociated glucocorticoid receptor modulator reduces airway hyperresponsiveness and inflammation in a mouse model of asthma. *J Immunol.* **188** (7), 3478-3487.
40. Gossye, V., Elewaut, D., van Beneden, K., Dewint, P., Haegeman, G. and De Bosscher, K. (2010) A plant-derived glucocorticoid receptor modulator attenuates inflammation without provoking ligand-induced resistance. *Ann Rheum Dis.* **69**, 291-296.
41. Saksida, T., Vujicic, M., Nikolic, I., Stojanovic, I., Haegeman, G. and Stosic-Grujicic, S. (2014) Compound A, a selective glucocorticoid receptor agonist, inhibits immunoinflammatory diabetes, induced by multiple low doses of streptozotocin in mice. *Br J Pharmacol.* **171** (14), 5898-5909.
42. Liberman, A. C., Antunica-Noguerol, M., Ferraz-de-Paula, V., Palermo-Neto, J., Castro, C. N., Druker, J., Holsboer, F., Perone, M. J., Gerlo, S., de Bosscher, K., Haegeman, G. and Arzt, E. (2012) Compound A, a dissociated glucocorticoid receptor modulator, inhibits T-bet (Th1) and induces GATA-3 (Th2) activity in immune cells. *PLoS One.* **7** (4), e35155.

43. Rauner, M., Goettsch, C., Stein, N., Thiele, S., Bornhaeuser, M., De Bosscher, K., Haegeman, G., Tuckermann, J. and Hofbauer, L. C. (2011) Dissociation of osteogenic and immunological effects by the selective glucocorticoid receptor agonist, compound A, in human bone marrow stromal cells. *Endocrinology*. **152** (1), 103-112.
44. Barnes, P. J. (2011) Glucocorticosteroids: current and future directions. *Br J Pharmacol*. **163** (1), 29-43.
45. Barnes, P. J. (1998) Anti-inflammatory actions of glucocorticoids: molecular mechanisms. *Clin Sci*. **94** (6), 557-572.
46. Stahn, C., Löwenberg, M., Hommes, D. W. and Buttgereit, F. (2007) Molecular mechanisms of glucocorticoid action and selective glucocorticoid receptor agonists. *Mol Cell Endocrinol*. **275** (1-2), 71-78.
47. Izake, E. L. (2007) Chiral discrimination and enantioselective analysis of drugs: An overview. *J Pharm Sci*. **96** (7), 1659-1679.
48. Sekhon, B. S. (2010) Enantioseparation of chiral drugs - An overview. *Int J Chem Tech Res*. **2** (2), 1584-1594.
49. Nguyen, L. A., He, H. and Pham-Huy, C. (2006) Chiral drugs: an overview. *Int J Biomed Sci*. **2**, 85-100.
50. Maier, N. M., Franco, P. and Lindner, W. (2001) Separation of enantiomers: needs, challenges, perspectives. *J Chromatogr A*. **906**, 3-33.
51. Martín, A. and Cocero, M. J. (2007) Separation of enantiomers by diastereomeric salt formation and precipitation in supercritical carbon dioxide. Application to the resolution of mandelic acid. *J Supercrit Fluids*. **40**, 67-73.
52. Prelog, V. and Heimchen, G. (1982) Basic principles of the CIP-system and proposals for a revision. *Angew Chem Int Ed Engl*. **21**, 567-583.
53. Miller, W. L., and Auchus, R. J. (2011) The molecular biology, biochemistry, and physiology of human steroidogenesis and its disorders. *Endocr Rev*. **32** (1), 81-151.
54. Schloms, L. (2015) The inhibition of adrenal steroidogenic enzymes and modulation of glucocorticoid levels *in vitro* and *in vivo* by *Aspalathus linearis* (Rooibos). Ph.D. thesis, Dept. Biochemistry, University of Stellenbosch.
55. Schloms, L., Storbeck, K.H., Swart, P., Gelderblom, W.C.A. and Swart, A.C. (2012) The influence of *Aspalathus linearis* (Rooibos) and dihydrochalcones on adrenal steroidogenesis: Quantification of steroid intermediates and end products in H295R cells. *J Steroid Biochem Mol Biol*. **128**, 128-138.

56. Ehrhart-Bornstein, M., Hinson, J. P., Bornstein, S. R., Scherbaum, W. A. and Vinson, G. P. (1998) Intraadrenal interactions in the regulation of adrenocortical steroidogenesis. *Endocr Rev.* **19** (2), 101-143.
57. Mescher, A. L. (2010) *Junqueira's Basic Histology: Text and Atlas*, 12th ed. McGraw-Hill, New York, USA.
58. Ehrhart-Bornstein, M. and Bornstein, S. R. (2008) Cross-talk between adrenal medulla and adrenal cortex in stress. *Ann NY Acad Sci.* **1148** (1), 112–117.
59. Mugari, M. B. (2015) The inhibitory effect of Rooibos on cytochromes P450 and downstream *in vitro* modulation of steroid hormones. M.Sc. thesis, Dept. Biochemistry, University of Stellenbosch.
60. Hu, J., Zhang, Z., Shen, W. J. and Azhar, S. (2010) Cellular cholesterol delivery, intracellular processing and utilization for biosynthesis of steroid hormones. *Nutr Metab.* **7** (47), 1-25.
61. Mason, J. I., and Rainey, W. E. (1987) Steroidogenesis in the human fetal adrenal: A role for cholesterol synthesized *de novo*. *J Clin Endocrinol Metab.* **64**, 140-147.
62. Mostaghel, E. A. (2013) Steroid hormone synthetic pathways in prostate cancer. *Transl Androl Urol.* **2** (3), 212-227.
63. du Toit, T. (2015) An investigation into the influence of Rooibos (*Aspalathus linearis*) on androgen metabolism in normal and prostate cancer. M.Sc. thesis, Dept. Biochemistry, University of Stellenbosch.
64. Sundahl, N., Bridelance, J., Libert, C., De Bosscher, K. and Beck, I. M. (2015) Selective glucocorticoid receptor modulation: New directions with non-steroidal scaffolds. *Pharmacol Ther.* **152**, 28-41.
65. Ortsäter, H., Sjöholm, A. and Rafacho, A. (2012) *Regulation of glucocorticoid receptor signalling and the diabetogenic effects of glucocorticoid excess*. In Tech, Croatia.
66. Klingenbergz, M. (1958) Pigments of rat liver microsomes. *Arch Biochem Biophys.* **75**, 376-386.
67. Garfinkel, D. (1958) Studies on pig liver microsomes. I. Enzymic and pigment composition of different microsomal fractions. *Arch Biochem Biophys.* **77** (2), 493-509.
68. Omura, T. and Sato, R. (1962) A new cytochrome in liver microsomes. *J Biol Chem.* **237**, 1375–1376.
69. Harding, B.W., Wong, S.H. and Nelson, D. H. (1964) Carbon monoxide-combining substances in rat adrenal. *Biochem Biophys Acta.* **92**, 415-417.
70. Sato, R. and Omura, T. (1978) *Cytochrome P-450*. Kodansha Ltd. and Academic Press Inc., Tokyo, pp. 173-175.

71. White, R. E. and Coon, M. J. (1980) Oxygen activation by cytochrome P-450. *Ann Rev Biochem.* **49**, 315-356.
72. Walsh, C. (1979) *Enzymatic reaction mechanisms*. W.H. Freeman and Company, San Francisco.
73. Cohen, B.S. and Estabrook, R. W. (1971) Microsomal electron transport reaction. *Arch Biochem Biophys.* **143**, 46-53.
74. Kimura, T. (1981) ACTH stimulation on cholesterol side chain cleavage activity of adrenocortical mitochondria. *Mol Cell Biochem.* **36**, 105-122.
75. Sagara, Y., Hara, T., Ariyasu, Y., Ando, F., Tokunaga, N. and Horiuchi, T. (1992) Direct expression in *Escherichia coli* and characterization of bovine adrenodoxins with modified amino-terminal regions. *FEBS Lett.* **300** (3), 208-212.
76. Suhara, K., Nakayama, K., Takikawa, O. and Karagiri, M. (1982) Two forms of adrenodoxin reductase from mitochondria of bovine adrenal cortex. *Eur J Biochem.* **125**, 659-664.
77. Suhara, K., Ikeda, Y., Takemori, S. and Katagiri, M. (1972) The purification and properties of NADPH-adrenodoxin reductase from bovine adrenocortical mitochondria. **28** (1), 45-47.
78. Kimura, T. (1968) *Biochemical aspects of iron-sulfur linkage in non-heme iron protein, with special reference to "adrenodoxin"*. Springer Berlin Heidelberg, Berlin, Heidelberg, pp. 1-40.
79. Lambeth, J. D., Seybert, D. W., Lancaster, J. R., Salerno, J. C. and Kamin, H. (1982) Steroidogenic electron transport in adrenal cortex mitochondria. *Mol Cell Biochem.* **45** (1), 13-31.
80. Lambeth, J. D., Lancaster, J. R. and Kamin, H. (1981) Steroidogenic electron transport by adrenodoxin reductase and adrenodoxin. *J Biol Chem.* **256** (8), 3674-3678.
81. Louw, A. (1998) A study of the mechanism of contraceptive action of naturally occurring and synthetic phenyl aziridines in rats. Ph.D. thesis, Dept. Biochemistry, University of Stellenbosch.
82. Rautenbach, M. (1998) The synthesis and characterization of analogues of the antimicrobial peptide iturin A2. Ph.D. thesis, Dept. Biochemistry, University of Stellenbosch.
83. McConathy, J. and Owens, M. J. (2003) Stereochemistry in drug action. *Prim Care Companion J Clin Psychiatry.* **5** (2), 70-73.
84. Blackmond, D. G. (2010) The origin of biological homochirality. *Cold Spring Harb Perspect Biol.* **2**, a002147.

85. Pálovics, E., Faigl, F. and Fogassy, E. (2012) *Separation of the mixtures of chiral compounds by crystallization processes*. In Tech, Hungary, pp. 3-6.
86. Ault, A. (1965) Resolution of D,L- α -phenylethylamine: An introductory organic chemistry experiment. *J Chem Educ.* **42**, 269.
87. Cheng, S.C. and Harding, B. W. (1973) Substrate-induced difference spectral, electron paramagnetic resonance, and enzymatic properties of cholesterol-depleted mitochondrial cytochrome P450 of bovine adrenal cortex. *J Biol Chem.* **248** (20), 7263–7271.
88. Ziegler, G. A, Vonnrhein, C., Hanukoglu, I. and Schulz, G. E. (1999) The structure of adrenodoxin reductase of mitochondrial P450 systems: electron transfer for steroid biosynthesis. *J Mol Biol.* **289**, 981–990.
89. Schiffler, B., Kiefer, M., Wilken, A., Hannemann, F., Werner Adolph, H. and Bernhardt, R. (2001) The interaction of bovine adrenodoxin with CYP11A1 (cytochrome P450_{scc}) and CYP11B1 (cytochrome P450_{11 β}). Acceleration of reduction and substrate conversion by site-directed mutagenesis of adrenodoxin. *J Biol Chem.* **276** (39), 36225–36232.
90. Omura, T., Sanders., E., Estabrook, R.W., Cooper, D.Y. and Rosenthal, O. (1966) Isolation from adrenal cortex of a non-heme iron protein and a flavoprotein functional as a reduced triphosphopyridine nucleotide cytochrome P-450 reductase. *Arch Biochem Biophys.* **117**, 660–673.
91. Swart, P., Polson, A. and van der Merwe, K. J. (1985) An apparatus for the concentration of large volumes of dilute protein solutions to a predetermined volume. *Prep Biochem.* **15**, 1–8.
92. Takemori, S., Sato, H., Gomi, T., Suhara, K. and Katagiri, M. (1975) Purification and properties of cytochrome P-450_{11 β} from adrenocortical mitochondria. *Biochem Biophys Res Commun.* **67** (3), 1151–1157.
93. Laemmli, U. K. (1970) Cleavage of structural proteins during the assembly of the head of bacteriophage T4. *Nature.* **227** (5259), 680-685.
94. Mentel, M., Blankenfeldt, W. and Breinbauer, R. (2009) The active site of an enzyme can host both enantiomers of a racemic ligand simultaneously. *Angew Chem Int Ed Engl.* **48**, 9084–9087.